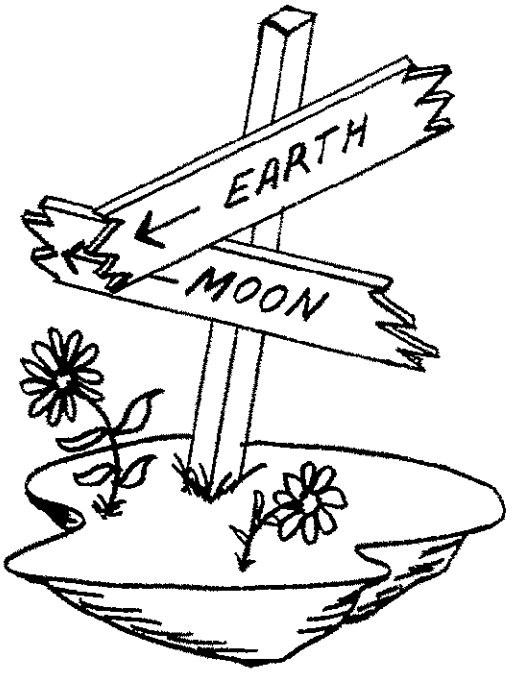

The Benchmark Satellite

Final Report

NGR06-002-085

Prepared by C. Byron Winn

DEPARTMENT OF MECHANICAL ENGINEERING
FORT COLLINS, COLORADO
COLORADO STATE UNIVERSITY

THE BENCHMARK SATELLITE

FINAL REPORT

NASA NGR 06-002-085

Department of Mechanical Engineering
Colorado State University
Fort Collins, Colorado

June 1970

TABLE OF CONTENTS

I. INTRODUCTION

A. Summary of Research

The primary purpose of the research reported herein was to investigate the possibilities of using satellites to obtain independent and more precise measurements of continental drift, polar wandering, and irregular variations in the earth's speed of rotation, than have been obtained by other means. An additional objective was to develop an active attitude control logic for controlling the attitude of spin-stabilized spacecraft. A final objective was to investigate the feasibility of using laser range measurements from a space base for satellite orbit determination.

B. Report Format

Several papers have been prepared as part of this program; some have been accepted for publication in the professional journals or for presentation before the professional societies while others are in the process of being submitted for publication. These papers form the basis of this report. Brief summaries of the research accomplishments are presented prior to the papers.

II. SUMMARIES OF RESEARCH ACCOMPLISHMENTS

A. Geodesy

It had been proposed to examine the use of a synchronous controlled satellite and precise laser range measurements for the determination of polar wandering, continental drift, and variations in the earth's rotation rate. Development of the

basic functional relationships between range and geodetic parameters has been completed and was based on one controllable synchronous satellite (the Benchmark Satellite) and one freely drifting synchronous satellite. The controllable satellite would be forced to remain earth-fixed by active thrusting and laser ranging to ground stations and therefore could serve as a known position or benchmark in space. The analysis developed in terms of ranging between a benchmark satellite and a freely drifting satellite was general and may be applied directly to ground based observations. Analysis of ground based observations has been initiated but no results can be reported at this time. The analytical development is presented in the paper on polar wandering.

An independent means for determining continental drift was also investigated. This technique involves the use of laser range data to subsynchronous satellites and it is demonstrated that the accuracy is essentially independent of satellite height beyond one earth radius and of ground station locations. This research is described in the paper on continental drift.

B. Research Accomplishments in Attitude-Control of Spinning Spacecraft

The accomplishments of this program include the following developments:

(a) A completely active control logic has been developed for controlling the attitude of a spin-stabilized axisymmetric spacecraft having arbitrary (but non-spherical) inertial

characteristics. The developed control logic is formulated from a direction-cosine kinematic model, and is accordingly not restricted by either small angle assumptions or by kinematic singularities. The formulated control logic can be realized by means of one body-fixed reaction jet, and makes use of existing sensor systems. Details of this development are included in the two enclosed papers: (i) Optimal Direction-Cosine Attitude-Control Logic for Spin-Stabilized Axisymmetric Spacecraft (submitted to AIAA Journal of Spacecraft and Rockets 15 May 1970), and (ii) Direction-Cosine Attitude-Control Logic for Spin-Stabilized Axisymmetric Spacecraft (accepted for publication in AIAA Journal of Spacecraft and Rockets 14 April 1970).

(b) A considerable quantity of work has been expended towards the development of an active control system for a moderately asymmetric spinning body. The enclosed report outlines an improved analytical solution for the torque-free motion of a spinning asymmetric body. This solution should be of considerable value in the development of impulsive control logic, since it is valid for large angles, and allows a time-varying spin-speed. Details of this analysis are included in the enclosed paper.

C. Space-Based Orbit Determination

Techniques involving range only data for orbit determination have been investigated in the past but have not included space-based

range data to arbitrary satellites. The purpose of this research was to develop an orbit determination program for arbitrary orbits using range only data obtained from a space-based tracking satellite. A program has been developed and is discussed, along with some results, in the paper on orbit determination. The tracking procedure has been simulated for various orbits and the program has converged to the orbit parameters to an accuracy of 1×10^{-6} within at most three iterations in all cases examined.

THE DETERMINATION OF POLAR WANDERING AND CONTINENTAL DRIFT BY LASER RANGING TO SATELLITES

Paul F. Mennemeyer*

C. Byron Winn**

* Graduate Student, Mechanical Engineering Department, Colorado State University

** Associate Professor, Mechanical Engineering Department, Colorado State University

MEP69-70CBW-PFM-3

TABLE OF CONTENTS

ABSTRACT

A method is presented for measuring the motion of the Earth with respect to its rotation axis using two synchronous satellites Laser range measurements are made between a free satellite and a controlled satellite which is forced to maintain its position relative to the Earth by active thrusting. Additional laser ranging between the controlled satellite and three ground stations is required. The amplitude of polar motion can be calculated to within 0.0001 seconds of arc.

II. POLAR WANDERING

Introduction

It is well known that the Earth's rotation axis undergoes a precession and nutation due to gravitational torques exerted by the sun and moon. In addition to this motion, the Earth has been observed to shift or wobble with respect to its axis of rotation. Evidence for such a motion consists primarily of astronomical observations conducted by the International Latitude Service (ILS) since the turn of the century. Since 1962, the International Polar Motion Service (IPMS) has carried on the work of the ILS, and an independent determination of polar motion has been made by the Bureau Internation de l'Heure (BIH) in Paris since 1955.

The amplitude of the wobble (Termed the Chandler Wobble) is on the order of 0''.1 to 0''.2, and the period is approximately 14 months. The most precise observatory instruments presently in use for latitude and sidereal time determinations are the photographic zenith tube (PZT) and the Danjon impersonal prismatic astrolabe. These instruments have a standard deviation of 0''.075 from 14 - 15 star observations during one night or 0''.2 from a single determination [Mueller, 1969]. Monthly averaging of such astronomical observations theoretically results in a probable error on the order of 0''.01 [Markowitz, 1968]. However, systematic differences of up to 0''.1 are present when the ILS-IPMS data are compared with results obtained by the BIH [Smylie and Manshina, 1968]. In addition to the Chandler Wobble, it is suspected that a secular shift in the mean pole position occurs at a rate of about 0''.002 - 0''.003 along a meridian 60° - 70° West. [Markowitz, 1968; Yumi and Wako, 1968].

It has been suggested that the motion of the pole is sustained by seasonal variations in the Earth's mass distribution [Munk and Macdonald, 1960] and by earthquakes [Smylie and Manshina, 1968], but the observational data presently available are of insufficient accuracy to allow proper investigation of such phenomena. It would be desirable to obtain more accurate data from an independent experiment.

A method of measuring the motion of the Earth with respect to its axis of rotation by means of two synchronous satellites is currently being investigated. The technique involves laser ranging between a controlled or proof satellite and a freely drifting satellite. The proof satellite is forced to maintain its position relative to the Earth by means of active thrusting and laser ranging to three ground stations. The free satellite is unaffected by small changes in the Earth's orientation. Therefore, intersatellite range measurements provide an indication of the motion of the Earth. Perturbations of the satellite orbits and the movement of the Earth's rotation axis in space are accounted for so as to permit calculation of the amplitude of any shift of the pole with respect to the rotation axis to within 0''.0001.

Polar Motion Coordinates

The pole of epoch is defined as the point of intersection of the Earth's axis of rotation with its surface at a particular time, called epoch. The polar axis of epoch is defined to be a geocentric axis passing through a fixed point on the Earth's surface corresponding to the pole of epoch. The term "polar motion" refers to a change in the position of the polar axis of epoch relative to the axis of rotation. Great circles normal to the polar axis of epoch and to the axis of rotation are called the earth-fixed equator and the rotation equator respectively. The position of the earth-fixed equator relative to the rotation equator is specified by the angle α between the two equatorial planes and the east longitude Γ of the ascending node of the earth-fixed equator with respect to a reference point P^1 on the rotation equator. The polar motion coordinates α and Γ are shown in Figure 1.

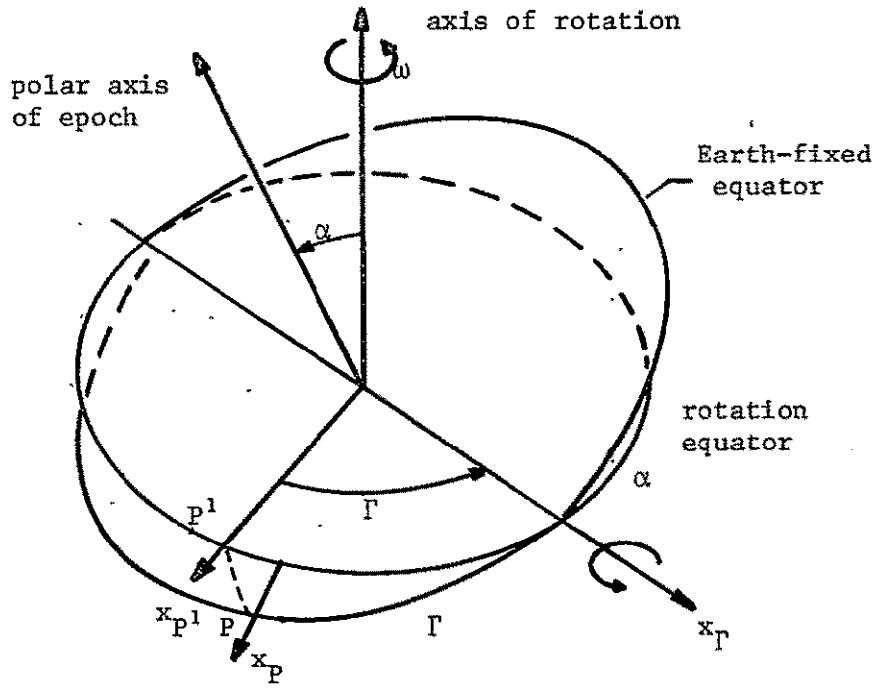

Fig. 1. Polar Motion Coordinates.

Relationship to Traditional Polar Motion Coordinates

Traditionally, the position of the axis of rotation relative to the polar axis of epoch is specified by the rectangular coordinates (x_1, x_2) as shown in Figure 2. The polar axis chosen as a reference is known as the Conventional International Origin (CIO), and corresponds to a mean pole of 1900-1905. It will prove advantageous in the following kinematical development to define a new pole of epoch to be the position of the spin axis at the time of initiation of a particular experiment. The change to a new pole of epoch involves a simple translation of the coordinate axes shown in Figure 2. As a consequence of the small magnitude of x_1 and x_2 (a few tenths of an arc second) it makes very little difference whether they are taken to be angles, as suggested by Figure 2, or direction cosines of the Earth's spin axis. The direction cosine interpretation is used in the following development of equations which relate x_1 and x_2 to the nodal coordinates α and Γ.

Let x_1, x_2, and x_3 be direction cosines of the spin axis with respect to an Earth-fixed coordinate system having its x, y, and z axes through the Greenwich meridian, 90° east longitude, and the pole of epoch respectively.

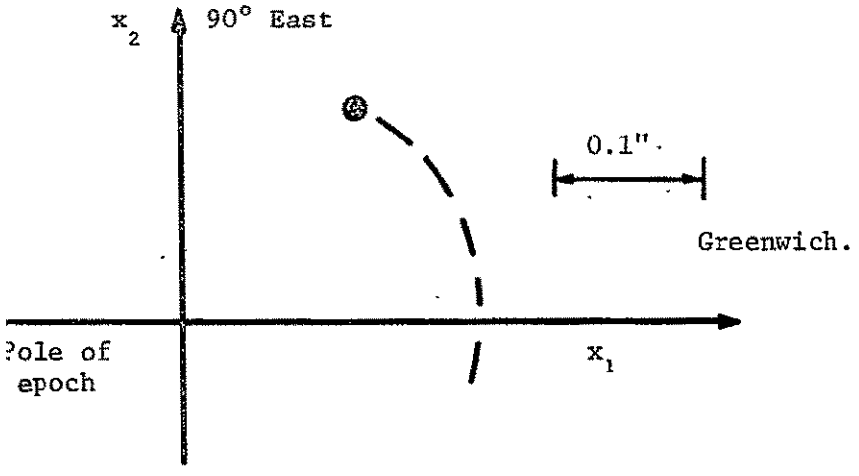

Fig. 2. Rectangular Polar Motion Coordinates.

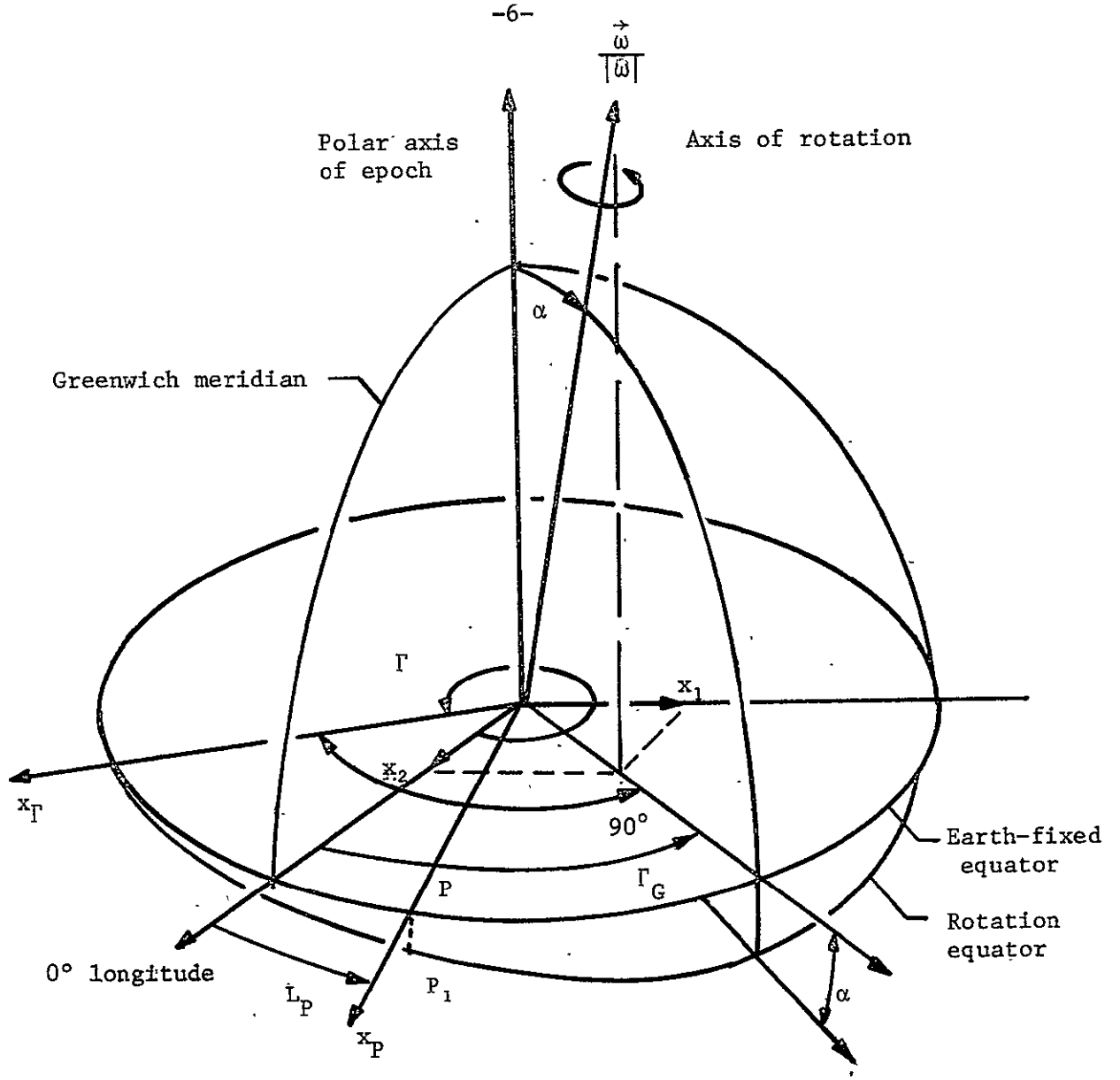

Fig. 3. Nodal Coordinates and Polar Motion Direction Cosines.

If L_P is the east longitude of reference point P (Figure 3) and Γ_G denotes east longitude of the spin axis relative to Greenwich, then

$$\Gamma = \Gamma_G - (L_P + \frac{\pi}{2}). \tag{1}$$

Since x_1, x_2, and x_3 are direction cosines, they satisfy

$$x_1^2 + x_2^2 + x_3^2 = 1$$

In view of the two preceding relationships, α and Γ are related to x_1 and x_2 by observing that

$$\alpha = \mathrm{Tan}^{-1} \frac{x_1^2 + x_2^2}{x_3} \tag{2}$$

and

$$\Gamma_G = \mathrm{Tan}^{-1} \frac{x_2}{x_1}$$

Rotation Axis Coordinates

The axis of rotation of the Earth does not remain stationary in space. The motion of the rotation axis is described as a precession and nutation relative to some inertial coordinate system. The precession is a coning motion with amplitude equal approximately to the obliquity of the ecliptic, 23°.5, and a period of about 25,800 years. The nutation is a relatively short periodic motion with an amplitude of about 9'' and a period of about 18.6 years. The position of the rotation axis and rotation equator at time of epoch serves as an inertial coordinate system to which subsequent motion of the rotation axis can be referred. The vernal equinox of epoch, γ_E, represents a fixed direction in space. Referral of longitude to an inertial axis x_E, 90° eastward from γ_E, insures that the longitude $\tilde{\Omega}$ of the ascending node of the rotation equator will be a small angle.* The inclination of the rotation equator with respect to the inertial equator of epoch is denoted by i. Note that $i > 0$ by definition. The rotation axis coordinates are shown in Figure 4.

*The rotation axis tips in the general direction of a moving vernal equinox, which progresses at about 50''.3 per year westward.

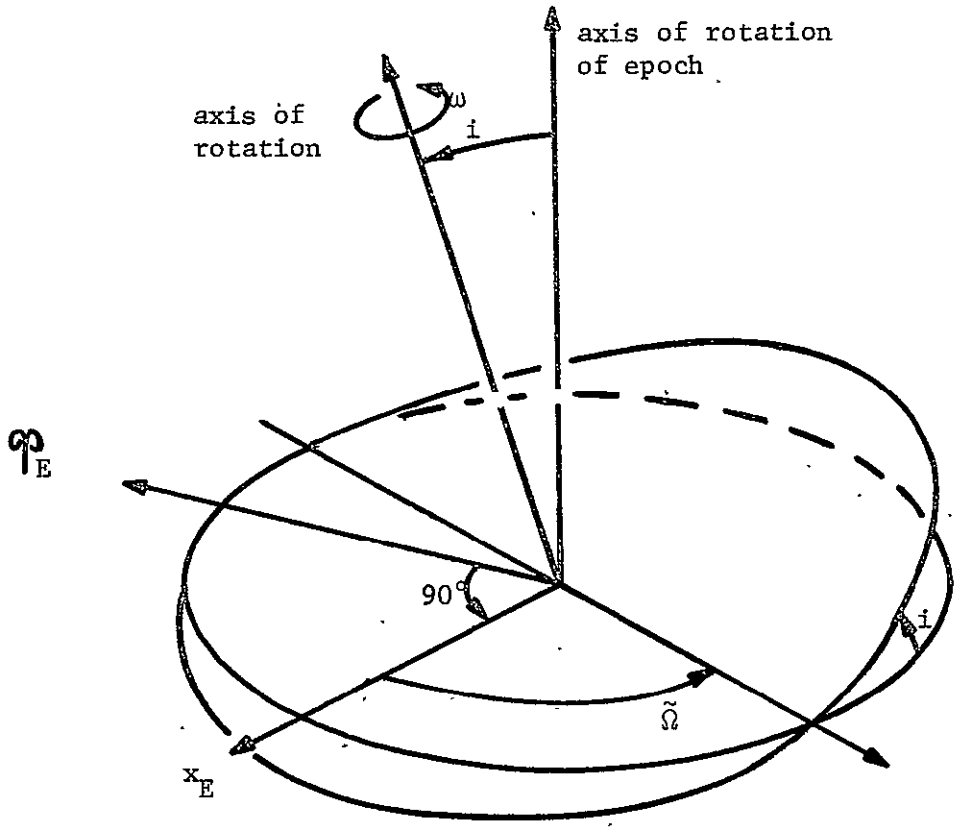

Fig. 4. Rotation Axis Coordinates.

Orbit of the Free Satellite

The ground track of a synchronous satellite resembles a figure eight as shown in Figure 5. The actively controlled proof satellite remains in the immediate vicinity of an arbitrary point P above the Earth-fixed equator. The free satellite is injected into a synchronous orbit whose ground track is centered over point P at the time of initiation of the experiment. This initial time is taken as the time of epoch.

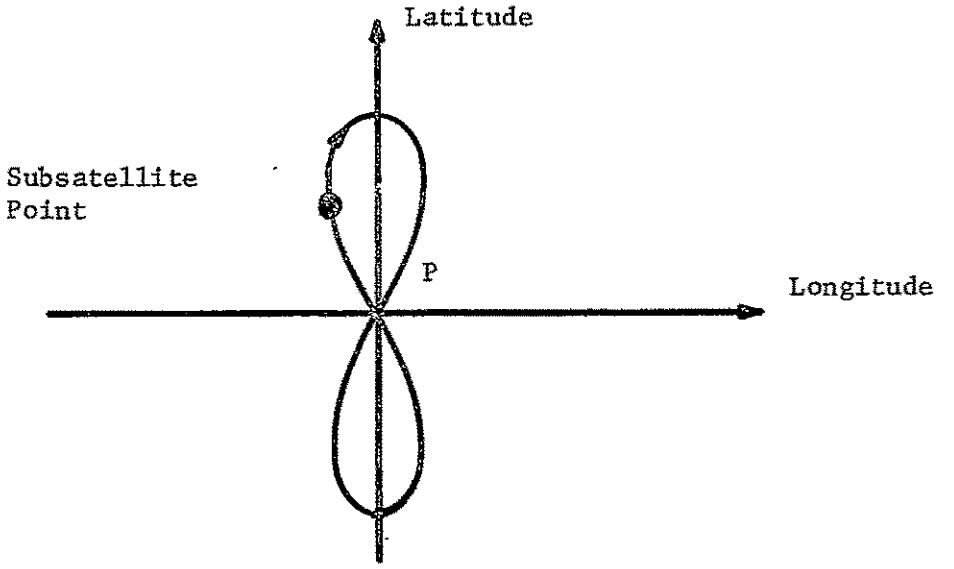

Fig. 5. Ground Track of a Synchronous Satellite.

Near circularity of the free satellite orbit permits specification of satellite positions at any time subsequent to epoch in terms of the four elements Ω, ρ, η, and λ of a circular reference orbit and perturbations $\delta\lambda$, $\delta\phi$, and $\delta\rho$ measured from a nominal point $\overline{P}_F$ which moves in the reference orbit as shown in Figure 6. In order to insure that the free satellite remains in the vicinity of point $\overline{P}_F$ during the extended period of time subsequent to epoch (possibly tens of years), it is necessary to regard the elements of the reference orbit as slowly osculating parameters with values Ω_E, ρ_E, η_E, and λ_E at epoch. Point $\overline{P}_E$ corresponds to point $\overline{P}_F$ at epoch, and λ_E is the argument of $\overline{P}_E$ measured from the node $\overline{x}_E$. The rate of change of λ_E with respect to time is defined to be

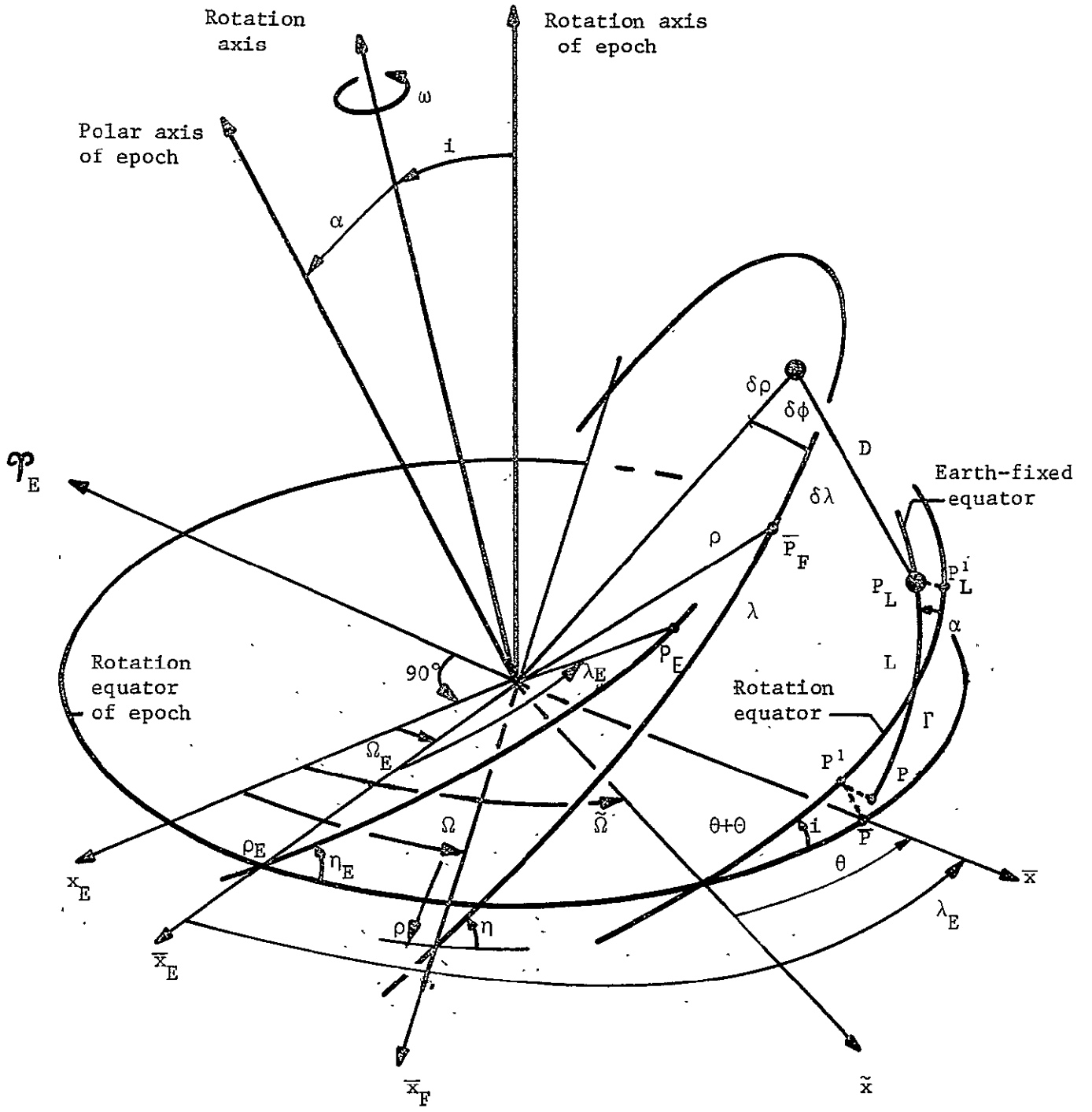

Fig. 6. Coordinate Systems.

$$\dot{\lambda}_E \equiv \omega_E \quad , \tag{3}$$

where ω_E is the Earth's absolute rate of rotation at epoch. λ is then specified by assigning a value to the slowly osculating parameter Λ, where

$$\lambda \equiv \lambda_E + \Lambda \quad . \tag{4}$$

ρ_E is defined to be the radius resulting in an orbital period equal to the period of the Earth's rotation at epoch. The parameters η_E and Ω_E specify the size of the free satellite ground track and the initial orientation of the orbit plane in space. The point $\bar{P}$ is defined to travel around the rotation equator of epoch, always being located at an angle λ_E eastward from the inertially fixed axis $\bar{x}_E$. The angle θ is defined as

$$\theta \equiv \lambda_E - (\tilde{\Omega} - \Omega_E). \tag{5}$$

Point P^1 is defined to correspond with $\bar{P}$ at epoch and to be located along the rotation equator $\theta + \Theta$ radians eastward from the node $\tilde{x}$, where Θ is a small, slowly varying parameter which takes into account any changes in the Earth's rotation rate subsequent to epoch. It will be shown later that proper orientation of the free satellite orbit renders the final results insensitive to Θ.

Ground-to-Satellite Ranging

An Earth-fixed rectangular coordinate system may be established as shown in Figure 7 with the origin at the center of the Earth and the x axis passing through point P on the Earth-fixed equator. Three ground stations are used having geocentric radius, east longitude, and north

latitude denoted by R_n, E_n, and N_n; (n = 1,2,3) respectively. The rectangular coordinates, X_n, Y_n, and Z_n of the nth ground station are given by

$$\begin{aligned} X_n &= R_n \cos N_n \cos E_n \ , \\ Y_n &= R_n \cos N_n \sin E_n \ , \\ Z_n &= R_n \sin N_n \ . \end{aligned} \tag{6}$$

If x, y, and z denote rectangular coordinates of either the free satellite or the proof satellite, and if the column vectors $\vec{R}_n$ and $\vec{x}$ are defined as

$$\vec{R}_n = \begin{bmatrix} X_n \\ Y_n \\ Z_n \end{bmatrix} \qquad (n = 1,2,3) \ , \tag{7}$$

and

$$\vec{x} = \begin{bmatrix} x \\ y \\ z \end{bmatrix} \tag{8}$$

then the three ground-to-satellite range vectors are given by

$$\vec{r}_n = -\vec{R}_n + \vec{x} \qquad (n = 1,2,3). \tag{9}$$

The ground ranging equation,

$$r_n^2 = R_n^2 + |\vec{x}|^2 - 2(X_n x + Y_n y + Z_n z) \ , \tag{10}$$

follows directly from equation 9, and is applicable to either the free satellite with coordinates (x_F, y_F, z_F), or to the proof satellite with coordinates (x_P, y_P, z_P).

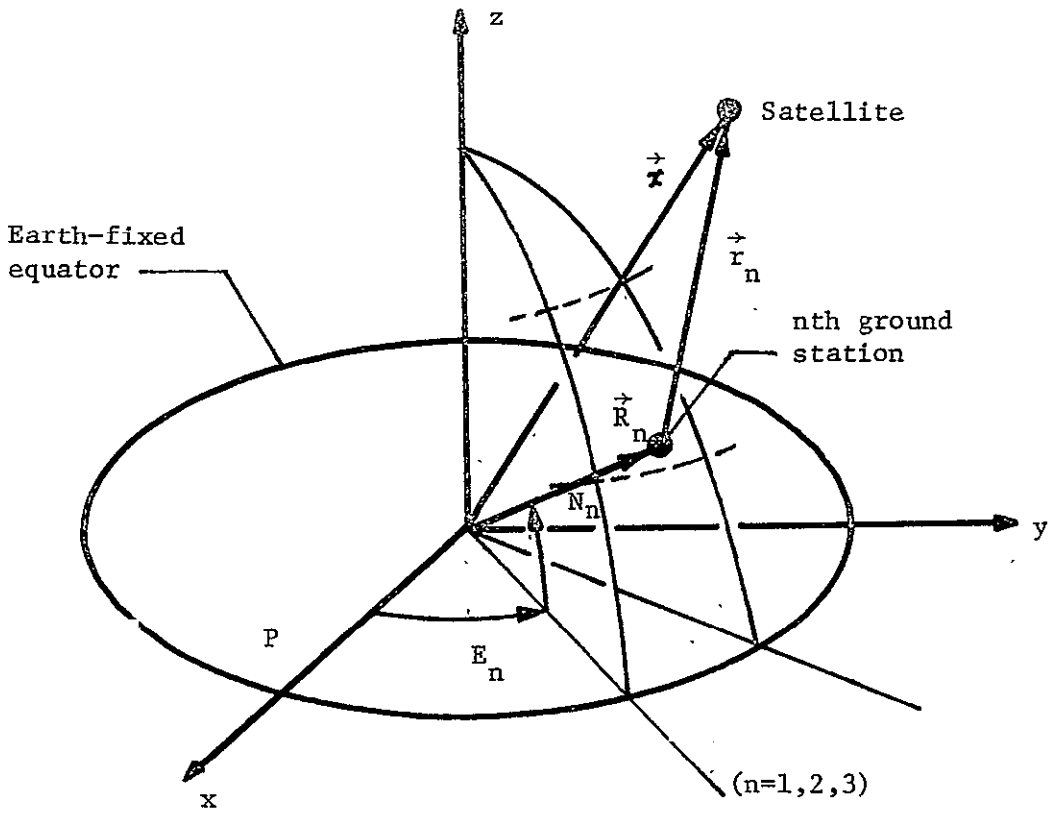

Fig. 7. Earth-fixed Coordinates.

The proof satellite is to be actively controlled in such a way that it remains in the vicinity of a point P_L which is located at synchronous radius ρ_E and at a specified east longitude L from point P on the Earth-fixed equator. L can be chosen so as to insure that the satellites do not collide. Deviation of the proof satellite from its nominal position is expressed in terms of the perturbations ε_1, ε_2, and ε_3 shown in Figure 8.

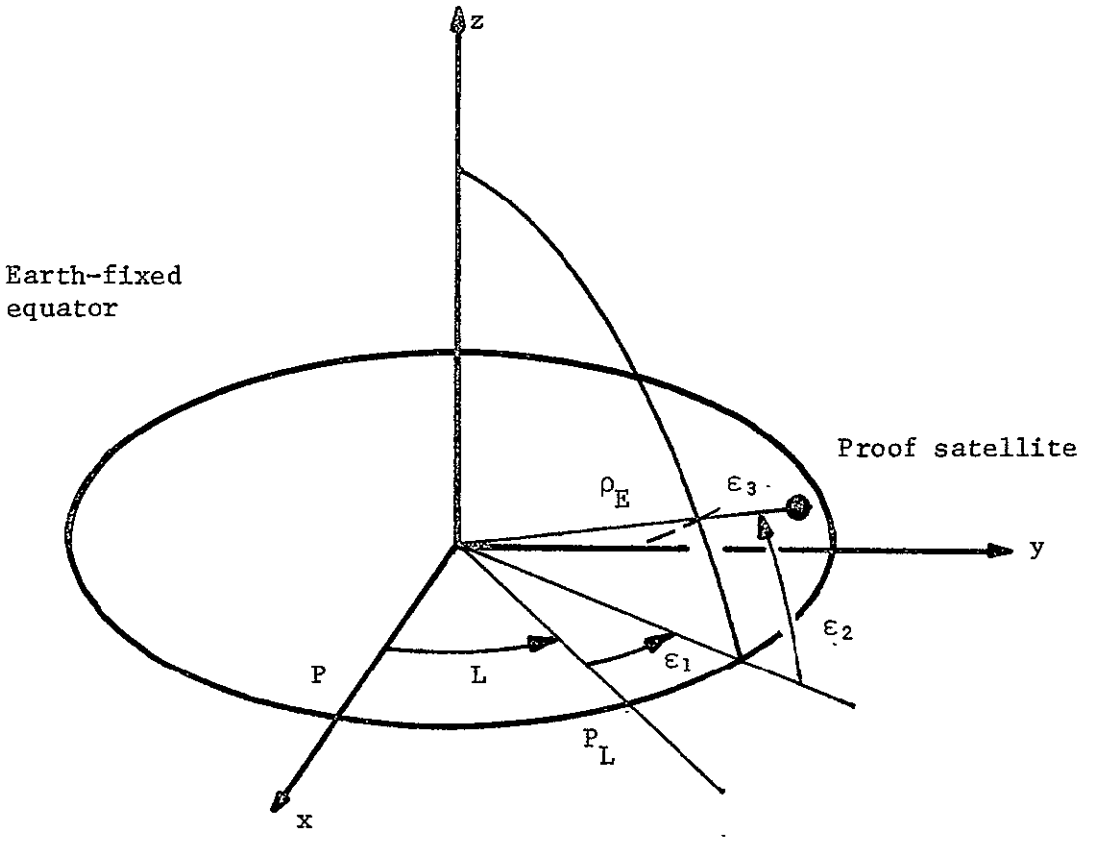

Fig. 8. Proof Satellite Coordinates.

The rectangular coordinates of the proof satellite are

$$\begin{aligned} x_P &= (\rho_E + \varepsilon_3) \cos \varepsilon_2 \cos(L + \varepsilon_1) , \\ y_P &= (\rho_E + \varepsilon_3) \cos \varepsilon_2 \sin(L + \varepsilon_1) , \\ z_P &= (\rho_E + \varepsilon_3) \sin \varepsilon_2 . \end{aligned} \tag{11}$$

Linearization of Equation (10) about the nominal point P_L, corresponding to $\varepsilon_1 = \varepsilon_2 = \varepsilon_3 = 0$, results in

$$\begin{bmatrix} \delta r_1 \\ \delta r_2 \\ \delta r_3 \end{bmatrix} = \begin{bmatrix} \\ \dfrac{\partial r_n}{\partial \varepsilon_k}_{P_L} \\ \\ \end{bmatrix} \begin{bmatrix} \delta \varepsilon_1 \\ \delta \varepsilon_2 \\ \delta \varepsilon_3 \end{bmatrix} \tag{12}$$

where

$$\begin{aligned} \left(\frac{\partial r_n}{\partial \varepsilon_1}\right)_{P_L} &= \frac{\rho_E}{(r_n)_{P_L}} \left[X_n \sin L - Y_n \cos L\right] , \\ \left(\frac{\partial r_n}{\partial \varepsilon_2}\right)_{P_L} &= -\frac{\rho_E}{(r_n)_{P_L}} Z_n , \\ \left(\frac{\partial r_n}{\partial \varepsilon_3}\right)_{P_L} &= \frac{1}{(r_n)_{P_L}} \left[\rho_E - X_n \cos L - Y_n \sin L\right] \end{aligned} \tag{13}$$

and $$(r_n)_{P_L} = R_n^2 - 2\rho_E \left[X_n \cos L + Y_n \sin L\right]$$

for (n = 1,2,3). Inversion of equation (12) gives the deviation of the proof satellite from point P_L in terms of the ground-station range residuals δr_1, δr_2, and δr_3, and therefore provides information necessary to control the proof satellite.

Intersatellite Ranging

The range D between the free satellite and the proof satellite is given by

$$D^2 = (x_F - x_P)^2 + (y_F - y_P)^2 + (z_F - z_P)^2 \tag{14}$$

The coordinates (x_F, y_F, z_F) of the free satellite in the Earth-fixed coordinate system of Figure 7 are obtained by first expressing the free satellite's position in terms of ρ, $\delta\lambda$, $\delta\phi$, and $\delta\rho$ using the coordinate

system of Figure 9, and then performing seven consecutive coordinate rotations ending with the Earth-fixed system of Figure 8.

The position of the free satellite is given by

$$\begin{aligned} x_F^{vii} &= (\rho + \delta\rho) \cos\delta\phi \cos\delta\lambda \,, \\ y_F^{vii} &= (\rho + \delta\rho) \cos\delta\phi \sin\delta\lambda \,, \\ z_F^{vii} &= (\rho + \delta\rho) \sin\delta\phi \end{aligned} \tag{15}$$

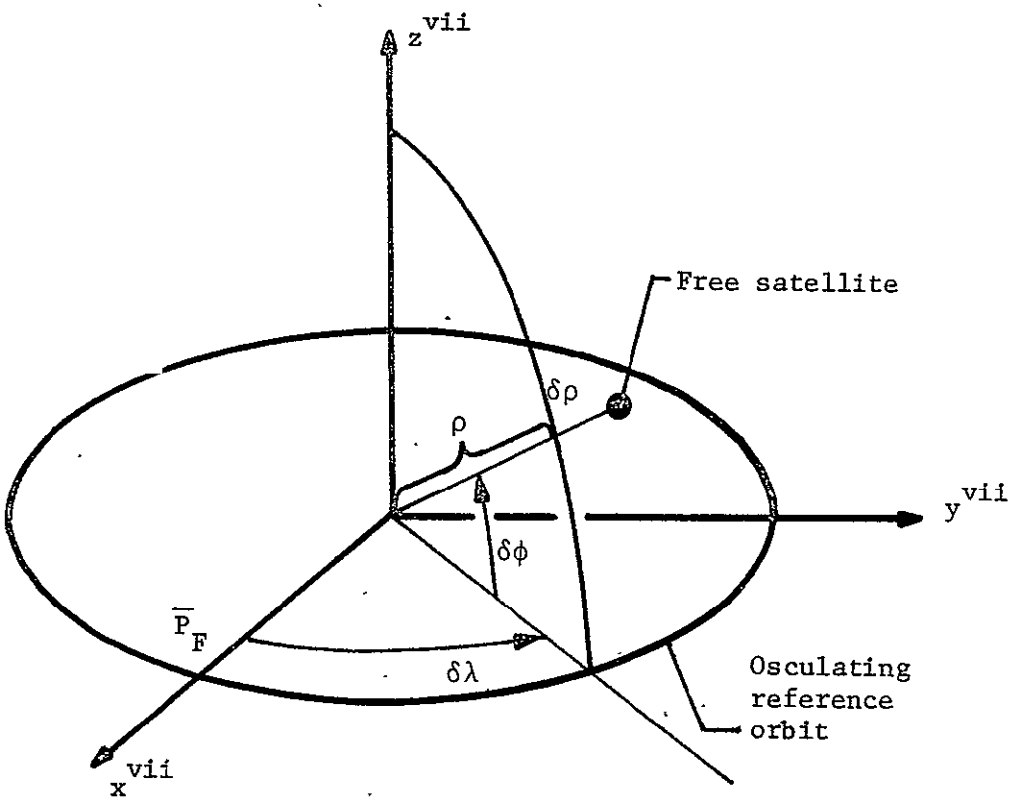

Fig. 9. Coordinates of the Free Satellite.

If $\vec{x}_F^{vii}$, $\vec{x}_F^{vi}$, $\cdots$, $\vec{x}_F^{i}$, $\vec{x}_F$ denote 3 x 1 component vectors in the respective coordinate systems, the rotations are expressed by

$$\vec{x}_F^{vi} = \begin{bmatrix} \cos\lambda & -\sin\lambda & 0 \\ \sin\lambda & \cos\lambda & 0 \\ 0 & 0 & 1 \end{bmatrix} \vec{x}_F^{vii} ,$$

$$\vec{x}_F^{v} = \begin{bmatrix} 1 & 0 & 0 \\ 0 & \cos\eta & -\sin\eta \\ 0 & \sin\eta & \cos\eta \end{bmatrix} \vec{x}_F^{vi} ,$$

$$\vec{x}_V^{iv} = \begin{bmatrix} \cos(\tilde{\Omega}-\Omega) & \sin(\tilde{\Omega}-\Omega) & 0 \\ -\sin(\tilde{\Omega}-\Omega) & \cos(\tilde{\Omega}-\Omega) & 0 \\ 0 & 0 & 1 \end{bmatrix} \vec{x}_F^{v} ,$$

$$\vec{x}_F^{iii} = \begin{bmatrix} 1 & 0 & 0 \\ 0 & \cos i & \sin i \\ 0 & -\sin i & \cos i \end{bmatrix} \vec{x}_F^{iv} ,$$

$$\vec{x}_F^{ii} = \begin{bmatrix} \cos(\lambda_E-\tilde{\Omega}+\Omega_E+\Theta+\Gamma) & \sin(\lambda_E-\tilde{\Omega}+\Omega_E+\Theta+\Gamma) & 0 \\ -\sin(\lambda_E+\tilde{\Omega}+\Omega_E+\Theta+\Gamma) & \cos(\lambda_E+\tilde{\Omega}+\Omega_E+\Theta+\Gamma) & 0 \\ 0 & 0 & 1 \end{bmatrix} \vec{x}_F^{iii} ,$$

$$\vec{x}_F^{i} \quad \begin{bmatrix} 1 & 0 & 0 \\ 0 & \cos\alpha & \sin\alpha \\ 0 & -\sin\alpha & \cos\alpha \end{bmatrix} \vec{x}_F^{ii} ,$$

and

$$\vec{x}_F \quad \begin{bmatrix} \cos\Gamma & -\sin\Gamma & 0 \\ \sin\Gamma & \cos\Gamma & 0 \\ 0 & 0 & 1 \end{bmatrix} \vec{x}_F^{i}$$

These rotations are combined to yield a functional relationship of the form

$$\vec{x}_F = \vec{x}_F(\alpha, \Gamma; \Omega, \eta, \lambda, \rho; \tilde{\Omega}, i; \lambda_E, \Theta; \delta\lambda, \delta\phi, \delta\rho). \qquad (16)$$

Sensitivity of Range to Geodetic Parameters

The kinematical relationships which have been developed are quite general and can, in fact, be applied to ground-based observations of a free satellite in an arbitrary orbit as well as to space-based observations. In order to see this, assume for a moment that the position of the proof satellite has been established in an Earth-fixed reference frame by means of monitoring the range residuals of Equation (12) and active thrusting. Such a satellite serves as a known reference point or "benchmark" in space and can be thought of as another tracking station.

In order to formulate these generalizations more precisely, let us identify the coordinates (x_p, y_p, z_p) of the benchmark satellite with the coordinates (X_n, Y_n, Z_n) of the n^{th} ground station and denote the coordinates of the satellite being observed by (x,y,z) in place of (x_F, y_F, z_F). Equations (10) and (14) are replaced by the single relationship

$$r_n^2 = (x - Y_n)^2 + (y - Y_n)^2 + (z - Z_n)^2 \quad , \tag{19}$$

where r_n is the range from a general observer with coordinates (X_n, Y_n, Z_n) to a satellite being observed. Nowhere in the range relationships and coordinate transformations has it been necessary to assume that the reference orbit of the satellite being observed is in fact circular. If ρ in Equation (16) is replaced by semimajor axis a, eccentricity e and longitude of perigee λ_p using

$$\rho = \frac{a(1 - e^2)}{1 + e \cos(\lambda - \lambda_p)} \tag{20}$$

then a general reference orbit with elements Ω, η, λ, a, e, and λ_p can be considered.

The functional dependence associated with Equation (19) is expressed by

$$r_n = r_n(X_n, Y_n, Z_n; \dot{x}, \dot{x}; \Omega, \eta, \lambda, a, e, \lambda_p; \Omega, i, H; \lambda_E; \delta\lambda, \delta\phi, \delta\rho) \quad . \tag{21}$$

The six elements of the reference orbit, together with the Earth's nominal angular position λ_E constitute reference numbers or definitions. The remaining arguments of expression (21) govern the variation of range r_n and range rate $\dot{r}_n$ with time. A least squares or minimum variance estimation procedure can be used to converge upon optimum values for these geodetic parameters.

The partial derivatives of r_n with respect to its various arguments provide insight regarding the degree to which range is influenced by the motion of the earth and by the orientation of the free satellite with respect to the tracking station at the time of observation. A system of rectangular coordinates with origin at the tracking station (ground station or benchmark satellite) has been introduced in order to aid interpretation of the sensitivity formulas which follow. The coordinates ℓ_{E_n}, ℓ_{N_n}, and ℓ_{R_n} refer to distance of the satellite from the n^{th} observer in the eastward, northward, and radial directions respectively as shown in Figure 10.

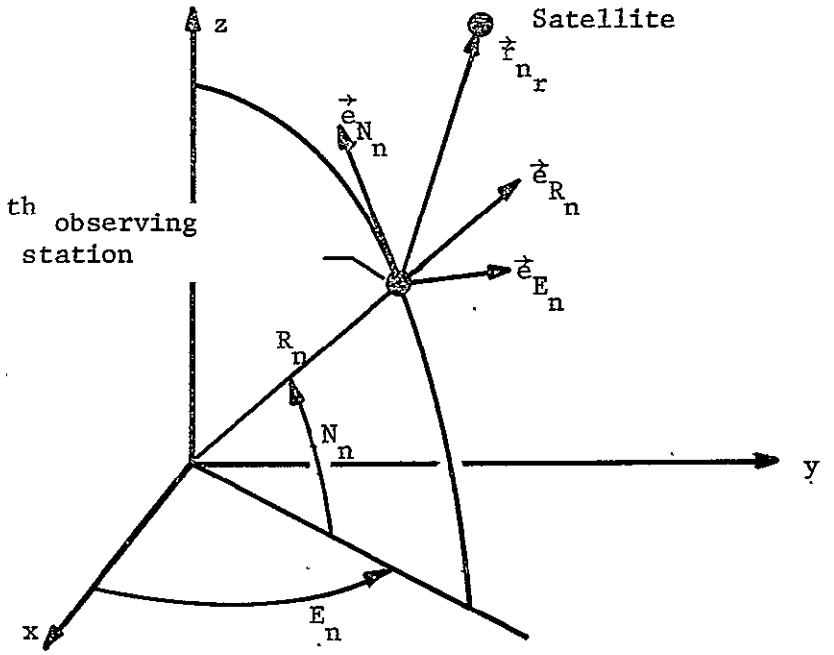

Fig. 10. Rectangular Station-Centered Coordinates.

The following sensitivity relationships are based upon the consecutive coordinate transformations preceding Equation 16 together with Equation 19:

Sensitivity of Range to Polar Motion

$$\frac{\partial r_n}{\partial x_1} = \frac{R_n}{r_n} \sum_{k=o}^{\infty} (k+1)\,(x_1^2 + x_2^2)^{\frac{k}{2}} \; x_2 \ell_{E_n} \cos N_n$$

$$- x_1^2\,(\ell_{E_n} \sin N_n \sin E_n + \ell_{N_n} \cos E_n)$$

$$- x_1 x_2 (-\ell_{E_n} \sin N_n \cos E_n + \ell_{N_n} \sin E_n)$$

$$-(\ell_{E_n} \sin N_n \sin E_n + \ell_{N_n} \cos E_n) \qquad (22)$$

$$\frac{\partial r_n}{\partial x_2} = \frac{\dot{R}_n}{r_n} \sum_{k=o}^{\infty} (k+1) \left(x_1^2 + x_2^2\right)^{\frac{1}{2}} - x_1 \ell_{E_n} \cos N_n$$

$$+ x_2^2 (\ell_{E_n} \sin N_n \cos E_n - \ell_{N_n} \sin E_n)$$

$$+ (\ell_{E_n} \sin N_n \cos E_n - \ell_{N_n} \sin E_n) \tag{23}$$

Sensitivity of Range to Coordinates of the Observer

$$\frac{\partial r_n}{\partial E_n} = - \frac{R_n}{r_n} \ell_{E_n} \cos N_n \tag{24}$$

$$\frac{\partial r_n}{\partial N_n} = - \frac{R_n}{r_n} \ell_{N_n} \tag{25}$$

$$\frac{\partial r_n}{\partial R_n} = - \frac{\ell_{r_n}}{r_n} \tag{26}$$

Sensitivity of Range to Earth Rotation Rate Correction

$$\frac{\partial r_n}{\partial H} = \frac{R_n}{r_n} \ell_{E_n} \sin N_n (x_1 \cos E_n + x_2 \sin E_n)$$

$$- x_3 \ell_{E_n} \cos N_n + \ell_{N_n} (-x_1 \sin E_n + x_2 \cos E_n) \tag{27}$$

Sensitivity of Range to Earth Precession

$$\frac{\partial r_n}{\partial \tilde{\Omega}} = \frac{R_n}{r_n} \ell_{E_n} \cos N_n \, x_3 \, (1 - \cos i)$$

$$+ \ell_{N_n} \cos E_n \, x_3 \cos \Gamma \sin i \cos \psi$$

$$+ \ell_{E_n} [\cos N_n (x_1^2 + x_2^2)^{\frac{1}{2}} \sin i \cos \psi$$

$$- s \, N_n (1 - \cos i) (x_2 \sin E_n + x_1 \cos E_n)]$$

$$- \ell_{N_n} (1 - \cos i) (x_1 \sin E_n - x_2 \cos E_n)$$

$$+ \sum_{k=1}^{\infty} \binom{\frac{1}{2}}{k} (x_1^2 + x_2^2)^k \sin i \cos \psi [\ell_{N_n} \cos (E_n - \Gamma)$$

$$+ \ell_{E_n} \sin N_n \sin (E_n - \Gamma)]$$

$$+ \sin i \, [\sin N_n \sin (\lambda_E + \Omega_E + H - \tilde{\Omega} + E_n)$$

$$+ \cos (\lambda_E + \Omega_E + H - \tilde{\Omega} + E_n)] \qquad (28)$$

Sensitivity of Range to Earth Nutation

$$\frac{\partial r_n}{\partial i} = \frac{R_n}{r_n} - \ell_{E_n} \cos (x_1^2 + x_2^2)^{\frac{1}{2}} \sin \psi$$

$$- \left(\sum_{k=1}^{\infty} \binom{\frac{1}{2}}{k} (x_1^2 + x_2^2)^k \sin \psi [\ell_{E_n} \sin N_n \sin (E_n - \Gamma) \right.$$

$$\left. + \ell_{N_n} \cos (E_n - \Gamma)] \right.$$

$$+ \ell_{E_n} \sin N_n \cos (\lambda_E + \Omega_E + H - \tilde{\Omega} + E_n)$$

$$+ \ell_{N_n} \sin (\lambda_E + \Omega_E + H - \tilde{\Omega} + E_n) \qquad (29)$$

ψ in the above equations is defined by

$$\psi = \dot{\lambda}_E + \Omega_E + H + \Gamma - \tilde{\Omega} \quad . \tag{30}$$

The sensitivity relationships can be used as a basis for determining optimum relative orientations of the free satellite with respect to an observer. Such considerations should lead in turn to the design of an optimal orbit orientation for the purpose of determining selected geodetic parameters.

In order to illustrate typical orders of magnitude which might occur in an application of the sensitivity relationships, two particular numerical examples are presented below. Case 1 involves a ground station with coordinates

$$E_1 = -80^\circ$$

$$N_1 = 34^\circ$$

$$R_1 = 6380 \text{ KM}$$

and Case 2 involves the benchmark satellite with coordinates

$$E_2 = -115^\circ$$

$$N_2 = 0^\circ$$

$$R_2 = 42{,}100 \text{ KM}$$

The satellite and station coordinates selected for Case 1 correspond roughly to a pass of Geos -A over Rosman, N.C. The east longitude of -115° for the benchmark satellite corresponds to a stable equilibrium point over the Pacific. A spin axis inclination of 10^{-4} radians is used in the calculations. Range is normalized to r_n/R_E, where $R_E = 6371$ KM.

The satellite being tracked from the ground station of Case 1 is observed at an elevation angle of 40° above the horizon. All of the sensitivity expressions except $\partial r_n/\partial R_n$ approach zero as the elevation angle approaches 90°, and below 40° atmospheric effects on the quality of range data become severe. Therefore, values listed for the sensitivities correspond to the largest that can be obtained in practice. The results of the example computations are presented as Figures 11 through 26 following the discussion.

Discussion

The maximum sensitivity of range to polar motion is an order of magnitude greater for the benchmark satellite (Fig. 25 and 26) than for the ground based observations (Fig. 23 and 24). This is due to the "lever arm" effect resulting from an increased geocentric radius R_n and from the fact that an elevation angle of 0° is permissible for the benchmark satellite. The same remarks hold true regarding sensitivity to precession and nutation of the Earth's spin axis.

In a sense, the benchmark satellite concept represents the ideal situation for a tracking station. Observations would be made in a vacuum and a much larger portion of the trajectory of a particular satellite would be visible. With regard to the polar motion determination, it is expected that intersatellite range measurements, together with the ground-to-satellite range information, will permit the determination of satellite positions to within about one centimeter. One centimeter at synchronous altitude corresponds to an angular uncertainty of 4.75×10^{-5} arc seconds or within 0''.0001.

The potential of ground based observations for precise determination of geodetic parameters is also clearly indicated by the results which have been obtained. For example, $\partial(r_1/R_E)/\partial x_2$ reaches approximately 0.8 for an aximuth of 80° (Fig. 24), so that a shift in the pole in the x_2 direction by, say 5 meters, produces a corresponding change of 4 meters in range.

LIST OF ILLUSTRATIONS FOR EXAMPLE COMPUTATIONS

E	=	-.80000000E+02	EAST LONGITUDE OF OBSERVER (DEGREES)
N	=	.34000000E+02	NORTH LATITUDE OF OBSERVER (DEGREES)
R	=	.63800000E+04	RADIUS OF OBSERVER (KILOMETERS)
LE	=	.15890000E+04	EAST COORD. OF SATELLITE RELATIVE TO OBSERVER (KILOMETERS)
LN	=	0.	NORTH COORD. OF SATELLITE RELATIVE TO OBSERVER (KILOMETERS)
LR	=	.13320000E+04	RADIAL COORD. OF SATELLITE RELATIVE TO OBSERVER (KILOMETERS)
X1	=	.10000000E-05	POLAR MOTION TOWARD GREENWICH (DIRECTION COSINE)
X2	=	.10000000E-05	POLAR MOTION COORDINATE TOWARD 90 DEGREES EAST (DIRECTION COSINE)
X3	=	.10000000E+01	COSINE OF ANGLE BETWEEN SPIN AXIS AND POLE OF EPOCH
INCLIN	=	.10000000E-05	SPIN AXIS INCLINATION (RADIANS)
AZ	=	0.00	AZIMUTH OF SATELLITE (DEGREES FROM DUE EAST)

POLAR MOTION

D (RN/RE) / D X1 = .42262836E+00
D (RN/RE) / D X2 = .74521245E-01

COORDINATES OF OBSERVER

D (RN/RE) / D (CAP R /RE) = -.94241131E+00
D (RN/RE) / D EN = -.03623862E+00
D (RN/RE) / D NN = -0.

EARTH ROTATION RATE CORRECTION

D (RN/RE) / D (CAP THETA) = -.03629917E+00

PRECESSION AND NUTATION OF THE EARTH

PSI (DEGREES)	D (RN/RE) / D (PRECESSION)	D (RN/RE) / D (NUTATION)
0.00	.52726542E-05	.35153786E+00
10.00	.11296989E-04	.38894043E+00
20.00	.16978167E-04	.41452525E+00
30.00	.22143569E-04	.42751494E+00
40.00	.26636247E-04	.42751480E+00
50.00	.30319693E-04	.41452485E+00
60.00	.33081987E-04	.38893977E+00
70.00	.34839199E-04	.35153696E+00
80.00	.35537936E-04	.30345287E+00
90.00	.35156908E-04	.24614853E+00
100.00	.33707870E-04	.18136509E+00
110.00	.31234673E-04	.11107097E+00
120.00	.27812523E-04	.37402013E-01
130.00	.23545400E-04	-.37403385E-01
140.00	.18562959E-04	-.11107230E+00
150.00	.13016569E-04	-.18136634E+00
160.00	.70748132E-05	-.24614966E+00
170.00	.91816940E-06	-.30345385E+00
180.00	-.52662758E-05	-.35153775E+00
190.00	-.11290611E-04	-.38894035E+00
200.00	-.16971791E-04	-.41452520E+00
210.00	-.22137194E-04	-.42751492E+00
220.00	-.26626874E-04	-.42751482E+00
230.00	-.30313322E-04	-.41452490E+00
240.00	-.33075619E-04	-.38893985E+00
250.00	-.34832833E-04	-.35153707E+00
260.00	-.35531573E-04	-.30345301E+00
270.00	-.35150608E-04	-.24614869E+00
280.00	-.33701513E-04	-.18136527E+00
290.00	-.31228318E-04	-.11107116E+00
300.00	-.27806170E-04	-.37402207E-01
310.00	-.23539050E-04	.37403191E-01
320.00	-.18556611E-04	.11107211E+00
330.00	-.13010242E-04	.18136617E+00
340.00	-.70684606E-05	.24614950E+00
350.00	-.91182313E-06	.30345371E+00
360.00	.52726223E-05	.35153763E+00

SENSITIVITY OF RANGE TO PRECESSION

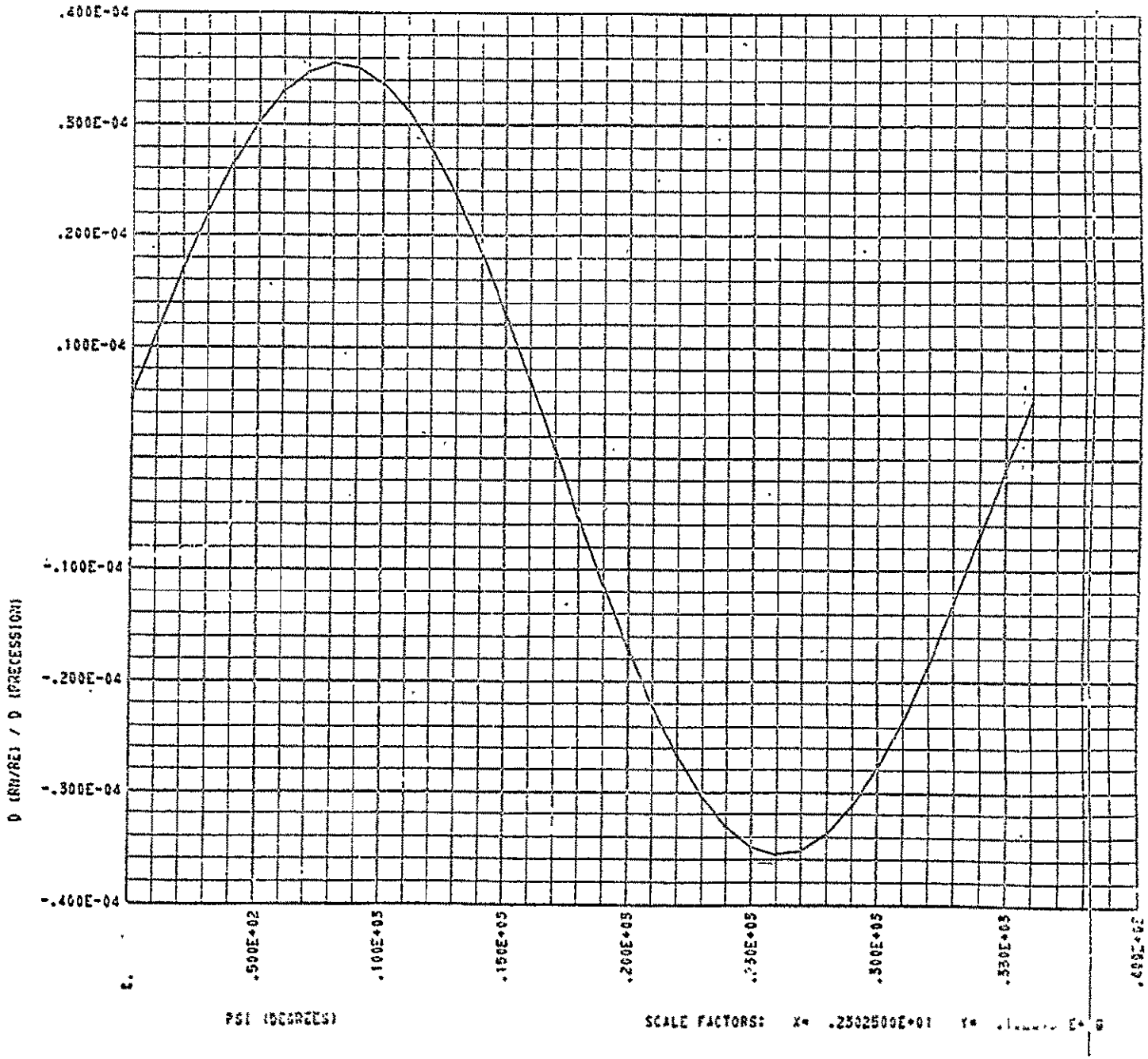

SENSITIVITY OF RANGE TO NUTATION

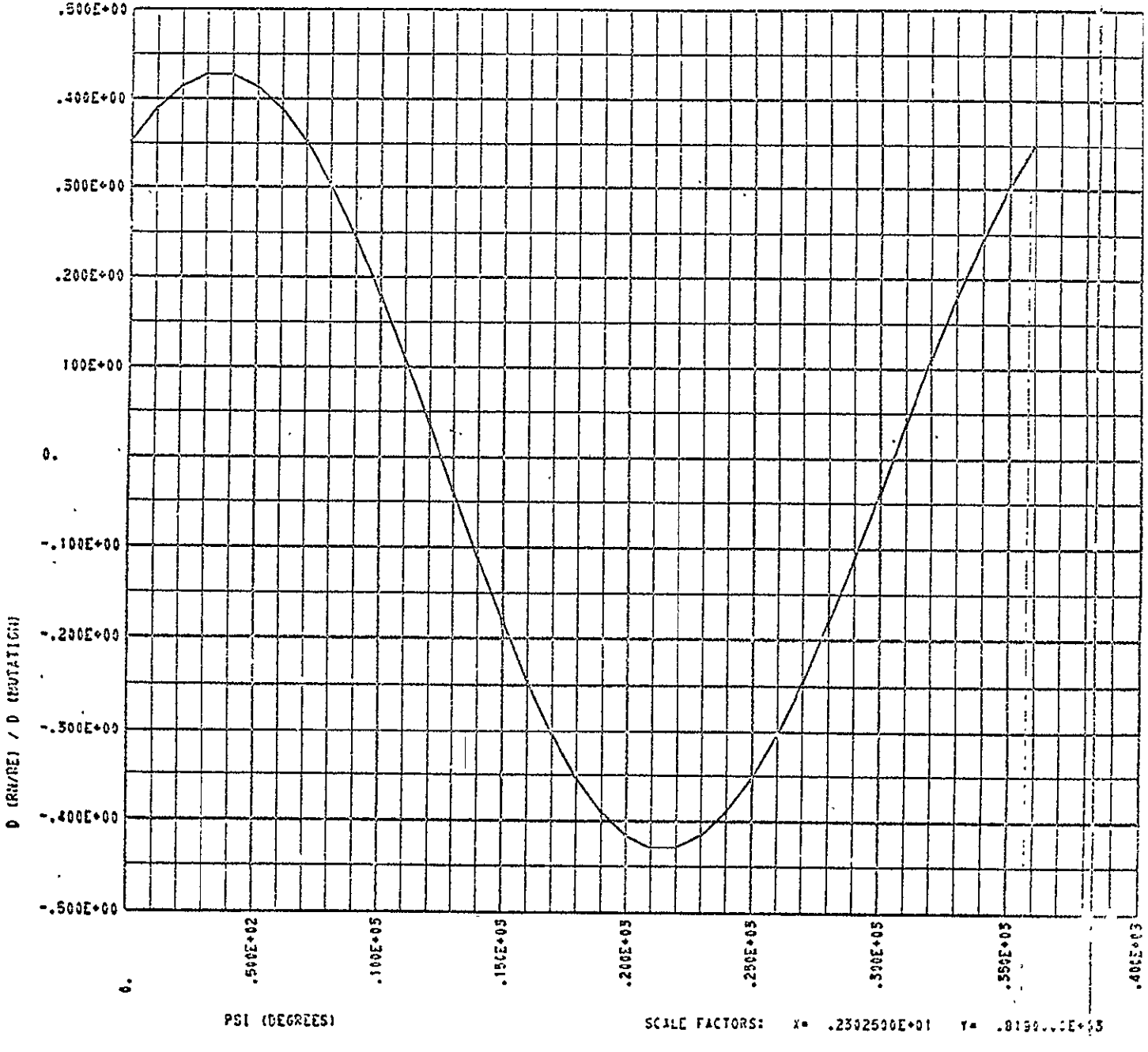

E	=	-.80000000E+02	EAST LONGITUDE OF OBSERVER (DEGREES)
N	=	.34000000E+02	NORTH LATITUDE OF OBSERVER (DEGREES)
R	=	.63800000E+04	RADIUS OFOBSERVER (KILOMETERS)
LE	=	.36037710E+03	EAST COORD. OF SATELLITE RELATIVE TO OBSERVER (KILOMETERS)
LN	=	.15890000E+04	NORTH COORD. OF SATELLITE RELATIVE TO OBSERVER (KILOMETERS)
LR	=	.13320000E+04	RADIAL COORD. OF SATELLITE RELATIVE TO OBSERVER (KILOMETERS)
1	=	.10000000E-05	POLAR MOTION TOWARD GREENWICH (DIRECTION COSINE)
2	=	.10000000E-05	POLAR MOTION COORDINATE TOWARD 90 DEGREES EAST (DIRECTION COSINE)
3	=	.10000000E+01	COSINE OF ANGLE BETWEEN SPIN AXIS AND POLE OF EPOCH
NCLIN	=	.10000000E-03	SPIN AXIS INCLINATION (RADIANS)
Z	=	90.00	AZIMUTH OF SATELLITE (DEGREES FROM DUE EAST)

POLAR MOTION

D (RN/RE) / D x1 = -.13326507E+00
D (RN/RE) / D x2 = .75578345E+00

COORDINATES OF OBSERVER

D (RN/RE) / D (CAP R /RE) = -.64241131E+00
D (RN/RE) / D FN = -.14420572E-06
D (RN/RE) / D NN = -.76744204E+00

EARTH ROTATION RATE CORRECTION

D (RN/RE) / D (CAP THETA) = .74752800E-06

RECESSION AND NUTATION OF THE EARTH

PSI (DEGREES)	D (RN/RE) / D (PRECESSION)	D (RN/RE) / D (NUTATION)
0.00	.53441973E-04	.44018697E+00
10.00	.50273835E-04	.32433524E+00
20.00	.45274308E-04	.19862875E+00
30.00	.38291454E-04	.66887034E-01
40.00	.30233600E-04	-.66887013E-01
50.00	.22072118E-04	-.19862873E+00
60.00	.14642300E-04	-.32433522E+00
70.00	.59642282E-04	-.44018695E+00
80.00	.52630064E-04	-.54266382E+00
90.00	.44018709E-04	-.62865214E+00
100.00	.34066808E-04	-.69553918E+00
110.00	.23085831E-04	-.74129262E+00
120.00	.11400343E-04	-.76452227E+00
130.00	-.63153782E-06	-.76452230E+00
140.00	-.12644230E-04	-.74129272E+00
150.00	-.24272734E-04	-.69553934E+00
160.00	-.35163723E-04	-.62865235E+00
170.00	-.44986201E-04	-.54266409E+00
180.00	-.53441954E-04	-.44018725E+00
190.00	-.60273640E-04	-.32433555E+00
200.00	-.65274297E-04	-.19862909E+00
210.00	-.68291449E-04	-.66887381E-01
220.00	-.69233600E-04	.66886666E-01
230.00	-.68072124E-04	.19862840E+00
240.00	-.64842311E-04	.32433491E+00
250.00	-.59642298E-04	.44018666E+00
260.00	-.52630064E-04	.54266358E+00
270.00	-.44018733E-04	.62865194E+00
280.00	-.34066895E-04	.69553903E+00
290.00	-.23085801E-04	.74129253E+00
300.00	-.11400374E-04	.76452224E+00
310.00	.63150641E-06	.76452233E+00
320.00	.12644199E-04	.74129281E+00
330.00	.24272704E-04	.69553948E+00
340.00	.35163769E-04	.62865255E+00
350.00	.44986257E-04	.54266433E+00
360.00	.53441934E-04	.44018754E+00

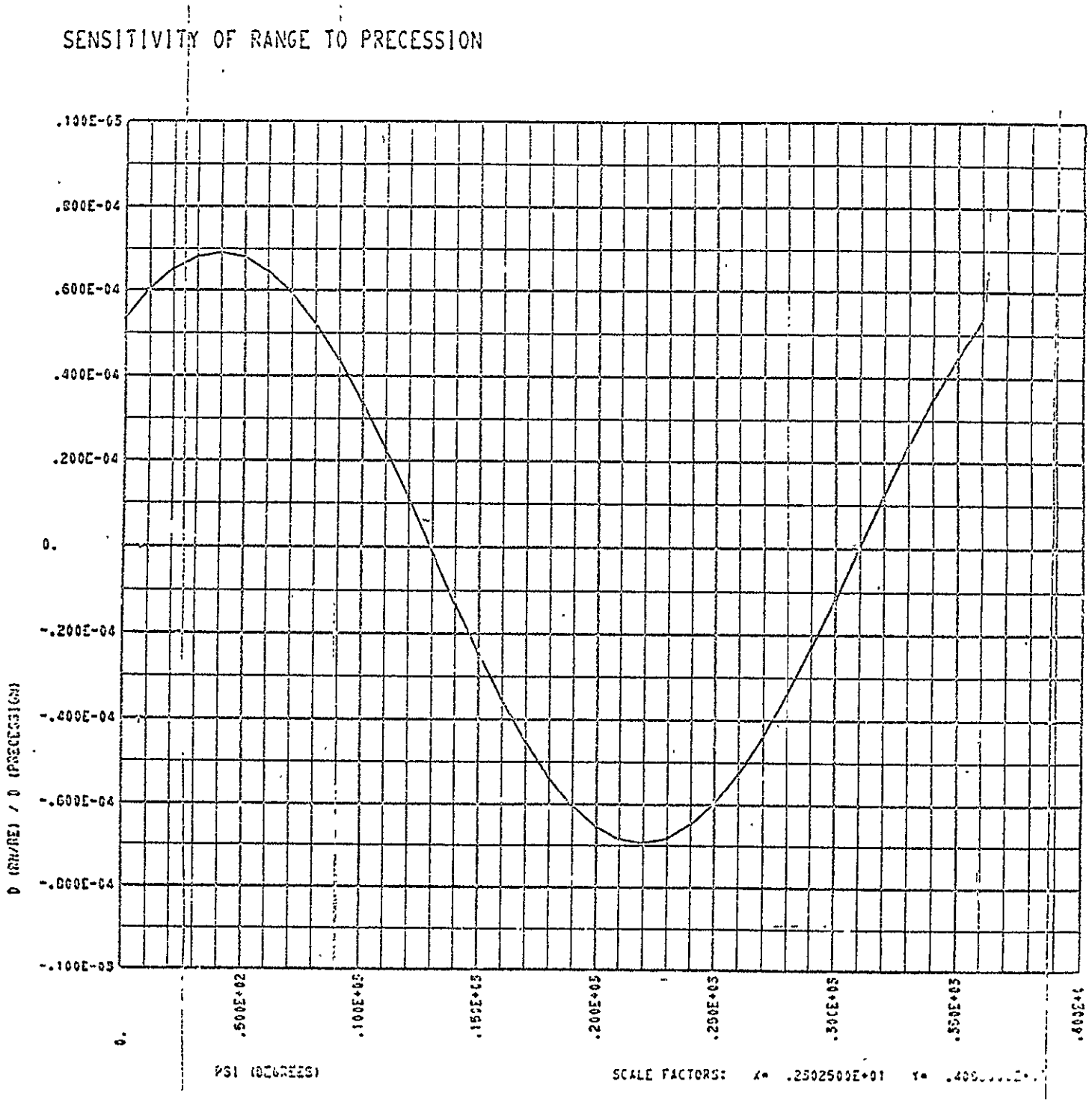
SENSITIVITY OF RANGE TO PRECESSION
.100E-03
.800E-04
.600E-04
.400E-04
.200E-04
0.
-.200E-04
-.400E-04
-.600E-04
-.800E-04
-.100E-03
0.
.500E+02
.100E+03
.150E+03
.200E+03
.250E+03
.300E+03
.350E+03
.400E+03
PSI (DEGREES)
SCALE FACTORS: X= .2502500E+01 Y= .400

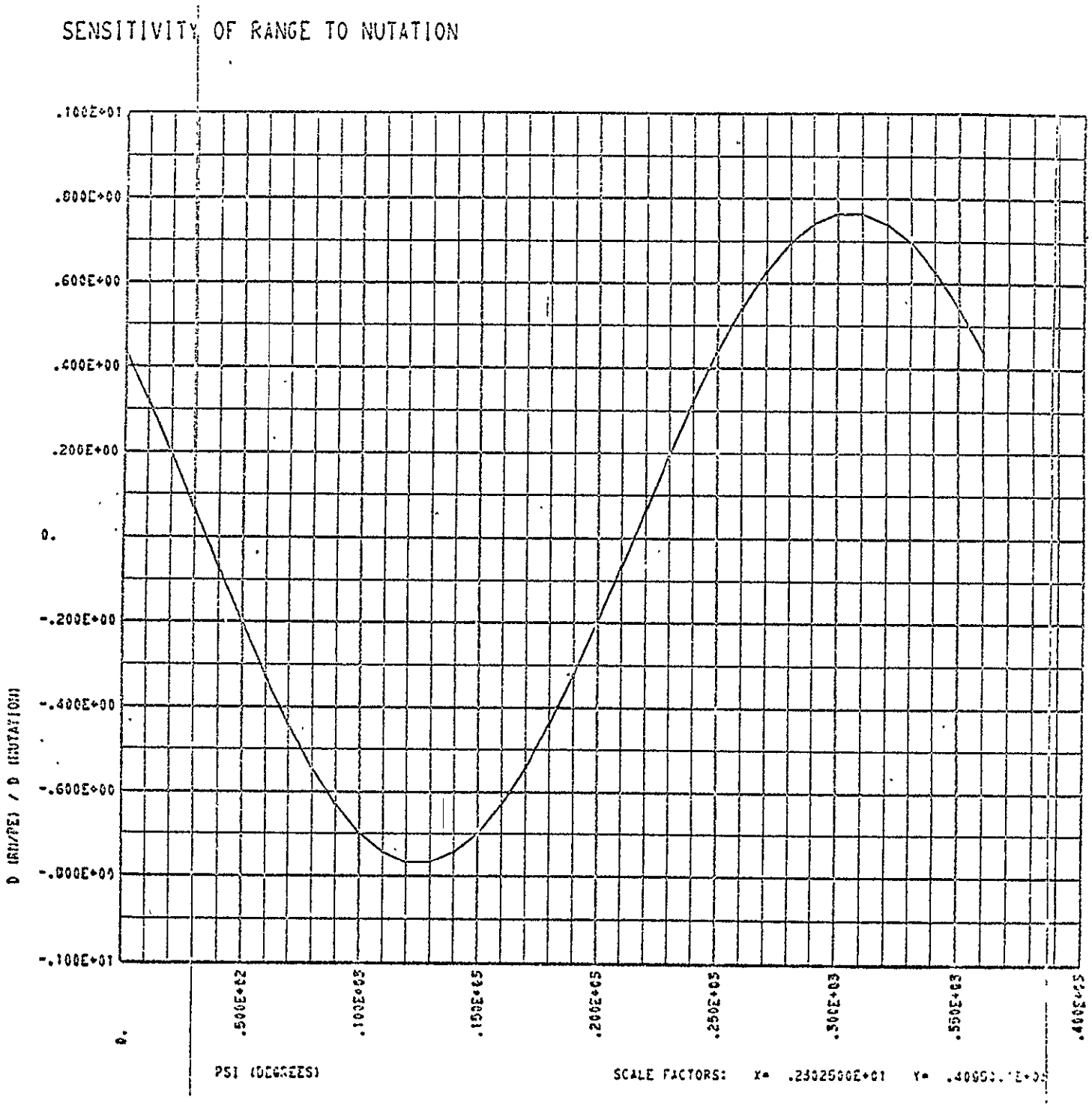
SENSITIVITY OF RANGE TO NUTATION
.100E+01
.800E+00
.600E+00
.400E+00
.200E+00
0.
-.200E+00
-.400E+00
-.600E+00
-.800E+00
-.100E+01
D (RANGE) / D (NUTATION)
0.
.500E+02
.100E+03
.150E+03
.200E+03
.250E+03
.300E+03
.350E+03
.400E+03
PSI (DEGREES)
SCALE FACTORS: X= .2502500E+01 Y= .4000

E	=	-.11500000E+03	EAST LONGITUDE OF OBSERVER (DEGREES)
N	=	0.	NORTH LATITUDE OF OBSERVER (DEGREES)
R	=	.42100000E+05	RADIUS OFOBSERVER (KILOMETERS)
LE	=	.22679490E-04	EAST COORD. OF SATELLITE RELATIVE TO OBSERVER (KILOMETERS)
LN	=	.10000000E+03	NORTH COORD. OF SATELLITE RELATIVE TO OBSERVER (KILOMETERS)
LR	=	0.	RADIAL COORD. OF SATELLITE RELATIVE TO OBSERVER (KILOMETERS)
X1	=	.10000000E-05	POLAR MOTION TOWARD GREENWICH (DIRECTION COSINE)
X2	=	.10000000E-05	POLAR MOTION COORDINATE TOWARD 90 DEGREES EAST (DIRECTION COSINE)
X3	=	.10000000E+01	COSINE OF ANGLE BETWEEN SPIN AXIS AND POLE OF EPOCH
INCLIN	=	.10000000E-03	SPIN AXIS INCLINATION (RADIANS)
AZ	=	90.00	AZIMUTH OF SATELLITE (DEGREES FROM DUE EAST)

POLAR MOTION

D (RN/RE) / D X1 = .27926884E+01
D (RN/RE) / D X2 = .59889441E+01

COORDINATES OF OBSERVER

D (RN/RE) / D (CAP R /RE) = -0.
D (RN/RE) / D EN = -.14986701E-05
D (RN/RE) / D NN = -.00080078E+01

EARTH ROTATION RATE CORRECTION

D (RN/RE) / D (CAP THETA) = .15976796E-05

PRECESSION AND NUTATION OF THE EARTH

PSI (DEGREES)	D (RN/RE) / ∩ (PRECESSION)	D (RN/RE) / D (NUTATION)
0.00	.42348202E-03	.62095519E+01
10.00	.32487610E-03	.57227537E+01
20.00	.21032209E-03	.50620726E+01
30.00	.09722376E-03	.42475830E+01
40.00	.01235483E-03	.33040328E+01
50.00	-.07478826E-03	.22600913E+01
60.00	-.14950399E-03	.11474780E+01
70.00	-.20834642E-03	-.74933787E-06
80.00	-.24850843E-03	-.11474795E+01
90.00	-.26095529E-03	-.22600927E+01
100.00	-.25798474E-03	-.33040341E+01
110.00	-.24866780E-03	-.42475842E+01
120.00	-.23602216E-03	-.50620736E+01
130.00	-.22347051E-03	-.57227545E+01
140.00	-.21473517E-03	-.62095524E+01
150.00	-.21026831E-03	-.65076763E+01
160.00	-.21855345E-03	-.66080678E+01
170.00	-.23092035E-03	-.65076766E+01
180.00	-.24234817E-03	-.62095529E+01
190.00	-.25248754E-03	-.57227552E+01
200.00	-.26103218E-03	-.50620745E+01
210.00	-.26772381E-03	-.42475853E+01
220.00	-.27235482E-03	-.33040354E+01
230.00	-.27478982E-03	-.22600941E+01
240.00	-.27495401E-03	-.11474810E+01
250.00	-.27283465E-03	-.22480143E-05
260.00	-.26850585E-03	.11474766E+01
270.00	-.26209554E-03	.22600899E+01
280.00	-.25379849E-03	.33040315E+01
290.00	-.24386807E-03	.42475819E+01
300.00	-.23260247E-03	.50620716E+01
310.00	-.22034708E-03	.57227530E+01
320.00	-.20736857E-03	.62095514E+01
330.00	-.19392797E-03	.65076758E+01
340.00	-.18055431E-03	.66080 7[illegible]+01
350.00	-.16922004E-03	.65076771E+01
360.00	-.16234914E-03	.62095540E+01

SENSITIVITY OF RANGE TO PRECESSION

SENSITIVITY OF RANGE TO MUTATION

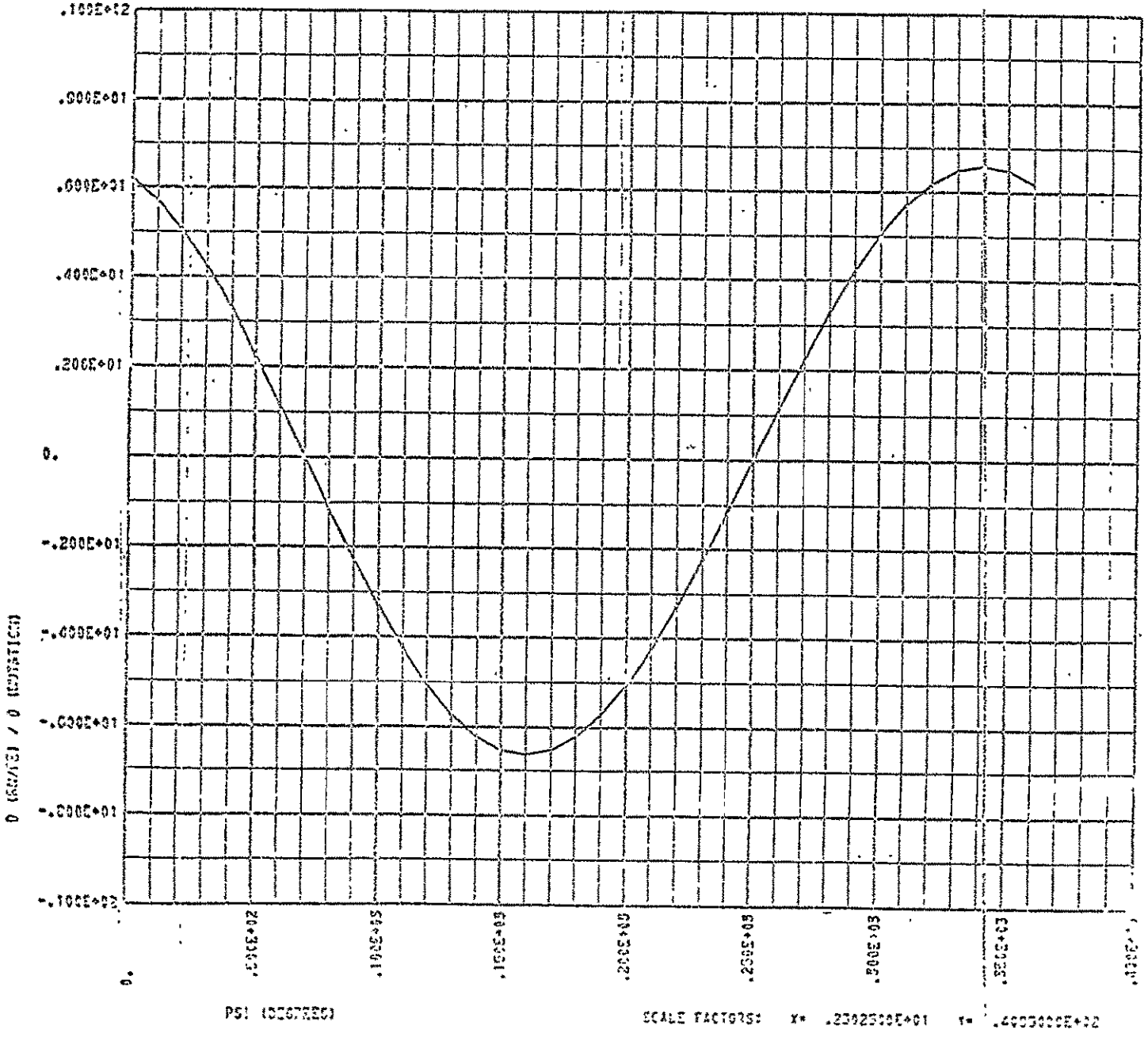

SENSITIVITY OF RANGE TO X1 VS. AZIMUTH

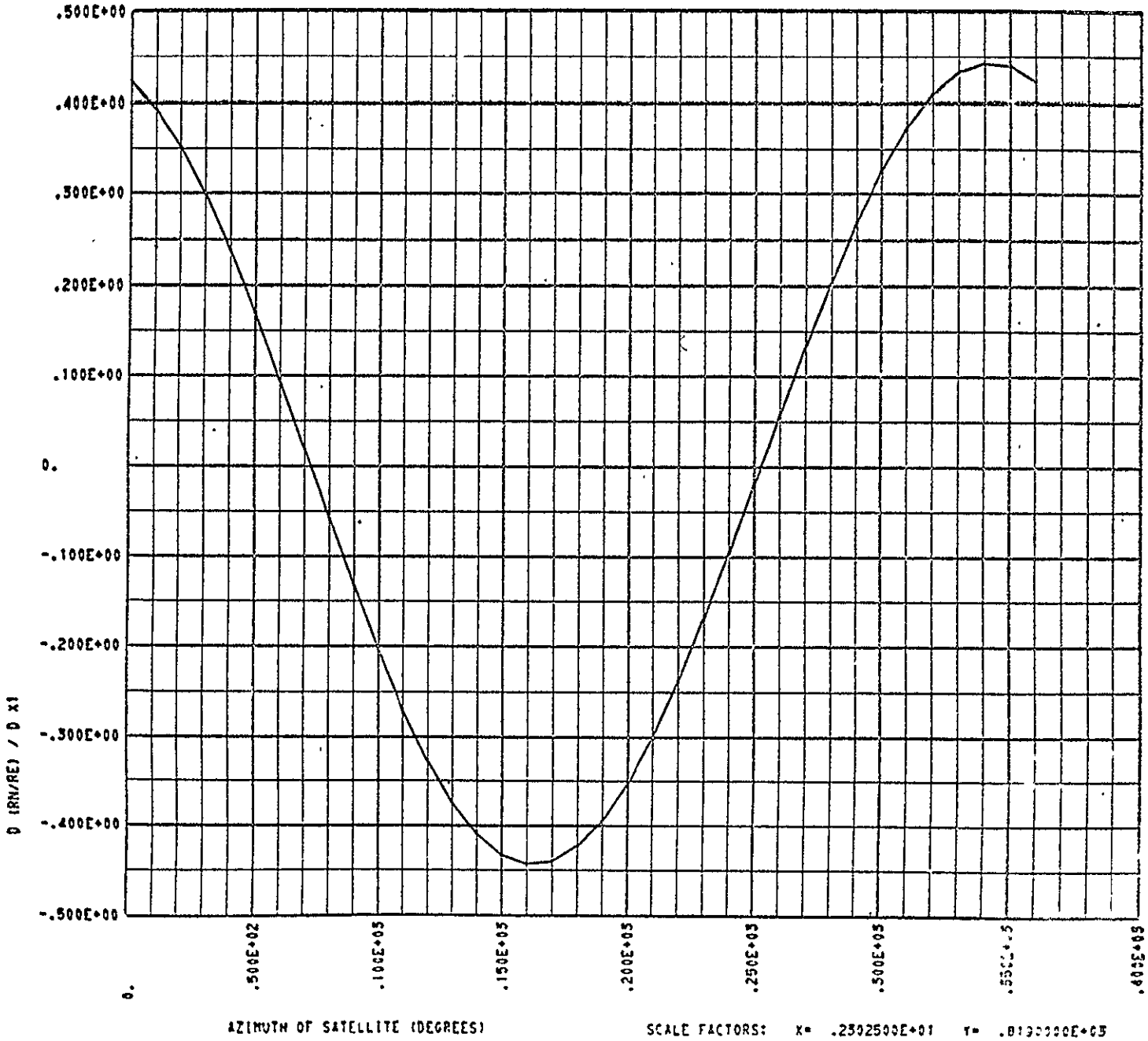

SENSITIVITY OF RANGE TO X2 VS. AZIMUTH

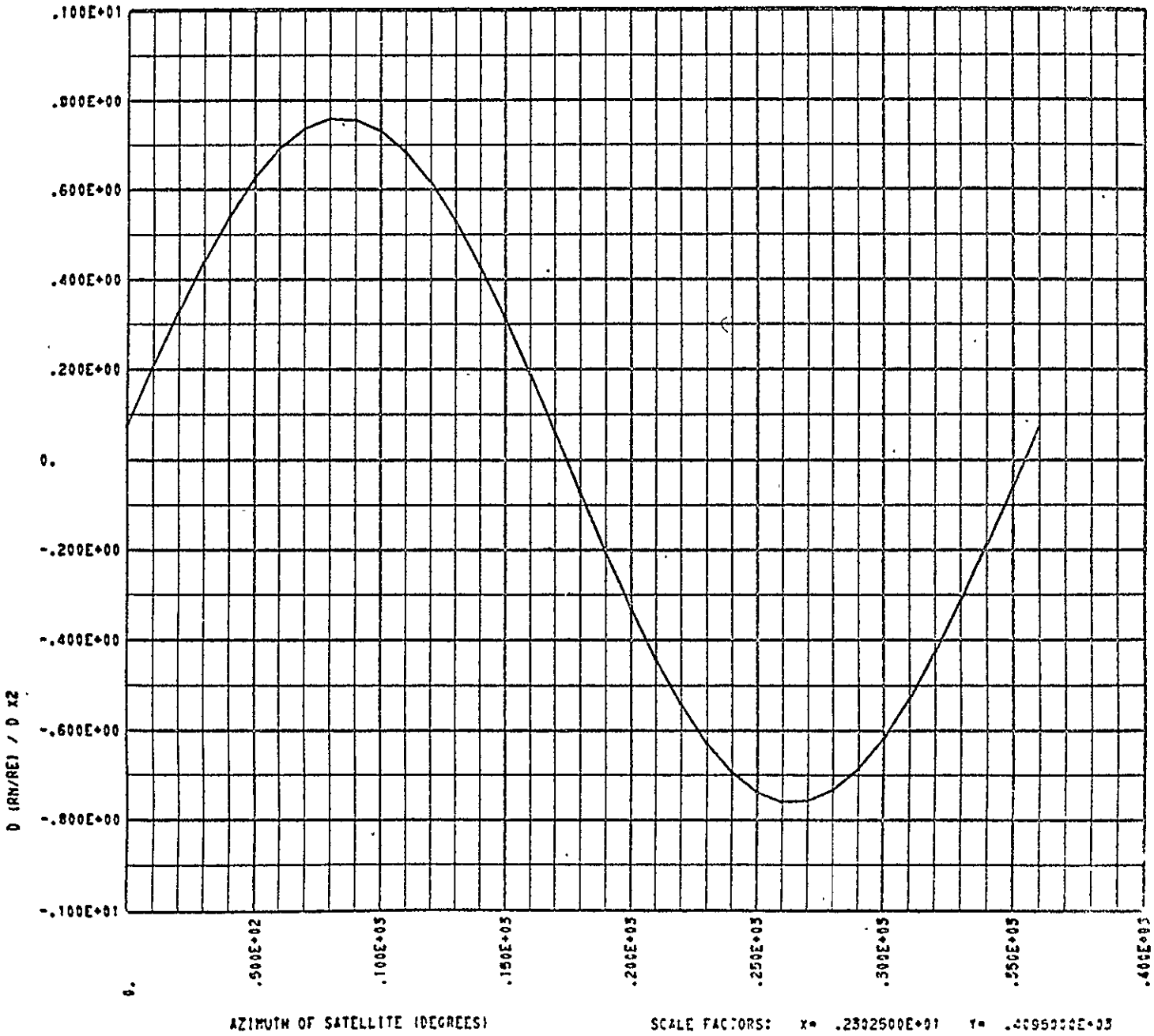

SENSITIVITY OF RANGE TO X1 VS. AZIMUTH

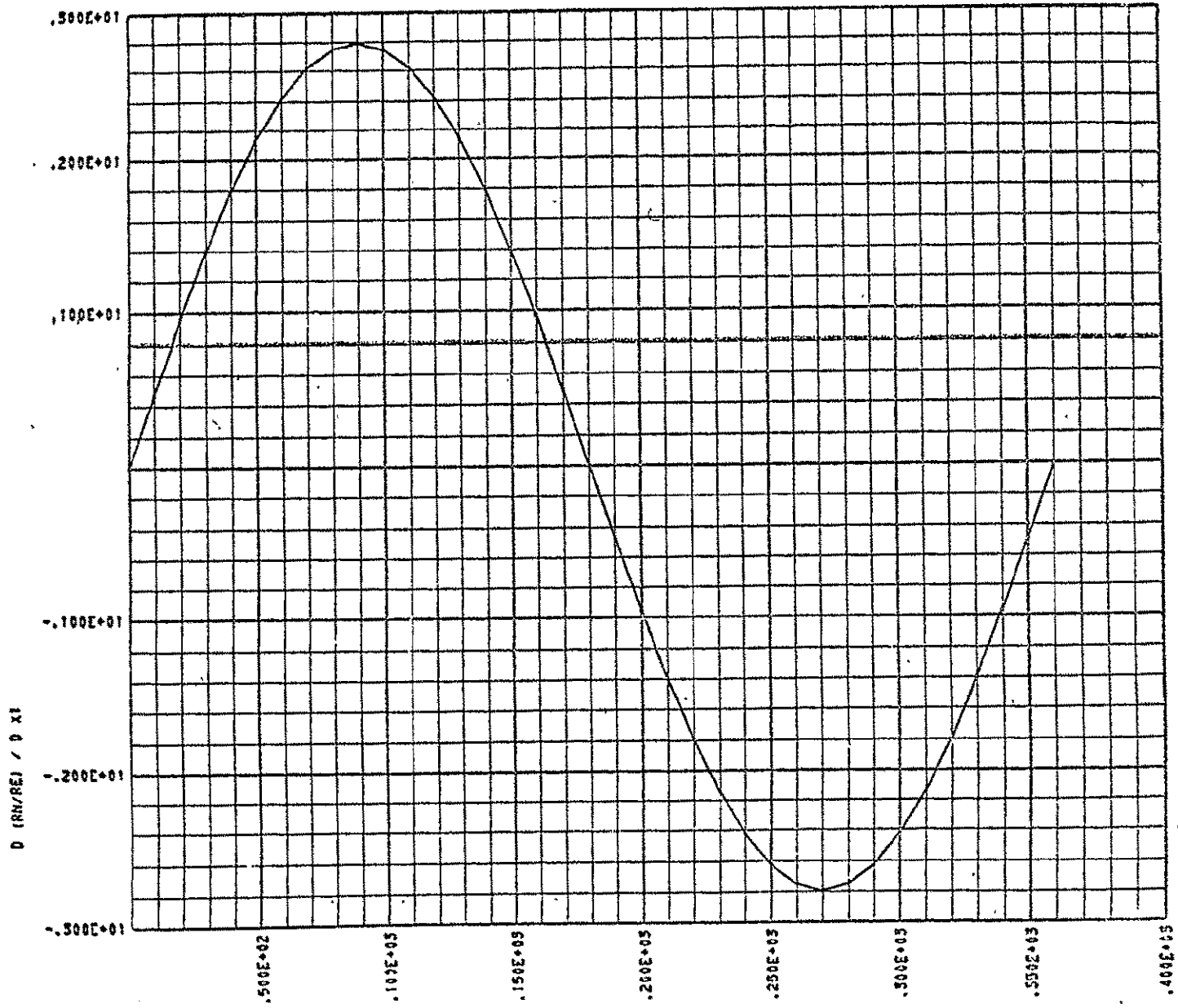

SENSITIVITY OF RANGE TO X2 VS. AZIMUTH

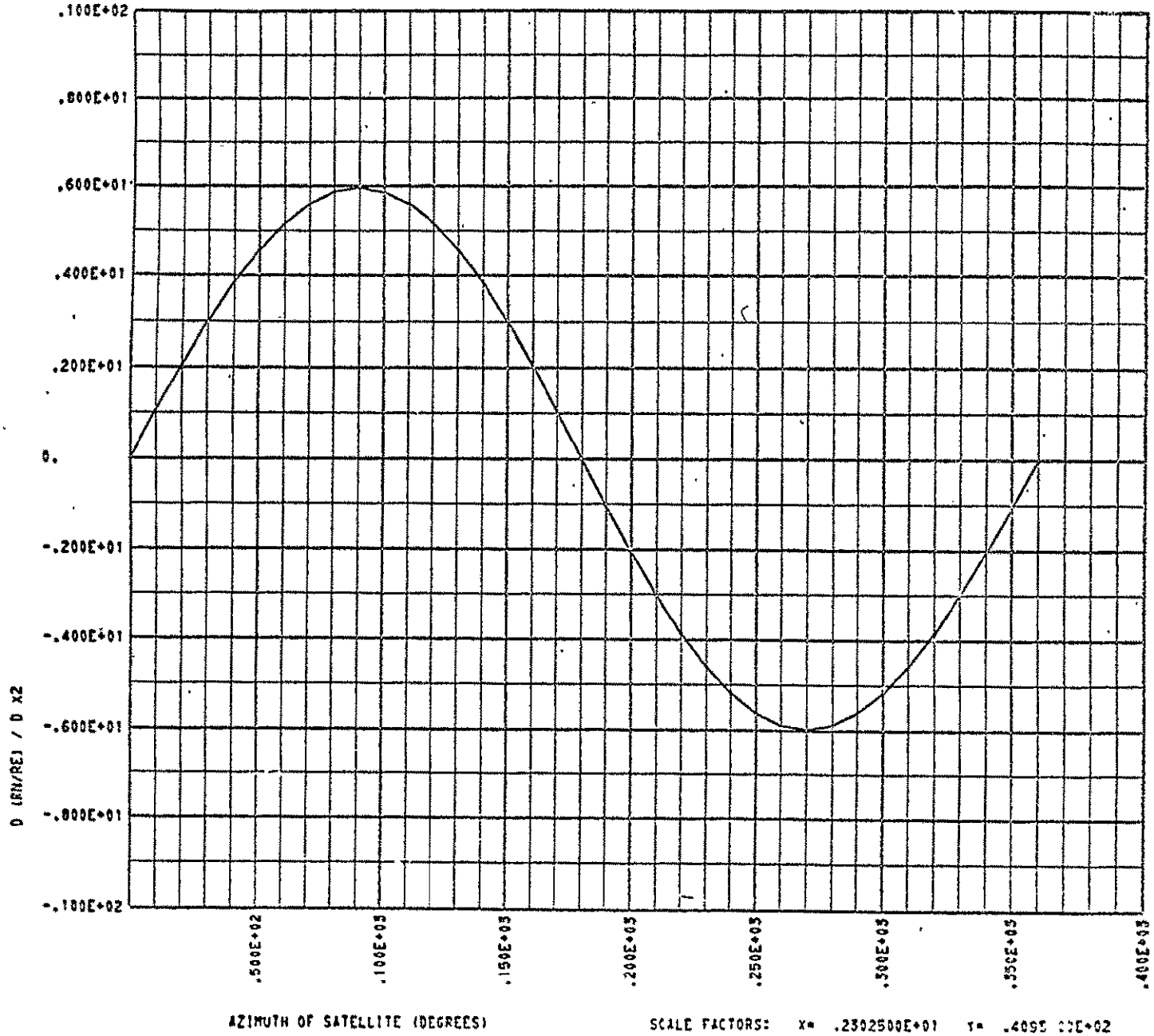

DETERMINATION OF CONTINENTAL DRIFT BY LASER RANGING TO SATELLITES*

C. Byron Winn

Associate Professor of Mechanical Engineering
Colorado State University
Fort Collins, Colorado

ABSTRACT

A geometrical technique for determining continental drift from laser range measurements is investigated. The method involves an arbitrary number of ground stations with at least four of the stations making nearly simultaneous range measurements to a satellite. The results are shown to be essentially independent of the satellite orbit for satellite altitudes beyond one earth radius. The standard deviations in interstation distances are calculated and are found to be approximately 0.5 meters.

---

*This work was supported in part under NASA Research Grant NGR 06-002-085. This financial support is gratefully acknowledged.

INTRODUCTION

A subject of great controversy for nearly three hundred years was the flattening of the earth. It was observed by French explorers in 1672 that their pendulum clocks ran more slowly near the equator than in Paris and this led to a postulated flattening of the earth and many subsequent studies to determine the degree of flattening. Many studies were geometric in nature and involved astronomical measurement techniques, many were dynamical and made use of observations of the moon, some involved hydrostatics and hydrodynamics, and none were in agreement with one another. In 1948 Sir Harold Jeffries combined the results of many previous studies and arrived at a value for the flattening that was generally accepted by geodesists. However, observations of satellites in 1958 resulted in a slightly different value for the flattening than was previously accepted. This was of significant importance to geophysicists and led to the abandonment of some theories of the earth's interior [1].

The purpose of this discussion is to emphasize the role that artificial satellites have played in resolving a highly controversial problem in geodesy. We are currently faced with several analogous situations. These involve the concepts of continental drift, polar wandering, and variations in the angular speed of the earth. These concepts have been debated vigorously for many years, many experiments have been performed to measure the quantities in question, and yet there is still not general agreement as to their existence and very little agreement as to their

cause. The situation is very similar to that of the degree of flattening and it would be of significant value if an independent experiment could be devised that would lead to more accurate measurements. The purpose of this paper is to present some results of an investigation of possible experiments involving a synchronous satellite (or satellites) that will result in precise determinations of continental drift, variations in angular speed, and the polar wandering.

CONTINENTAL DRIFT

The possibility that the continents of the earth have been drifting relative to one another throughout the earth's history has been discussed for three hundred years and debated vigorously for the past fifty years [2]. The hypothesis of continental drift has been strongly supported in many recent books and papers ([3], [4], [5]) and many estimates have been presented for the drift rates ([3], [4]). However, its validity is regarded with scepticism by many scholars [2] and even denied by some [6]. If the drift rates were accurately determined, substantial questions regarding the structure of the earth's upper mantle could be answered and the cause of drift might be determined. This could lead to a better understanding of the origin of the earth and may be of value in determining man's future on the earth.

It is pointed out by Wilson [2] that the arguments about continental drift resolve themselves into three questions. The first question is whether drift has occurred and whether it is still occurring. If the occurrence of drift can be verified, the second question is to determine the pattern of drift of all the continents that gives a best fit to the observations. Finally, the third question to be answered is to determine

the nature of the forces that cause the drift. All three of these questions are currently unresolved. The original hypothesis of continental drift was based on the obvious similarities that exist between the coastlines of various land masses. This concept has been further explored recently by using a digital computer to assemble the continents in a "best fit" manner [8]. However, the primary results in support of continental drift have been obtained by analysis of palaeomagnetic data. By measuring magnetic anomaly patterns along faults various investigators have determined drift rates between continents. Morgan [3] divides the earth into twenty blocks, each one bounded by rises, trenches, or faults, and determines the relative motions of the blocks. It is found, for example, that the Antarctic block has a maximum spreading rate relative to the Pacific block of 5.7 ± 0.2 cm/year. It should be pointed out however, that the use of rock magnetic data in investigations of continental drift depends on postulating a model geomagnetic field because it is not known how the actual geomagnetic field behaved over long intervals of geological time. The validity of conclusions drawn from magnetic data depends on the accuracy of the model geomagnetic field [9]. However, the evidence obtained in this manner lends strong support to the hypothesis of drift.

Another technique that has proved to be of some consequence is to employ astronomical evidence. The most satisfactory results have been obtained by the International Latitude Service (ILS) by using a chain of five zenith telescopes around the earth at latitude 39°08' N [10]. Data have been taken almost continuously since the end of the last century and

these data have been extensively analyzed [11]. The results indicate that the observing stations have been fixed in latitude with respect to the earth within 0.01 seconds of arc over a half century and so secular motions in the north-south direction appear to be less than one centimeter per year at the present time [10]. However, this technique does not provide adequate information with respect to variations in longitude and does not exclude the possibility of east-west motions of up to one-half meter per year.

The prospects for improvement in determining continental drift are varied. The astronomical techniques may be extended to provide coverage on a more nearly world-wide basis but not without considerable expenditures. The magnetic anomaly approach may be extended by obtaining and analyzing additional data. However, this is complicated by the fact that measurements over most of Asia are currently denied. Satellites offer the opportunity of observing large portions of the earth's surface simultaneously and may provide the means of performing independent, and very precise, experiments to ascertain the current existence of continental drift.

DESCRIPTION OF METHOD

It has been estimated that a Q-switched laser with an output pulse of 10 ns can be used to determine the range to a satellite to a precision of 15 cm or less [12]. By making simultaneous range observations to a satellite from four ground stations and by repeating this for thirty satellite positions the interstation distances may be determined to within an average error of 50 cm. Therefore it should be possible to obtain a

direct measurement of continental drift rates after only two or three years of observations. The approach is briefly described below.

Suppose that R^j represents the vector from the origin of some arbitrary coordinate system to the satellite at the time of the j^{th} range measurement. Let c^{ji} represent the vector to the i^{th} station and r^{ji} represent the range vector (see Figure 1). The vectors are related by the following expression:

$$c^{ji} + r^{ji} = R^j \qquad \begin{matrix} i = 1,\cdots,4 \\ j = 1,\cdots,30 \end{matrix}$$

For a given j this provides four equations for five unknowns. In terms of components there are 120 equations for 126 unknowns (36 station coordinates and 90 satellite coordinates). The system can be made determinate by specifying six of the unknowns. This cannot be done arbitrarily but it can be done as follows. Specify the coordinates of one station (arbitrarily), then two components of the direction of motion of a second station relative to the first, and finally one component of the relative motion of a third station. The following relative displacements were selected for this analysis:

$$\delta c_1^{12} = \delta c_2^{12} = \delta c_3^{12} = \delta c_1^{11} = \delta c_2^{11} = \delta c_3^{10} = 0.$$

The range equation may be written in terms of components as

$$\sum_{k=1}^{3} (R_k^j)^2 + \sum_{k=1}^{3} (c_k^{ji})^2 - 2 \sum_{k=1}^{3} R_k^j c_k^j - |r^{ji}|^2 = f^j = 0$$

Perturbation equations may be written as

$$\sum_{k=1}^{3} (R_k^j - c_k^{ji}) \, \delta c_k^{ji} - \sum_{k=1}^{3} (R_k^j - c_k^{ji}) \, \delta R_k^j + \frac{1}{2} f^j(x^N) = 0$$

where x^N represents the vector (c,R) about which perturbations are taken. The above perturbation equation may be expressed in matrix form as

$$[A] \left\{ \frac{\delta c}{\delta R} \right\} = f$$

which may be inverted to give

$$\left\{ \frac{\delta c}{\delta R} \right\} = [A]^{-1} f \quad .$$

This provides an iterative procedure for locating stations and determining interstation distances. The iterative procedure is described as follows:

1. Guess nominal values for R, c.
2. Obtain a complete set of range measurements r.
3. Iterate to obtain the correct values of R, c.

The interstation distances are obtained from

$$D^2(I,J) = \sum_{k=1}^{3} [c(I,K) - c(J,K)]^2$$

where D(I,J) represents the distance between stations I and J.

After once obtaining the interstation distances from one complete set of measurements additional measurements may be taken and the interstation distances may be updated. This will provide a direct measurement of drift rates.

The ground stations that were selected are listed in Table 1. No attempt has been made to locate the stations at points of maximum relative movement; rather, they have been selected to be distributed somewhat uniformly over the Earth's surface. It was found, however, that if the station at Houston is replaced in favor of one at Goddard Space Flight Center, then the standard deviations in the determination of the inter-station distances increased significantly. Also, it is not required that 12 stations be used; in fact, if L represents the number of stations used at each observation time, M represents the number of observation times, and N represents the number of stations, then all that is required is that $LM = 3(N + M) - 6$, where $L \leq N$. For example, the ten stations to be employed in the current Isogex experiment could be used in the analysis. This is currently being examined.

ORBIT SELECTION

The technique requires that the satellite pass approximately over the midpoint of each great circle arc connecting all of the ground stations. It was considered to be desirable to maximize the number of times that the satellite passes near the required points in order to increase the opportunities for making the range measurements.

The problem is to determine the orbit parameters that result in maximizing the opportunities for observation. Two analytical formulations of the problem are described below.

Let ℓ_k, δ_k represent the longitude and latitude of the particular points of interest. Let $L(t)$, $\delta(t)$ represent the longitude and latitude

of the satellite at any time (t) and let L_o, δ_o be the initial values of longitude and latitude. The problem may then be stated as a parameter optimization problem as follows. Determine L_o, δ_o, and the orbit inclination and period to minimize the cost function

$$J = \int_o^T \sum_{k=1}^{N} \{(\ell_k - L(t))^2 + (\delta_k - \delta(t))^2\}\, dt$$

where N represents the number of regions of interest and T represents some specified time. A somewhat simpler formulation would be to define $\phi_k(t)$ as the great circle arc between the ground point and the projection of the satellite on the ground. Then let $\phi_k^* = \min \phi_k(t)$ and find the orbit parameters to minimize $J = \sum_{k=1}^{N} \phi_k^*$.

The expressions for latitude, longitude, and miss distance are given for a circular orbit as

$$L(t) = L_o - \omega_e t + \tan^{-1}[\cos i \tan \beta\, t]$$

$$\lambda(t) = \lambda_o + \sin^{-1}[\sin i \sin \beta\, t]$$

and
$$\phi_k(t) = \cos^{-1}\{\sin \delta_k \sin[\lambda_o + \sin^{-1}(\sin i \sin \beta\, t)] + \cos[\delta_k \cos \lambda_o + \sin^{-1}(\sin i \sin \beta\, t)] \cos[L_o - \omega_e t + \tan^{-1}(\cos i \tan \beta\, t) - i\, \ell_k]\},$$

where $\beta = (\mu/r^3)^{1/2}$.

In either approach an infinite number of points would have to be examined unless the time is restricted to be in some finite interval. Therefore it is reasonable to examine situations in which the ground track is periodic. Let the subsatellite trace repetition parameter [13]

be defined as

$$Q = \frac{360}{S}$$

where $S = \omega_e P_N - \Delta\Omega$

and ω_e is the earth rotation rate, P_N is the nodal period, and $\Delta\Omega$ is the inertial rotation of the line of nodes (measured positive westward) during one nodal period. Then Q may be approximated to first order in $(\frac{R}{a})$, where R is the earth's mean equatorial radius and a is the semi-major axis, by

$$Q = \frac{24}{k} a^{-3/2} \left\{ 1 + \frac{1}{36}\left(\frac{R}{a}\right)^{7/2} \cos i \right\}$$

where $K = 2.77 \times 10^{-6}$ and a is measured in kilometers. The significance of Q is that it represents the number of satellite revolutions that occurs during one rotation of the earth relative to the osculating orbit plane. The procedure was to select Q, which determines the number of revolutions required before the trace is repeated, and then examine the miss distances ϕ_k^* for various values of a and i. The orbit that was selected on that basis is a direct circular orbit at 285 NM altitude with Q = 15.5 and at an inclination of 70 degrees and launched from the Western Test Range. For Q of 15.5 the trace repeats after every 31 revolutions. The approximate minimum miss distances (in degrees) are shown in Table 2.

SENSITIVITES AND STANDARD DEVIATIONS

The precision of the determination of the interstation distances (and hence continental drift) is dependent on the precision of the range

measurements. The expression for the interstation distances in terms of station coordinates was given earlier. The variation in D(I,J) due to a variation in the station coordinates may be written as

$$D(I,J) = \sum_{k=1}^{3} [c(I,K) - c(J,K)][\delta c(I,K) - \delta c(J,K)]$$

or $\delta D = B\delta c$.

The variations in coordinates with respect to variations in the range measurements may be written as

$$\left\{ \frac{\delta \underline{c}}{\delta \underline{R}} \right\} = A^{-1} |r| \delta r \quad .$$

These expressions may be combined to give

$$\delta D = \tilde{B}\delta r$$

where $\tilde{B}(I,J) = \sum_{k} b_{I,K} a_{K,J} r_J$

The standard deviations in the interstation distances are given by

$$\sigma(D(I)) = \sum_{J} (\tilde{b}_{I,J})^2 \sigma(r)$$

where $\sigma(r)$ represents the standard deviation in the range measurements. The standard deviations are show in Table 3 and are based on a standard deviation $\sigma(r)$ of 15 cm. This value of $\sigma(r)$ is subject to question and is being examined currently at the Wave Propagation Laboratory of the Environmental Sciences Services Administration at Boulder, Colorado. Sensitivities were also calculated based on a common error of 15 cm. in all range measurements. These were all less than 10 centimeters.

It is apparent on examination of the standard deviations for this orbit that they are too large to allow for a direct measurement of continental drift rates. An investigation of the effect of orbit altitude on the standard deviations resulted in the curve shown on Figure 2, where $\tilde{\sigma}$ represents the average of the standard deviations in the inter-station distances. In order to keep the standard deviations small and also increase the opportunities for observations an orbit having $a/R \sim 2$ should be selected. Choosing $Q = 6$, $a/R = 2.015$, and $i = 65$ degrees provided the miss distances and standard deviations shown in Tables 4 and 5.

DISCUSSION

The analysis has indicated the feasibility of obtaining direct measurements of continental drift by laser ranging to satellites. The results of this experiment would also serve for mapping purposes, as has been pointed up in many papers. The method is not actually dependent upon having a satellite pass directly over the midpoints of the arcs joining the ground stations and could be implemented with currently existing satellites having corner reflectors.

REFERENCES

1. D. King-Hele, Observing Earth Satellites, St. Martin's Press, 1966, p. 164.

2. J. Wilson, "Some Rules for Continental Drift," Continental Drift, The Royal Society of Canada, 1966, pp. 3-17.

3. W. Morgan, "Rises, Trenches, Great Faults, and Crustal Blocks," Journal of Geophysical Research, Vol. 73, No. 6, March 15, 1968, pp. 1959-1982.

4. X. LePichon, "Sea-Floor Spreading and Continental Drift," Journal of Geophysical Research, Vol. 73, No. 12, June 15, 1968, pp. 3661-3697.

5. J. Maxwell, "Continental Drift and a Dynamic Earth," American Scientist, Spring, 1968, pp. 35-51.

6. E. Lyustikk, "Criticism of Hypotheses of Convection and Continental Drift," Geophysical Journal, 1967, 14, pp. 347-352.

7. G. Macdonald, "Mantle Properties and Continental Drift," Continental Drift, The Royal Society of Canada, 1966, pp. 18-27.

8. E. Bullard, J. Everett, A. Smith, Philosophical Trans. Royal Society, Symposium on Continental Drift, 258, 41, 1965.

9. K. Creer, "A Synthesis of World-wide Palaeomagnetic Data," Mantles of the Earth and Terrestrial Planets, Interscience, 1967, pp. 361-382.

10. R. Tanner, "Astronomical Evidence on the Present Rate of Continental Drift," Continental Drift, The Royal Society of Canada, 1966, pp. 71-74.

11. W. Markowitz, "Latitude and Longitude, and the Secular Motion of the Pole," Methods and Techniques in Geophysics, Vol. 1, 1960, Interscience, pp. 325-361.

12. Bender, P. L., Alley, C. O., Currie, D. G., and Fallen, J. E., "Satellite Geodesy Using Laser Range Measurements Only," Journal of Geophysical Research, Vol. 73, No. 16, August 15, 1968.

13. H. Karrenberg, E. Levin, R. Luders, "Orbit Synthesis," Air Force Report No. SAMSO-TR-68-341, Aerospace Corporation, June 1968.

Table 1

STATION LOCATIONS

Station Number	Latitude (N)	Longitude (E)	Location
1	29°30'	265°	Houston, Texas
2	14°45'	342°30'	Dakar, Senegal
3	36°15'	59°37'	Mashhad, Iran
4	31°23'	130°51'	Kanoya, Japan
5	20°43'	203°44'	Maui, Hawaii
6	-25° 4'	229°54'	Pitcairn Island (U.K.)
7	-31°57'	294°51'	Villa Dolores, Argentina
8	-33°55'	18°29'	Cape Town, South Africa
9	-12°11'	96°50'	Cocos Island (Australia)
10	-30°17'	149°36'	Culgoora, Australia
11	76°30'	291°28'	Thule, Greenland
12	-77°50'	166°40'	McMurdo Station, Antarctic (U.S.A.)

Table 2

MINIMUM MISS DISTANCES
285 NM Altitude

ORBIT NB'R	ϕ_1	ϕ_2	ϕ_3	ϕ_4	ϕ_5	ϕ_6	ϕ_7	ϕ_8	ϕ_9	ϕ_{10}	ϕ_{11}	ϕ_{12}	ϕ_{13}	ϕ_{14}	ϕ_{15}	ϕ_{16}	ϕ_{17}	ϕ_{18}	ϕ_{19}	ϕ_{20}	ϕ_{21}	ϕ_{22}	ϕ_{23}	ϕ_{24}	ϕ_{25}	ϕ_{26}	ϕ_{27}	ϕ_{28}	ϕ_{29}	ϕ_{30}
1				0												3		7			3									
2																														
3																							0							
4									0								1				1									
5			0									0																		
6																														
7								0											5							1				
8										3				1														0		
9																														
10		2																												
11															1										3					
12					0								1																	
13																														
14	0																													
15																								0		1				
16				0					5							3					3									
17																							0							
18																														
19									0								1				1				3					
20			0									0										2								
21																														
22						5		0																		1				
23														1														0		
24																														
25							5																							
26															0										3					8
27					0								1														6			
28																			5											
29	0																												5	
30																								0						
31																														

Table 3

STANDARD DEVIATIONS IN INTERSTATION DISTANCE (METERS)

285 NM Altitude

1	1.04	1.53	1.41	.69	.98	1.04	1.56	1.53	1.51	.66	1.69
2	.91	1.53	1.26	1.60	.87	.69	1.53	1.45	.89	1.51	
3	.84	1.41	1.37	1.51	1.05	.81	1.39	.89	1.57		
4	.84	1.39	1.37	1.52	.76	.89	1.10	1.36			
5	.76	1.33	1.25	1.37	1.07	.89	1.34				
6	.85	1.52	1.47	1.02	1.37	.88					
7	.87	1.64	1.53	1.46	.96						
8	.99	1.42	1.51	.88							
9	.70	1.64	1.09								
10	1.51	.65									
11	1.42										

Table 4

MINIMUM MISS DISTANCES (DEG)

3490 NM Altitude

ORBIT NB'R	ϕ_1	ϕ_2	ϕ_3	ϕ_4	ϕ_5	ϕ_6	ϕ_7	ϕ_8	ϕ_9	ϕ_{10}	ϕ_{11}	ϕ_{12}	ϕ_{13}	ϕ_{14}	ϕ_{15}	ϕ_{16}	ϕ_{17}	ϕ_{18}	ϕ_{19}	ϕ_{20}	ϕ_{21}	ϕ_{22}	ϕ_{23}	ϕ_{24}	ϕ_{25}	ϕ_{26}	ϕ_{27}	ϕ_{28}	ϕ_{29}	ϕ_{30}
1		10		3					9	.8	1					.6					5		2							
2	6						12	13				.2								10					15		18			
3						2							1		4		5		15			5		7					8	
4														7				16										11		4
5			1																											
6					0.5																					1				

Table 5

STANDARD DEVIATIONS IN INTERSTATION DISTANCE (METERS)

3490 NM Altitude

1	.32	.63	.55	.24	.28	.31	.76	.86	.62	.22	.64
2	.33	.71	.68	.68	.31	.31	.71	.91	.30	.71	
3	.27	.64	.89	.79	.38	.28	.59	.29	.74		
4	.28	.58	.89	.74	.25	.28	.32	.60			
5	.26	.59	.94	.60	.35	.29	.59				
6	.27	.70	.63	.30	.58	.27					
7	.34	.74	.59	.62	.30						
8	.34	.60	.75	.32							
9	.23	.63	.32								
10	.66	.22									
11	.88										

LIST OF FIGURES

Fig. 1. B. Winn

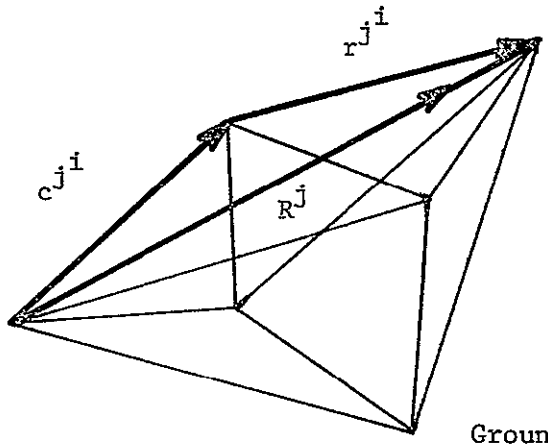

Fig. 2. B. Winn

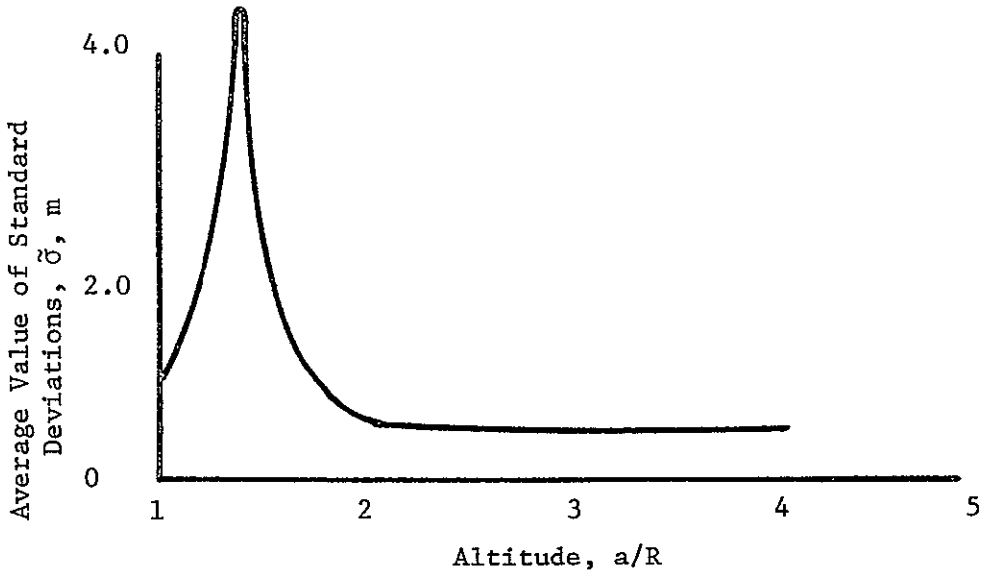
Average Value of Standard Deviations, $\tilde{\sigma}$, m
4.0
2.0
0
1
2
3
4
5
Altitude, a/R

DIRECTION-COSINE ATTITUDE-CONTROL LOGIC FOR SPIN-STABILIZED AXISYMMETRIC SPACECRAFT

Dara W. Childs*
Colorado State University
Fort Collins, Colorado

ABSTRACT

The developments of this study yield a control logic for the active attitude control of a spin-stabilized axisymmetric spacecraft. The derived control logic makes use of direction cosines for attitude definition, and is not restricted by either small angle assumptions or by the kinematic singularities associated with Euler angles. The active torqueing capability is provided by means of a reaction-jet system, and the control logic is simplified by assuming that control torques may be applied impulsively. The control logic formulated is optimal in the sense that each control impulse is delivered in such a manner as to cause a maximum reduction in "system error."

INTRODUCTION

The basic objective of the analysis which follows is the synthesis of an active feedback attitude-control logic for spin-stabilized axisymmetric spacecraft. Control torques are to be generated by means of a reaction-jet system, and the proposed control logic is simplified by assuming that control torques may be applied impulsively. Pulse-width modulation is suggested for generating the derived control impulses.

---

*Assistant Professor of Mechanical Engineering

Windeknecht [1]* was the first of several authors [2, 3] to suggest impulsive control logic for passively damped spacecraft. Since passive damping systems are only effective if the spin-axis moment of inertia is greater than either transverse-axis moment of inertia [4], the control logic suggested in [1 - 3] is not workable for many spacecraft configurations. In contrast to these systems, Porcelli and Connolly [5] have suggested a control logic for the active control of slender (i.e., "pencil-shaped") spacecraft. Childs [6] has recently suggested a control logic which is applicable for axisymmetric spacecraft of arbitrary inertial proportions; i.e., it would be used to control a "disk-shaped" body, a "pencil-shaped" body, or any configuration lying between these extremes.

All of the above cited control approaches employ Euler angles as kinematic variables and are restricted in application to situations which do not require "large" angular reorientations. The control logic suggested by Porcelli and Connolly and by Childs are based on linearized Euler angle models which become questionable for angular reorientations in excess of 15° (approximately). While these control approaches could be extended by changes in reference, a more fundamental approach consists of employing a kinematical representation which does not have the inherent kinematic singularity associated with Euler angles. The components of the direction cosine matrix [7, 8] are such a representation, and the analysis of this study makes use of them in a development similar to that of Childs [6].

THE CONTROL MODEL

The basic attitude-control requirement for spin-stabilized spacecraft is that the spin axis be placed and maintained within some small defined

---

*Identifies listing in reference section

neighborhood of a prescribed orientation. The physical variables which must be controlled are angular rates and angular displacements. The angular rates may be defined by Euler's equations of motion for a rigid body which, for an axisymmetric body, are stated as

$$\begin{aligned} \dot{\omega}_1 + a\Omega\omega_2 &= M_1/I = u(t)\cos\eta(t) \\ \dot{\omega}_2 - a\Omega\omega_1 &= M_2/I = u(t)\sin\eta(t) \\ \omega_3(t) &= \omega_3(0) = \Omega \end{aligned} \tag{1}$$

where

$$a = (I_3 - I)/I \tag{2}$$

and the subscripts 1, 2, 3 identify body-fixed x_1, x_2, x_3 axes with the x_3 axis the axis of symmetry. The origin of the x_1, x_2, x_3 system coincides with the mass center of the rigid body. The variables ω_1, ω_2, ω_3 and M_1, M_2 are, respectively, the components of the angular velocity vector of the body and the external torque vector. The parameters I and I_3 are, respectively, the transverse ($I_1 = I_2 = I$) and spin-axis moment of inertias. The form of (1) implies that control is to be supplied by a gimballed torqueing system, i.e., that $\eta(t)$ is an unbounded control variable.

The angular orientation of the body-fixed x_i system relative to an inertial X_i system may be defined by the direction cosine matrix [A]. If the components of the arbitrary vector V in the x_i and X_i systems are denoted, respectively, by $(v)_i$ and $(v)_I$, the direction cosine matrix satisfies

$$(v)_i = [A](v)_I \quad ; \quad (v)_I = [A]^T(v)_i \tag{3}$$

where "T" denotes the matrix transpose operation. Further, the matrix [A] is related ([7], [8]) to the components of the angular velocity vector cited in (1) by

$$[\dot{A}] = -[(\omega)][A] \tag{4}$$

where

$$[(\omega)] = \begin{bmatrix} 0 & -\omega_3 & \omega_2 \\ \omega_3 & 0 & -\omega_1 \\ -\omega_2 & \omega_1 & 0 \end{bmatrix} \tag{5}$$

Since only the spin-axis orientation orientation is significant, one extracts from (4)

$$\begin{aligned} \dot{a}_{13} &= \Omega a_{23} - \omega_2 a_{33} \\ \dot{a}_{23} &= -\Omega a_{13} + \omega_1 a_{33} \\ \dot{a}_{33} &= \omega_2 a_{13} - \omega_1 a_{23} \end{aligned} \tag{6}$$

These variables are not independent, since they satisfy the kinematic constraint

$$a_{13}^2 + a_{23}^2 + a_{33}^2 = 1 \tag{7}$$

Equations (1) and (6) constitute the system of governing equations. The kinematic definition given in (6) is not restricted by either small angle approximations or by kinematic singularities.

The control logic derived in this study is based on the assumption that the effect of a "short-duration" firing of the gimballed reaction jet can be adequately approximated by an impulse. Since a reaction jet is essentially an "on-off" device, i.e.,

$$u = U > 0, \text{ or } u = 0$$

the magnitude of a control impulse is approximately defined by

$$J = UI\Delta t .$$

where Δt is the firing duration. By varying Δt one obtains impulses of varying magnitude. This approach is commonly referred to as pulse-widt modulation.

To determine the effect of a control impulse, Eq's (1) and (6) are restated as

$$\dot{\omega} = ia\Omega\omega + \hat{u}(t) \tag{8}$$

and

$$\begin{aligned} \dot{\alpha} &= ia_{33}\omega - i\Omega\alpha \\ \dot{a}_{33} &= \omega_2 a_{13} - \omega_1 a_{23} \end{aligned} \tag{9}$$

where

$$\omega = \omega_1 + i\omega_2 = |\omega|e^{i\theta} \quad ; \quad \alpha = a_{13} + ia_{23} = |\alpha|e^{i\phi} \tag{10}$$

$$\hat{u}(t) = u(t)e^{i\eta(t)}$$

The solution to (8) for the control impulse

$$u(t) = (J^1/I)\delta(t-t^1) = (|J^1|/I)e^{i\eta^1}\delta(t-t^1) \tag{11}$$

can be expressed as

$$\begin{aligned} \omega(t) &= \omega^0 e^{ia\Omega t} && 0 \le t < t^1 \\ \omega(\tau) &= \omega^1 e^{ia\Omega\tau} && 0 \le \tau \end{aligned} \tag{12}$$

where

$$\begin{aligned} &\tau = t-t^1 \quad , \quad \omega^0 = \omega(0) = |\omega^0|e^{i\theta^0} \\ &\omega^1 = \omega(t^1) = \omega^0 e^{ia\Omega t^1} + (J^1/I) \end{aligned} \tag{13}$$

From (12), Eq. (9) is reduced to a system of linear time-varying differential equations. The transformation

$$\alpha = ze^{i(a\Omega t + \theta^0)} = (z_1 + iz_2)e^{i(a\Omega t + \theta^0)} \tag{14}$$

further reduces (9) to the linear time-invariant system

$$\begin{aligned} \dot{z} + i\mu z &= i|\omega^0|a_{33} \\ \dot{a}_{33} &= -|\omega^0|z_2 \end{aligned} \tag{15}$$

where

$$b = a + 1 = I_3/I \quad , \quad \mu = b\Omega \tag{16}$$

The solution of (15) is readily obtained, and from (14) yields for $t<t^1$

$$\begin{aligned} \alpha(t) &= \alpha^0 e^{ia\Omega t} \\ &\quad - i|\alpha^0||\omega^0|^2\beta_0^{-2} \sin(\phi^0-\theta^0)(1-\cos\beta_0 t)e^{i(a\Omega t+\theta^0)} \\ &\quad + (a_{33}^0\omega^0 - \mu\alpha^0)\beta_0^{-2}[\mu(1-\cos\beta_0 t) + i\beta_0 \sin\beta_0 t]e^{ia\Omega t} \end{aligned} \tag{17}$$

and

$$\begin{aligned} a_{33}(t) &= a_{33}^0\,\beta_0^{-1}\,(\mu^2 + |\omega^0|^2\cos\beta_0 t) \\ &\quad + \mu|\alpha^0||\omega^0|\beta_0^{-1}\cos(\phi^0-\theta^0)(1-\cos\beta_0 t) \\ &\quad - |\alpha^0||\omega^0|\beta_0^{-1}\sin(\phi^0-\theta^0)\sin\beta_0 t \end{aligned} \tag{18}$$

where

$$\beta_0^2 = \mu^2 + |\omega^0|^2 = [(I_3\Omega)^2 + (I|\omega^0|)^2]/I^2 \tag{19}$$

Hence,

$$\beta_0 = |H^0|/I \tag{20}$$

where H^0 is the initial angular-momentum vector of the rigid body. The solution for $t \geq t^1$ (or $\tau \geq 0$) is obtained from Eq's (17) through (20) by replacing the index 0 by 1 and substituting τ for t.

Although the solution developed above is formally correct, it is physically unmotivating, and a more meaningful solution format is obtained via the following definitions.

$$\sin \delta^0 = I|\omega^0|/|H^0| = |\omega^0|/\beta_0$$
$$\cos \delta^0 = I_3\Omega/|H^0| = \mu/\beta_0 \qquad (21)$$

$$a_{33} = \cos \gamma_3 \quad , \quad |\alpha| = \sin \gamma_3 \qquad (22)$$

$$H^0_{X_3} = |H^0| \cos \lambda^0 \qquad (23)$$

The angles defined above are illustrated in Fig. 1, and one observes that λ^0 is the angle between the angular-momentum vector H^0 and the inertial X_3 axis, while δ^0 is the angle between the angular-momentum vector and the spin axis. The angle γ_3 obviously lies between the x_3 axis and the X_3 axis.

Of these three angles λ^0 and δ^0 are piecewise-constant functions of time (stepping dicsontinuously when an impulse is applied), while γ_3 is a continuous function of time. From the last of (3) and (23), one obtains

$$\cos \lambda^0 = \cos \gamma_3^0 \cos \delta^0 + \sin \gamma_3^0 \sin \delta^0 \cos (\phi^0 - \theta^0) \qquad (24)$$

which yields, in conjunction with (21) and (22),

$$a_{33}(t) = \cos \delta^0 \cos \lambda^0 + (\cos \gamma_3^0 - \cos \delta^0 \cos \lambda^0) \cos \beta_0 t - \sin \gamma_3^0 \sin \delta^0 \sin (\phi^0 - \theta^0) \sin \beta_0 t$$

for (18). This result is further simplified by the substitution

$$\sin \zeta^0 = \sin \gamma_3^0 \sin (\phi^0 - \theta^0)/\sin \lambda^0$$
$$\cos \zeta^0 = (\cos \gamma_3^0 - \cos \delta^0 \cos \lambda^0)/\sin \delta^0 \sin \lambda^0 \qquad (25)$$

which yields

$$a_{33}(t) = \cos \delta^0 \cos \lambda^0 + \sin \delta^0 \sin \lambda^0 \cos (\zeta^0 + \beta_0 t) \qquad (26)$$

The planar representation of Fig. 2 illustrates the spherical trigonometry involved in this torque-free rigid-body solution with the spin axis

precessing about the angular momentum vector at the rate β_0. Eq's (24) and (26) are simply an expression of the law of cosines for arcs from spherical trignometry.

CONTROL SYNTHESIS

By a suitable definition of the inertial X_i system, the general attitude-control objective can be interpreted as the requirement that the x_3 axis (spin axis) be placed and maintained in coincidence with the inertial X_3 axis. In terms of the state variables, the desired terminal state is then defined by

$$\begin{aligned} &\omega_1(T) = \omega_2(T) = a_{13}(T) = a_{23}(T) = 0 \\ &a_{33}(T) = 1 \Rightarrow \gamma_3(T) = 0 \end{aligned} \tag{27}$$

where T is the first time for which (27) is satisfied, and is unspecified.

From (26), the solution for a_{33} following application of a control impulse is given by

$$a_{33}(\tau) = \cos \delta^1 \cos \lambda^1 + \sin \delta^1 \sin \lambda^1 \cos (\zeta^1 + \beta_1 \tau) \tag{28}$$

A given control impulse will be defined as optimal if it minimizes the system error which follows the impulse. In view of the desired terminal conditions cited in (27), system error is defined as the maximum value of the spin axis angle γ_3, i.e.,

$$E = \max \gamma_3(t) \tag{29}$$

Hence, the initial system error is defined by $E^0 = \lambda^0 + \delta^0$. Equivalently, a control impulse is optimal if it maximizes the minimum value of $a_{33}(\tau)$ which occurs following a control impulse. From Eq. (28) the quantity to be maximized is

$$G(|J^1|, \eta^1, t^1) = \cos (\lambda^1 + \delta^1) \tag{30}$$

The necessary conditions of optimality, $\partial G/\partial|J^1| = \partial G/\partial t^1 = \partial G/\partial \eta^1 = 0$, are satisfied by

$$\sin(\zeta^0 + \beta_0 t^1) = 0 \quad , \quad \cos(\zeta^0 + \beta_0 t^1) = 1 \tag{31}$$

$$\sin(a\Omega t^1 + \theta^0 - \eta^1) = 0 \quad , \quad \cos(a\Omega t^1 + \theta^0 - \eta^1) = -1 \tag{32}$$

Although the formal confirmation of these results is lengthy, their kinematic significance is easily appreciated from Fig. 3. Eq. (31) implies that the optimal firing time t^1 occurs when $a_{33}(t)$ is a maximum (or $\gamma_3(t)$ is a minimum), while Eq. (32) implies that the "new" angular-momentum vector H^1 is to lie in the plane defined by the initial angular-momentum vector H^0 and the inertial X_3 axis. This latter statement can be better appreciated by noting from (13) that

$$|\omega^1|^2 = |\omega^0|^2 + 2\,|\omega^0||J^1|/I \cos(a\Omega t^1 + \theta^0 - \eta^1) + (|J^1|/I)^2$$

If in addition to (32), one also has

$$|J^1| = I\,|\omega^0|$$

then $|\omega^1| = 0$, and the resultant angular-momentum vector H^1 would lie in the $H^0 - X_3$ plane. The firing time t^1 and impulse phase η^1 defined, respectively, by (31) and (32) affect this desired result irrespective of the impulse magnitude $|J^1|$. As a consequence, one obtains

$$\lambda^1 + \delta^1 = \gamma_3^1 = \lambda^0 - \delta^0 \tag{33}$$

The form of the definition for the control phase provided by (32) is not entirely satisfactory, since its implementation would require measurement of the angular velocity components ω_1 and ω_2. A control logic that requires only angular measurements would be more attractive from a sensor viewpoint

and can be readily developed from the kinematic interpretation given above and in Fig. 3 for Eq.'s (31) and (32). The following additional angle definitions are required. The angles between the X_3 and x_1 axes and between the X_3 and x_2 axes are denoted, respectively, as γ_1 and γ_2; hence, $a_{13} = \cos\gamma_1$, $a_{23} = \cos\gamma_2$. The angle between the $X_3 - x_1$ and $X_3 - x_2$ planes is denoted as ξ while the angle between the $X_3 - x_1$ and $X_3 - H^0$ planes is ψ. Finally, one denotes $\bar{\eta}^1 = \eta^1 - \pi$. With these definitions one obtains from Fig. 4 via spherical trigonometry (the law of cosines for arcs)

$$\begin{aligned} \cos\bar{\eta}^1 &= -\cos\gamma_1 \sin\gamma_3 + \sin\gamma_1 \cos\gamma_3 \cos\psi \\ \sin\bar{\eta}^1 &= -\cos\gamma_2 \sin\gamma_3 + \sin\gamma_2 \cos\gamma_3 \cos(\xi - \psi) \end{aligned} \tag{34}$$

Using the same relationship, one obtains from Fig. 5

$$\begin{aligned} 0 &= \cos\gamma_1 \cos\gamma_3 + \sin\gamma_1 \sin\gamma_3 \cos\psi \\ 0 &= \cos\gamma_2 \cos\gamma_3 + \sin\gamma_2 \sin\gamma_3 \cos(\xi - \psi) \end{aligned} \tag{35}$$

Hence, from (34) and (35)

$$\cos\bar{\eta}^1 = -\cos\gamma_1/\sin\gamma_3 \quad , \quad \sin\bar{\eta}^1 = -\cos\gamma_2/\sin\gamma_3 \tag{36}$$

, and from (10) and (22)

$$\cos\eta^1 = \cos\phi^1 \quad , \quad \sin\eta^1 = \sin\phi^1 \tag{37}$$

Eq. (37) may them be used in place of (32) to define η^1.

The necessary conditions of optimality ($\partial G/\partial|J^1| = \partial G/\partial t^1 = \partial G/\partial\eta^1 = 0$) do not yield a unique value for $|J^1|$. A graphical illustration of this statement is provided in Fig. 6 where one notes that any $|J^1|$ in the range

$$I|\omega^0| \leq |J^1| \leq I|\omega^0| + I_3\Omega \tan(\lambda^0 - \delta^0) \tag{38}$$

yields the same optimal performance index

$$G^1|_{opt.} = \cos(\lambda^0 - \delta^0) \Rightarrow E^1 = \lambda^0 - \delta^0 \tag{39}$$

In review then, the general solution for the optimal firing time t^1, impulse angle η^1, and impulse magnitude $|J^1|$ are defined, respectively, by (31), (37), and (38). There are two special cases not covered by this general solution, namely, $\lambda^0 = 0$ and $|\omega^0| = 0$. In both cases, there is no preferred firing time t^1 since $\gamma_3(t)$ is constant. In these cases t^1 is chosen arbitrarily with (37) and (38) used to define η^1 and $|J^1|$. In both of these cases the optimal control impulse does not reduce system error; however, any other non-zero control impulse increases system error.

A single control impulse, even if unrestrained in magnitude, can not in general achieve the desired terminal conditions given in (27). Since control impulses will in fact be magnitude limited, a sequence of best impulses, $\Sigma J^i \delta(t-t^i)$, will be required to drive the system error into an acceptable neighborhood of the point defined by (27). The constraint cited in (38) for optimal impulse magnitude makes no provision for physical limitations on impulse magnitudes $|J^i|$, although they are in fact bounded both above and below as follows

$$|J|_{min} \leq |J^i| \leq |J|_{max} \tag{40}$$

The lower bound arises because of physical limitations while the upper bound is necessary to insure that the "impulsive character" of control torques is preserved. With this in mind, two non-optimum possibilities become evident in (38), namely,

$$|J|_{max} < I|\omega^0| \tag{41}$$

and

$$|J|_{min} > I|\omega^0| + I_3\Omega \tan(\lambda^0 - \delta^0) \tag{42}$$

Condition (41) would be likely to arise in the acquisition phase of control when $|J|_{max}$ is too small to achieve the desired optimum given in (39), while condition (42) would be encountered near limit-cycle operation with $|J|_{min}$ exceeding the allowable desired maximum. From Fig. 6, however, one would conclude that a control impulse will always reduce system error providing

$$|J|_{min} < I|\omega^0| + I_3\Omega \tan \lambda^0 \tag{43}$$

If control is applied when $|J|_{min} > I|\omega^0| + I_3\Omega \tan \lambda^0$, system error (as defined by $\max \gamma(t)$) will be increased. Eq. (43) effectively defines the idealized limit-cycle accuracy of the control logic in terms of $|J|_{min}$.

SUMMARY AND CONCLUSIONS

A control logic is developed herein which allows one to compute a sequence of optimum impulses which force the solution of (8) and (9) into a predictable (Eq. (43)) idealized neighborhood of the point (27). The control logic is not restricted by either small-angle approximations or by the kinematic singularities customarily associated with Euler angles. Further, the control logic obtained does not necessarily require sensor measurement of the angular-velocity components ω_1 and ω_2, although it would be necessary to make angular or direction-cosine measurements.

The developments of this study are predicated on a gimballed torqueing system, and the resultant simplicity of the control logic is, to a large extent, purchased at the expense of mechanical complexity. There is no reason, however, that the analytical approach employed in this study could not be applied to a simpler mechanical system. For example, with a single-axis body-fixed torqueing system one would obtain for (1)

$$\dot{\omega}_1 + a\Omega\omega_2 = M_1/I = u_1 \tag{44}$$

$$\dot{\omega}_2 - a\Omega\omega_1 = 0$$

where the control element u_1 is bounded by

$$u_1 = \pm U_1 \quad \text{,or} \quad u = 0 \tag{45}$$

The analysis is actually simpler in this case since the impulse phase is known to be either 0 or π. The development of a control logic for this type of torqueing system (with direction cosines as kinematic variables) is currently in progress.

REFERENCES

1. Windeknecht, T. G., "A Simple System for Sun Orientation of a Spinning Satellite," National IAS-ARS Joint Meeting, Los Angeles, California, 1961.

2. Grubin, C., "Generalized Two Impulse Scheme for Reorienting a Spin-Stabilized Vehicle," Progress in Astronautics and Rocketry, Vol. 8, Guidance and Control, Editors: R. E. Roberson and J. S. Farrior, Academic Press, New York-London, 1962, pp. 644-468.

3. Grubin, C., "Two-Impulse Attitude Reorientation of an Asymmetric Spinning Vehicle," AIAA Journal of Spacecraft and Rockets, Vol. 4, No. 3, March, 1967, pp. 306-310.

4. Thomson, W. T., and Reiter, G. S., "Motion of an Asymmetric Spinning Body with Internal Dissipation," AIAA Journal, Vol. 1, No. 6, June, 1963.

5. Porcelli, G., and Connolly, A., "Optimal Attitude Control of a Spinning Space Body - A Graphical Approach," IEEE Transactions on Automatic Control, July, 1966, pp. 580-596.

6. Childs, D. W., "A Versatile Attitude-Control System for Spin-Stabilized Axisymmetric Spacecraft," Submitted to AIAA Journal of Spacecraft and Rockets, 18 April 1969.

7. C. F. Harding, "Solution of Euler's Gyrodynamics, ASME Journal of Applied Mechanics, pp. 325-328, June, 1964.

8. A. Sabroff, et al., "Investigation of the Acquisition problem in Satellite Attitude Control," Air Force Flight Dynamics Laboratory, Wright-Patterson Air Force, Ohio, Tech. Report AFFDL-TR-65-115, December, 1965.

LIST OF FIGURES

Fig. 1 D. Childs

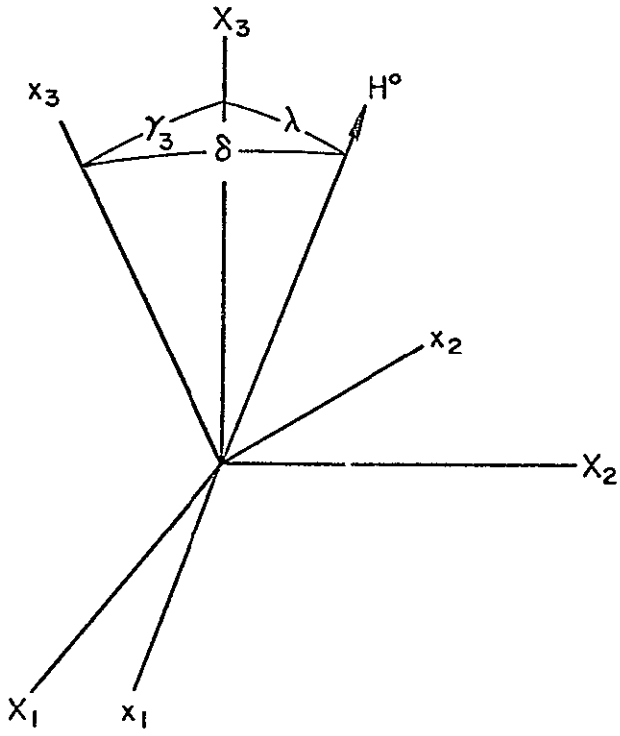

Fig. 2 D. Childs

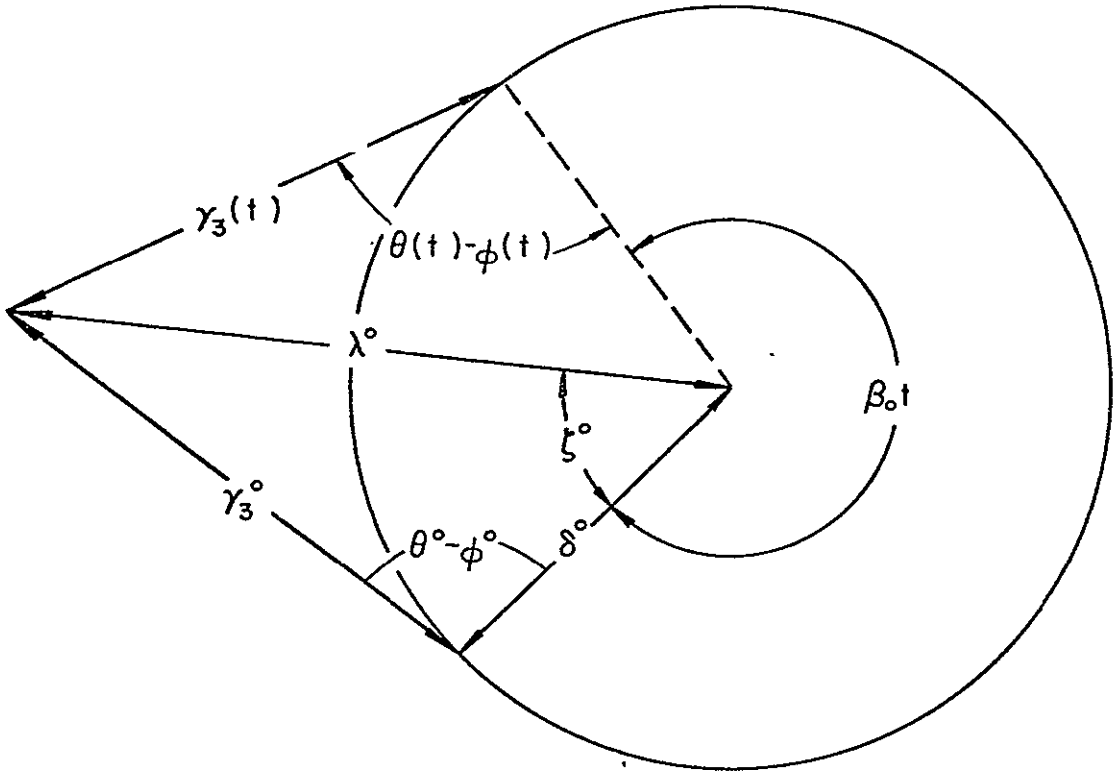

Fig. 3 D. C..ilds

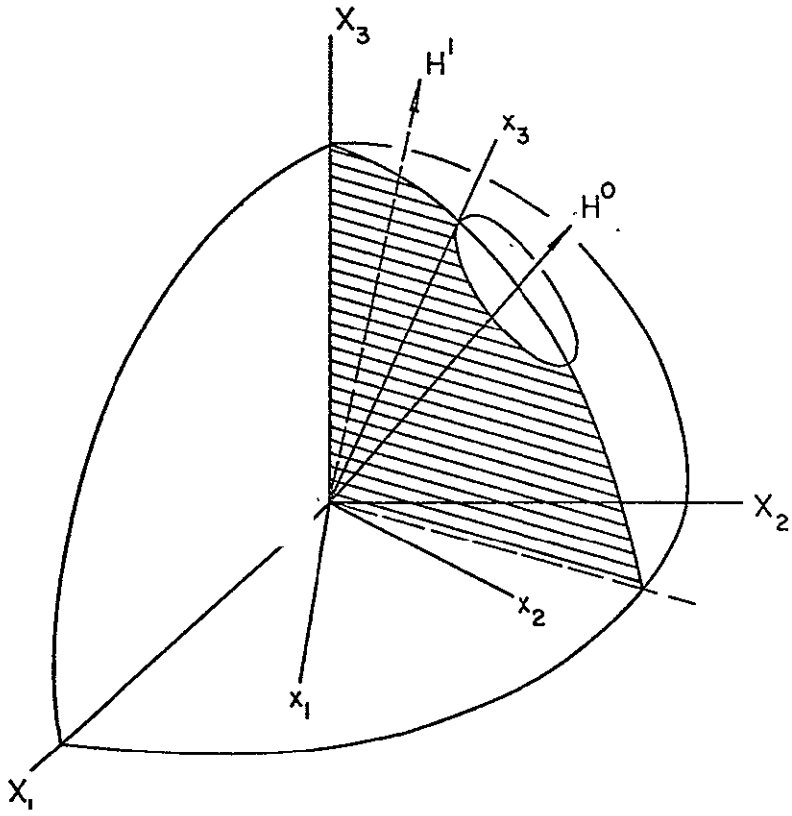

Fig. 4 D. Childs

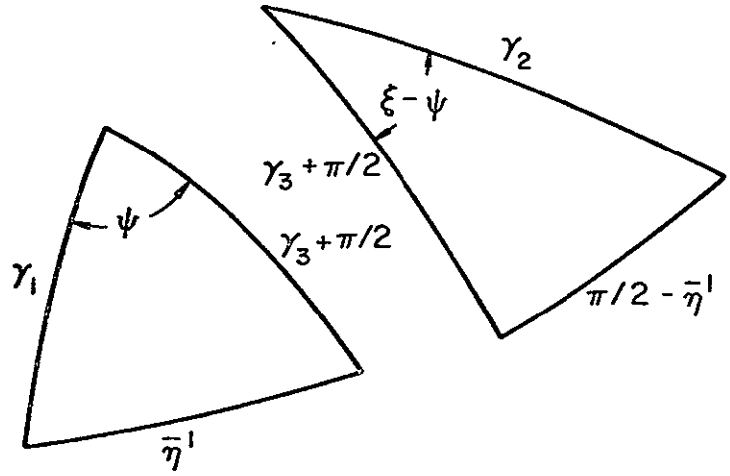

Fig. 5 D. Childs

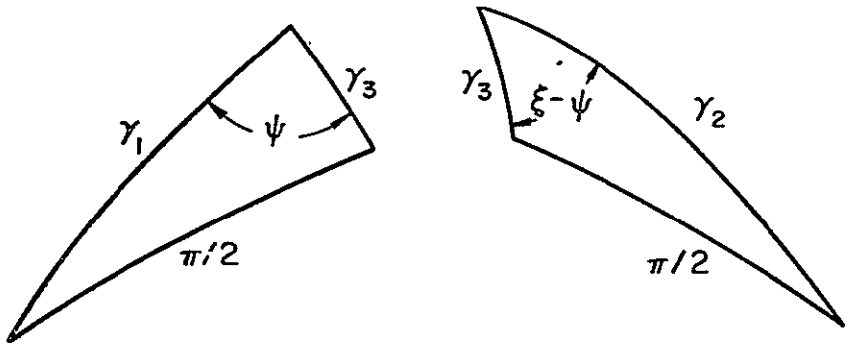

Fig. 6 D. Childs

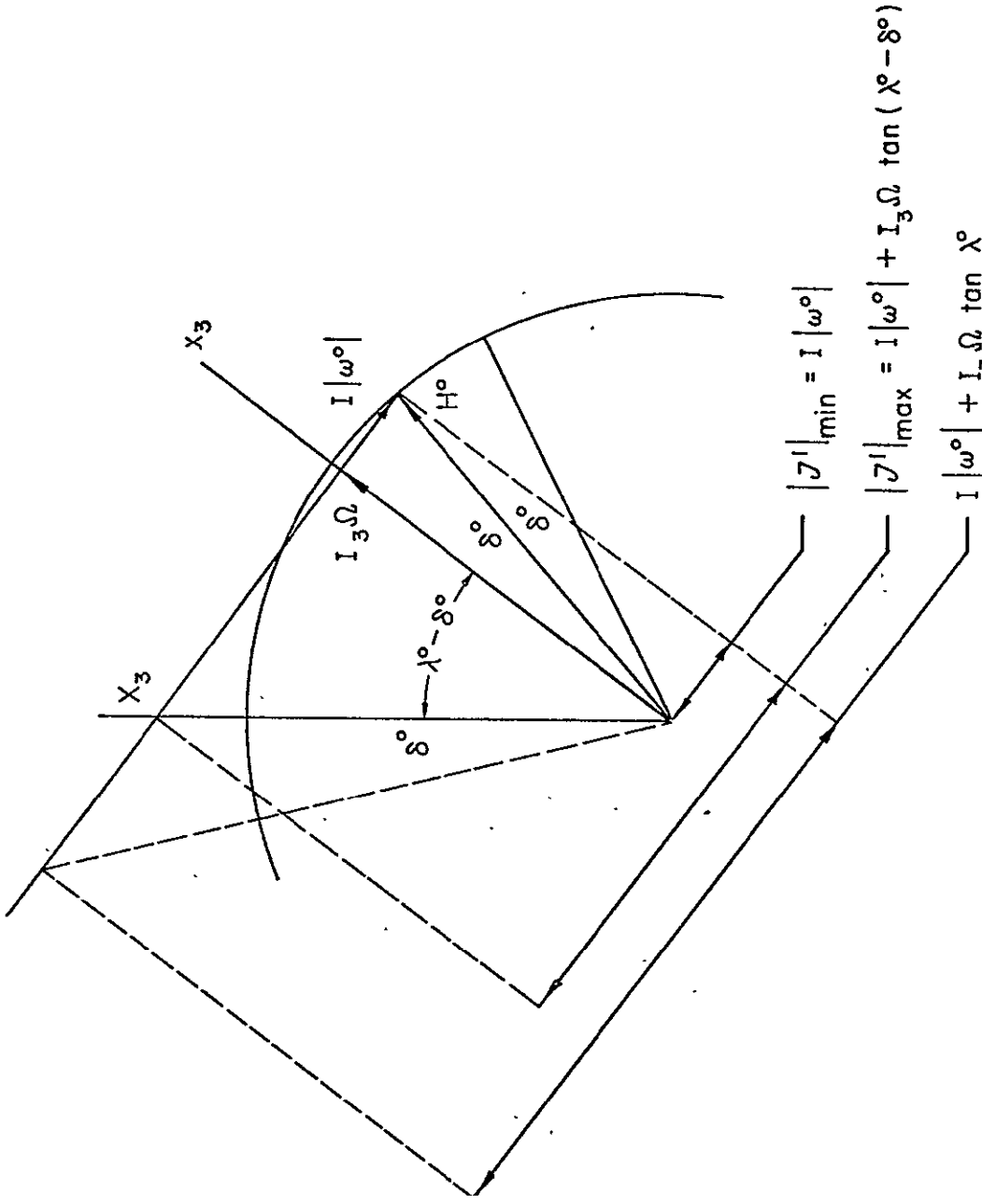

OPTIMAL DIRECTION-COSINE ATTITUDE-CONTROL LOGIC FOR SPIN-STABILIZED AXISYMMETRIC SPACECRAFT*

Dara W. Childs
Assistant Professor of Mechanical Engineering
Colorado State University
Fort Collins, Colorado

ABSTRACT

Necessary conditions are developed for the fuel-optimal attitude control of a spin-stabilized axisymmetric spacecraft with the attitude of the spacecraft defined by direction cosines, and the control torques provided via a gimballed reaction jet. The optimal solutions for free final time with unbounded control magnitude are demonstrated to be either (a) two impulses separated by a coasting arc or (b) an impulse followed by a singular arc (depending on the initial conditions). A proposed suboptimal control mechanization is outlined which requires a single, body-fixed reaction jet and incorporates several existing control approaches.

*This work was supported in part under NASA Research Grant NGR 06-002-085 and NSF Grant No. GK-5560. This financial support is gratefully acknowledged.

INTRODUCTION

Problems associated with the active attitude control of spin-stabilized axisymmetric spacecraft have been discussed in the literature for some time, and largely fall into the following two categories: (a) Control of passively damped spacecraft [1]*, [2], and (b) control of undamped spacecraft for small pointing and coning errors [3], [4]. Recently, two analyses [5], [6] have been reported which treat the large-angle attitude-control problem. Porcelli in [5] allows large pointing errors but retains the assumption of small coning errors, while Childs [6] considers the general case of arbitrary pointing and coning angle magnitudes. In both of these papers, impulsive-control strategies are developed from an analysis of the free motion of the spacecraft. In the analysis which follows, an optimal, unbounded control solution is demonstrated, and a suboptimal control logic based upon it is proposed. The proposed control logic is not restricted by the small coning angle assumptions of [5], and is simpler than that suggested by Childs [6].

THE CONTROL MODEL

The basic attitude-control requirement for spin-stabilized spacecraft is that the spin axis be placed and maintained within some small defined neighborhood of a prescribed orientation. The physical variables which must be controlled are angular rates and angular displacements. The angular rates may be defined by Euler's equations of motion for a rigid body which, for an axisymmetric body, are stated as

---

*Identifies listing in reference section.

$$\dot{\omega}_1 - a\Omega\omega_2 = M_1/I = u(t)\cos\eta(t)/I$$

$$\dot{\omega}_2 + a\Omega\omega_1 = M_2/I = u(t)\sin\eta(t)/I \qquad (1)$$

$$\omega_3(t) = \omega_3(0) = \Omega$$

where

$$a = (I - I_3)/I \qquad (2)$$

and the subscripts 1, 2, 3 identify body-fixed x_1, x_2, x_3 principal axes with the x_3 axis the axis of symmetry. The origin of the x_1, x_2, x_3 system coincides with the mass center of the rigid body. The variables ω_1, ω_2, ω_3 and M_1, M_2 are, respectively, the components of the angular velocity vector of the body and the external torque vector. The parameters I and I_3 are, respectively, the transverse ($I_1 = I_2 = I$) and spin-axis moment of inertias. The form of (1) implies that control is to be supplied by a gimballed torqueing system, i.e., that $\eta(t)$ is an unbounded control variable.

The angular orientation of the body-fixed x_i system relative to an inertial X_i system may be defined by the direction cosine matrix [A]. If the components of the arbitrary vector v in the x_i and X_i systems are denoted, respectively, by $(v)_i$ and $(v)_I$, the direction cosine matrix satisfies

$$(v)_i = [A](v)_I \quad ; \quad (v)_I = [A]^T(v)_i \qquad (3)$$

where "T" denotes the matrix transpose operation. Further, the matrix [A] is related [7] to the components of the angular velocity vector cited in (1) by

$$[\dot{A}] = -[(\omega)][A] \tag{4}$$

where

$$[(\omega)] = \begin{bmatrix} 0 & -\omega_3 & \omega_2 \\ \omega_3 & 0 & -\omega_1 \\ -\omega_2 & \omega_1 & 0 \end{bmatrix} \tag{5}$$

Since only the spin-axis orientation is significant, one extracts from (4).

$$\begin{aligned} \dot{a}_{13} &= \Omega a_{23} - \omega_2 a_{33} \\ \dot{a}_{23} &= -\Omega a_{13} + \omega_1 a_{33} \\ \dot{a}_{33} &= \omega_2 a_{13} - \omega_1 a_{23} \end{aligned} \tag{6}$$

These variables are not independent, since they satisfy the kinematic constraint

$$a_{13}^2 + a_{23}^2 + a_{33}^2 = 1 \tag{7}$$

Equations (1) and (6) constitute the system of governing equations. The kinematic definition given in (6) is not restricted by either small angle approximations or by kinematic singularities. Analytical solution of the state equations is expedited by restatement in the following complex variable format

$$\begin{aligned} \dot{\omega} + ia\Omega\omega &= ue^{i\eta}/I \\ \dot{\alpha} + i\Omega\alpha - ia_{33}\omega &= 0 \\ \dot{a}_{33} - \omega_2 a_{13} + \omega_1 a_{23} &= 0 \end{aligned} \tag{8}$$

where

$$\omega = \omega_1 + i\omega_2 = |\omega|e^{i\theta}, \quad \alpha = a_{13} + ia_{23} = |\alpha|e^{i\phi} \tag{9}$$

By a suitable definition of the reference X_i system, the general attitude-control problem may be expressed as the requirement that the body-fixed x_3 axis be placed and maintained in alignment with the X_3 axis.

NECESSARY CONDITIONS FOR UNBOUNDED, FREE-TIME, FUEL-OPTIMAL CONTROL

The problem to be examined in this section is as follows. Determine those control variables $u(t)$, $\eta(t)$ which transfer the state solutions from arbitrary initial conditions to the specified final state

$$\omega_1(T) = \omega_2(T) = a_{13}(T) = a_{23}(T) = 0 \;,\; a_{33}(T) = 1 \tag{10}$$

while minimizing the fuel-performance index

$$J = \int_0^T ku\,dt \tag{11}$$

In the above, the product ku defines the rate of fuel consumption where $u \geq 0$, and the final time T is not specified.

The Hamiltonian function for this system is defined as

$$\begin{aligned} H = {} & -ku + p_0(a_{13}^2 + a_{23}^2 + a_{33}^2 - 1) \\ & + p_1(a\Omega\omega_2 + u\cos\eta) + p_2(-a\Omega\omega_1 + u\sin\eta) \\ & + p_3(\Omega a_{23} - \omega_2 a_{33}) + p_4(-\Omega a_{13} + \omega_1 a_{33}) \\ & + p_5(\omega_2 a_{13} - \omega_1 a_{23}) \end{aligned} \tag{12}$$

The costate differential equations can then be expressed as

$$\begin{aligned} \dot{p} + ia\Omega p &= i(a_{33}q - \alpha p_5) \\ \dot{q} + i\Omega q - i\omega p_5 &= 2p_0(t)\alpha \\ \dot{p}_5 - p_3\omega_2 + p_4\omega_1 &= 2p_0(t)a_{33} \end{aligned} \tag{13}$$

where

$$p = p_1 + ip_2 \quad , \quad q = p_3 + ip_4$$

with the complex variables α and ω defined in (9). The maximum of the function H with respect to the control angle η is satisfied by

$$\sin\eta = p_2/|p| \quad , \quad \cos\eta = p_1/|p| \tag{14}$$

Hence, the functional dependence of H upon u becomes

$$H(u) = u(-k + |p|)$$

For unbounded u, it is necessary that

$$|p| \leq k \tag{15}$$

If $|p| < k$, $u = 0$, while if $|p| = k$, the control u can be either unbounded (impulsive control), or bounded (singular or coasting arcs). The costate variables are required to be continuous, and the Hamiltonian function must satisfy

$$H(t) = 0 \ , \tag{16}$$

since the final time is unspecified, and H is not an explicit function of time.

EXTREMAL FUEL-OPTIMAL SOLUTIONS

The nature of the extremal solutions for the system considered is most easily explained in terms of the properties of the motion of the system. The free motion solution for the state equations (8) may be developed as follows. The solution to the first of (8) for $u = 0$ is

$$\omega(t) = \omega^0 e^{-i\alpha\Omega\tau} \quad , \quad \omega^0 = \omega(0) \tag{17}$$

Substitution from (17) into the remainder of (8), together with the transformation

$$\alpha = ze^{i(\theta^0 - a\Omega t)} = (z_1 + iz_1)e^{i(\theta^0 - a\Omega t)} \tag{18}$$

yields the linear time-invariant system [6]

$$\dot{z} + ib\Omega z = i|\omega^0|a_{33} \quad , \quad \dot{a}_{33} = -|\omega^0|z_2 \tag{19}$$

where

$$b = 1 - a = I_3/I \tag{20}$$

The solution for (19) is straightforward, and may be expressed as

$$\begin{aligned} a_{33}(t) &= \cos\delta^0 \cos\lambda^0 + \sin\delta^0 \sin\lambda^0 \cos\psi \\ z(t) &= \sin\delta^0 \cos\lambda^0 - \cos\delta^0 \sin\lambda^0 \cos\psi + i \sin\lambda^0 \sin\psi \\ \psi &= \psi^0 + \beta_0 t \end{aligned} \tag{21}$$

where

$$\beta_0 = [(I_3\Omega)^2 + (I|\omega^0|)^2]^{1/2}/I = |H^0|/I \quad , \tag{22}$$

and $|H^0|$ is the initial moment-of-momentum vector magnitude. Additionally,

$$\sin\delta^0 = I|\omega^0|/|H^0| \quad , \quad \cos\delta^0 = I_3\Omega/|H^0| \tag{23}$$

$$\cos\lambda^0 = H^0_{X_3}/|H^0| \tag{24}$$

$$a_{33} = \cos\gamma_3 \quad , \quad |\alpha| = |z| = \sin\gamma_3 \tag{25}$$

Fig. 1 illustrates the three angles γ_3, λ^0, and δ^0 while the planar representation of Fig. 2 shows the spherical trigonometry involved in this torque-free rigid-body solution with the spin axis precessing about the angular momentum vector at the rate β_0. The first of Eq. (21) is simply an expression of the law of cosines for arcs from spherical trigonometry.

The same basic distinction between initial condition classes noted by Porcelli and Connolly [3] for the small angle model holds here as well.

Specifically, there are two basic optimal strategies depending on whether $\lambda^0 > \delta^0$ or $\lambda^0 < \delta^0$. The optimal strategy for $\lambda^0 < \delta^0$ is the simpler, and consists of the two-impulse strategy

$$\begin{aligned} u(t) &= -J^1 e^{i(\theta^0 - a\Omega t^1)}\delta(t-t^1) \\ &\quad -J(T)e^{i(\theta^1 - a\Omega T)}\delta(t-T) \end{aligned} \tag{26}$$

where $\delta(\ )$ is the delta-dirac function. In (26) above, the initial firing time t^1 is arbitrary, and the phase of ω at t^1, θ^1, is defined by $\theta^1 = \theta^0 + a\Omega t^1$. The nature of the solution is illustrated in Fig. 3 where one notes that the first impulse generates a new angular momentum vector H^1 such that the spin axis precesses into alignment with the X_3 axis, i.e., after the first impulse $\lambda^1 = \delta^1$. The terminal impulse reduces ω to zero when x_3 and X_3 are aligned, i.e., when $\alpha(t) = 0$. The costate solution which accompanies this strategy is given from (12), (14), (15), and (26) by

$$\begin{aligned} p(t) &= -ke^{i(\theta^0 - a\Omega t)} \quad , \quad 0 \le t \le T \\ q(t) &= p_5(t) = 0 \end{aligned} \tag{27}$$

This costate solution, together with the state solutions, identically satisfies the necessary conditions of optimality. This large angle optimal solution for $\lambda^0 > \delta^0$ is identical with the small angle solution first formulated by Porcelli and Connolly [3] with a cost of

$$J = kI|\omega^0| \tag{28}$$

By contrast, there is a marked difference between the optimal solutions for the small angle model [3], [4] and the large angle direction-cosine solution for $\lambda^0 > \delta^0$ initial conditions. The small-angle solutions which

have been developed consist of two impulses, while the optimum large-angle strategy consists of an impulse followed by a singular arc. This statement is most easily confirmed by considering the special initial condition class $\delta^0 = 0$. The optimal control strategy consists of a forced precession which is not accompanied by coning, and is accomplished by directing a constant-magnitude control torque towards X_3^*, i.e.,

$$\dot{\omega} + ia\Omega\omega = Ue^{i\phi}/I \tag{29}$$

where ϕ is defined in (17), and U is a fixed control magnitude. The state solutions which correspond to (29) are

$$\begin{aligned} \omega(t) &= -i(U/I_3\Omega)e^{i\phi(t)} \\ \alpha(t) &= \sin\gamma_3(t)e^{i\phi(t)} \\ a_{33}(t) &= \cos\gamma_3(t) \end{aligned} \tag{30}$$

where

$$\phi(t) = \phi^0 - \Omega t \quad , \quad \gamma_3(t) = \lambda^0 - (U/I_3\Omega)t \tag{31}$$

The costate solutions are

$$\begin{aligned} q(t) &= -b\Omega k\cos\gamma_3 e^{i\phi} \\ p_5(t) &= b\Omega k\sin\gamma_3 \\ p(t) &= ke^{i\phi} \end{aligned} \tag{32}$$

The state and costate solutions given in (30) through (32) yield an identical satisfaction of the necessary conditions except for the $H(t) = 0$ condition given in (16), for which substitution yields

$$H(t) = kU/I_3$$

---

*This is the customary [8] ideal control path which is taken in controlling passively damped spacecraft for which $\delta^0 = 0$.

Since the execution time T and control magnitude U are related by

$$U = I_3\Omega\gamma_3^0/T = I_3\Omega\lambda^0/T ,$$

Eq. (16) is satisfied for $T \to \infty$ and $U \to 0$.

The optimal control policy for general $\lambda^0 > \delta^0$ initial conditions (i.e., $\delta^0 \neq 0$) is illustrated in Fig. 4, and consists of a coasting arc from the initial state to the point

$$\begin{aligned} \gamma_3(t) &= \gamma_3\big|_{min} = \gamma_3^1 = (\lambda^0 - \delta^0) \\ \psi(t) &= \psi^0 + \beta_0 t^1 = 2\pi \end{aligned} \tag{33}$$

At this time the impulse

$$J^1\delta(t - t^1) = -I|\omega^0|e^{i(\theta^0 - a\Omega t^1)} \tag{34}$$

is applied which eliminates ω, and places the spin axis on the singular arc to the origin. The cost of this transfer is

$$J = k[I|\omega^0| + I_3\Omega(\lambda^0 - \gamma^0)] \tag{35}$$

The costate solution for the complete $\lambda^0 > \delta^0$ transfer is given by*

$$\begin{aligned} p(t) &= k[-\sin^2\delta^0 - \cos^2\delta^0 \cos\psi + i \cos\delta^0 \sin\psi]e^{i(\theta^0 - a\Omega t)} \\ q(t) &= kb\Omega \left\{ \begin{array}{l} \sin\delta^0 \sin\lambda^0 + \cos\delta^0 \cos\lambda^0 \cos\psi \\ \quad - i \cos\lambda^0 \sin\psi \end{array} \right\} e^{i(\theta^0 - a\Omega t)} \\ p_s(t) &= kb\Omega[\sin\lambda^0 \cos\delta^0 - \cos\lambda^0 \sin\delta^0 \cos\psi] \end{aligned} \tag{36}$$

for $0 \le \tau \le t^1$. For $t^1 \le t \le T$ one has from (30) through (32)

$$\begin{aligned} p(\tau) &= ke^{i\phi} \\ q(\tau) &= -b\Omega k \cos\gamma_3 e^{i\phi} \quad , \quad p_s(\tau) = b\Omega k \sin\gamma_3 \end{aligned} \tag{37}$$

*Development of the general coast-arc costate solutions is given in Appendix A.

where

$$\tau = t - t^1$$

$$\phi(\tau) = \phi^1 - \Omega\tau = \ , \quad \phi^1 = \theta^1 + \pi = \theta^0 - a\Omega t^1 + \pi \tag{38}$$

$$\gamma_3(\tau) = \gamma_3{}^1 - (U/I_3\Omega)\tau = (\lambda^0 - \delta^0) - (U/I_3\Omega)\tau$$

The state and costate solutions cited for $0 \le t \le t^1$ identically satisfy the necessary conditions (including $H(t) = 0$). The solutions for $t^1 \le t \le T$ have the same properties as previously noted for the $\delta^0 = 0$ case. The costate variables are continuous for all time, $0 \le t \le T$. In particular, they are continuous at $t = t^1$.

CONTROL MECHANIZATION

To understand the control logic which is discussed in this section, it is worthwhile to review the following current control approach [8] employed for the active control of passively damped spacecraft. During the acquisition phase of control, the passive damper forces the spin-axis and moment-of-momentum vector into coincidence, effectively eliminating $|\omega|$. The reaction-jet system is then employed in an attempt to precess the spin-axis x_3 towards the reference X_3 axis. This precession is accomplished by a series of impulses designed to approximate the singular arc noted in the preceding section. A control impulse can either increase or decrease $|\omega|$, and it is generally speculated [5] that the net result of a sequence of impulses is a negligible change in $|\omega|$; however, should $|\dot{\omega}|$ (and hence δ) become too large, one simply waits until the passive damper reduces $|\omega|$ sufficiently, and then continues forced precessional motion.

It is proposed that a completely active control system is near optimal when operated in a manner analogous to this active control of a passively damped system. Specifically, active control is to consist of the following two sequential modes:

Mode A. Eliminate the transverse angular velocity magnitude without regard for position (angular orientation).

Mode B. Once $|\omega|$ is minimized by Mode A, initiate by repeated impulses a transfer of x_3 towards X_3. If during this transfer $|\omega|$ and hence δ) become too large, return to Mode A.

In short, Mode A control is an active replacement for the passive damper, and the development of such a system has been reported [9]. Mode B control logic does not differ from existing active-control approaches for passively damped systems [8]. By following this simplified control policy, the maximum increase in cost over the optimal $\lambda^0 < \delta^0$ cost given in (28) would be

$$\Delta J_{max} = kI_3\Omega(\lambda^0 + \delta^0) \leq 2kI_3\Omega\delta^0$$

while the increase over the $\lambda^0 > \delta^0$ optimal cost cited in (35) would be

$$\Delta J_{max} = 2kI_3\Omega\delta^0$$

Hence, the average increase in fuel-consumption would be $kI_3\Omega\delta^0$, and if one follows Porcelli's arguments [5] that δ^0 is "small" this simplified policy is seen to be quite economical.

In summary, the control mechanization suggested incorporates existing active coning control systems [9] for Mode A control and existing precessional control approaches for Mode B control [8]. Such a control

approach will closely approximate the optimal control strategy. Since it is basically a geometric control concept, it would be relatively insensitive to inertia ratios, and could be adapted to any axisymmetric configuration of interest (including time-varying systems).

SUMMARY AND CONCLUSIONS

Extremal solutions are developed herein for the unbounded, free-time, fuel-optimal control of an axisymmetric spinning body. The optimal control strategy is shown to be quite similar to existing control policies which have been separately developed for coning [9] and precessional [8] control, and a suboptimal control policy is proposed which makes use of these existing control approaches. The control approach is conceptually adequate for arbitrary initial errors, arbitrary (but non-spherical) axisymmetric inertia properties, and can be realized with one body-fixed reaction jet.

Possible extensions of this work include analysis of asymmetric spin-stabilized vehicles, and the development of additional extremal solutions for the present problem. Specifically, small angle analyses suggest the presence of another type of singular arc for control of the form

$$u(t) = -Ue^{i(\theta^0 - a\Omega t)}$$

for $\lambda^0 < \delta^0$ initial conditions with a costate solution similar to (27).

REFERENCES

1. Windeknecht, T. G., "A Simple System for Sun Orientation of a Spinning Satellite," National IAS-ARS Joint Meeting, Los Angeles, California, 1961.

2. Grubin, C., "Generalized Two Impulse Scheme for Reorienting a Spin-Stabilized Vehicle," Progress in Astronautics and Rocketry, Vol, 8, Guidance and Control, Editors: R. E. Roberson and J. S. Farrior, Academic Press, New York-London, 1962, pp. 649-668.

3. Porcelli, G., and Connolly, A., "Optimal Attitude Control of a Spinning Space Body - A Graphical Approach," IEEE Transactions on Automatic Control, July, 1966, pp. 241-249.

4. Childs, D., Tapley, B., and Fowler, W., "Suboptimal Attitude Control of a Spin-Stabilized Axisymmetric Spacecraft," IEEE Transactions on Automatic Control, Dec. 1969, pp. 736-740.

5. Porcelli, G., "Large-Angle Attitude Control of a Spinning Space Body," IEEE Transactions on Automatic Control, Dec. 1969, pp. 731-736.

6. Childs, D., "Direction-Cosine Attitude-Control Logic for Spin-Stabilized Axisymmetric Spacecraft," Accepted for publication in AIAA Journal of Spacecraft and Rockets, 14 April 1970.

7. C. F. Harding, "Solution of Euler's Gyrodynamics," ASME Journal of Applied Mechanics, pp. 325-328, June 1964.

8. NASA SP-57, Orbiting Solar Observatory Satellite, 1965.

9. Connolly, A., "An Active Nutation Control for a Spinning Spacecraft," Proceedings of the Symposium on Attitude Stabilization and Control of Dual-Spin Spacecraft, August 1967, Air Force Report SAMSO-TR-68-191, pp. 111-118.

APPENDIX A: COAST-ARC COSTATE SOLUTIONS

An interesting fact about the formulated optimization problem is that the kinematic constraint given in (7) and included in the Hamiltoni (12) has no influence on the optimal solution. This fact is verified by considering the last two equations in (13) (which are linear if $\omega(t)$ is specified). The complete solution to these equations is

$$\begin{aligned} q(t) &= q^h(t) + A(t)\,\alpha(t) \\ p_5(t) &= p_5{}^h(t) + A(t)\,a_{33}(t) \end{aligned} \tag{A.1}$$

where the superscript h denotes the homogeneous solution and the scalar function $A(t)$ is defined by $\dot{A}(t) = 2p_0(t)$. Substitution from (A.1) into the first of (13) yields

$$\dot{p} + ia\Omega p = i(a_{33}q^h - \alpha p_5{}^h)$$

Hence, the terms $2p_0\alpha$ and $2p_0a_{33}$ which arise in (13) (due to the constraint (7)) have no influence on the switching function. In addition, substitution from (A.1) into (12) confirms that these terms have no influence on $H(t)$ either, and the system whose solution is sought becomes from (13)

$$\begin{aligned} \dot{p} + ia\Omega p &= i(a_{33}q - \alpha p_5) \\ \dot{q} + i\Omega q - i\omega p_5 &= 0 \\ \dot{p} - p_3\omega_2 + p_4\omega_1 &= 0 \end{aligned} \tag{A.2}$$

In analogy with (18), the transformation

$$q(t) = ve^{i(\theta^0 - a\Omega t)} \tag{A.3}$$

yields the solution for v and p_5

$$
\begin{aligned}
v/B &= \sin\delta^0 \cos\Lambda^0 - \cos\delta^0 \sin\Lambda^0 \cos\Psi + i \sin\Lambda^0 \sin\Psi \\
p_5/B &= \cos\delta^0 \cos\Lambda^0 + \sin\delta^0 \sin\Lambda^0 \cos\Psi
\end{aligned}
\qquad (A.4)
$$

where B is a scalar constant, and

$$\Psi = \Psi^0 + \beta_n t$$

The solution for the first of (A.2) is

$$p(t) = p^0 e^{-ia\Omega t} + ie^{-ia\Omega t} \int_0^t e^{ia\Omega x}(a_{33}q - \alpha p_5)dx$$

From (A.3) and (18),

$$p(t) = p^0 e^{-ia\Omega t} + ie^{i(\theta^0 - a\Omega t)} \int_0^t (a_{33}v - zp_5)dx$$

Substituting from (A.4) and (21) followed by integration yields

$$p(t) = p^0 e^{-ia\Omega t} + ie^{i(\theta^0 - a\Omega t)} B\, Z(t)/\beta_0$$

where

$$
\begin{aligned}
Z(t) = {} & -i \cos\delta^0 \cos\lambda^0 \sin\Lambda^0(\cos\Psi - \cos\Psi^0) \\
& +i \cos\delta^0 \cos\Lambda^0 \sin\lambda^0(\cos\psi - \cos\psi^0) \\
& -\cos\lambda^0 \sin\Lambda^0(\sin\Psi - \sin\Psi^0) \\
& +\sin\lambda^0 \cos\Lambda^0(\sin\psi - \sin\psi^0) \\
& +i\, t \sin\lambda^0 \sin\delta^0 \sin\Lambda^0 \sin(\Psi^0 - \psi^0,
\end{aligned}
$$

LIST OF FIGURES

Figure 1
D. Childs

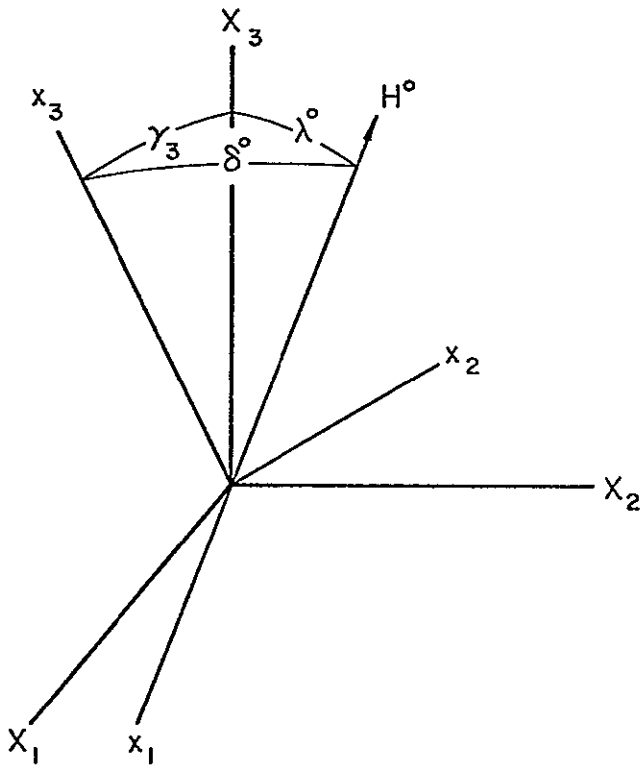

Figure 2
D. Childs

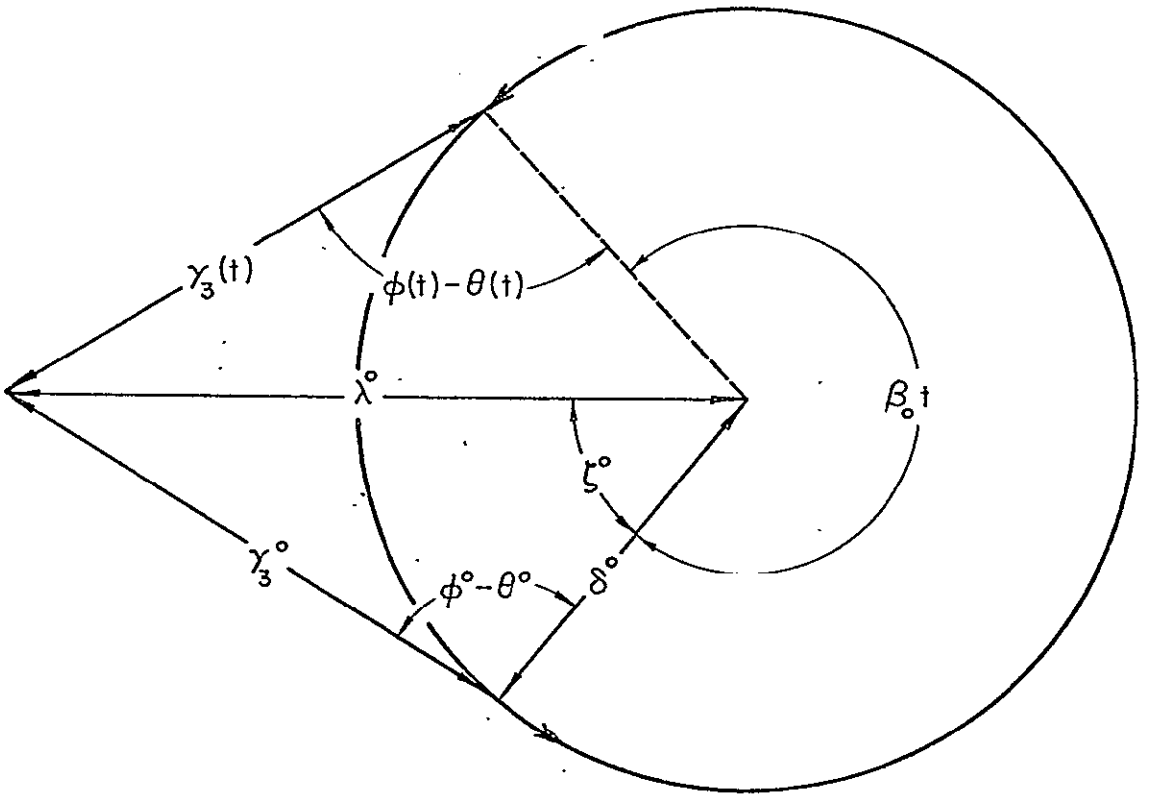

Figure 3.
D. Childs

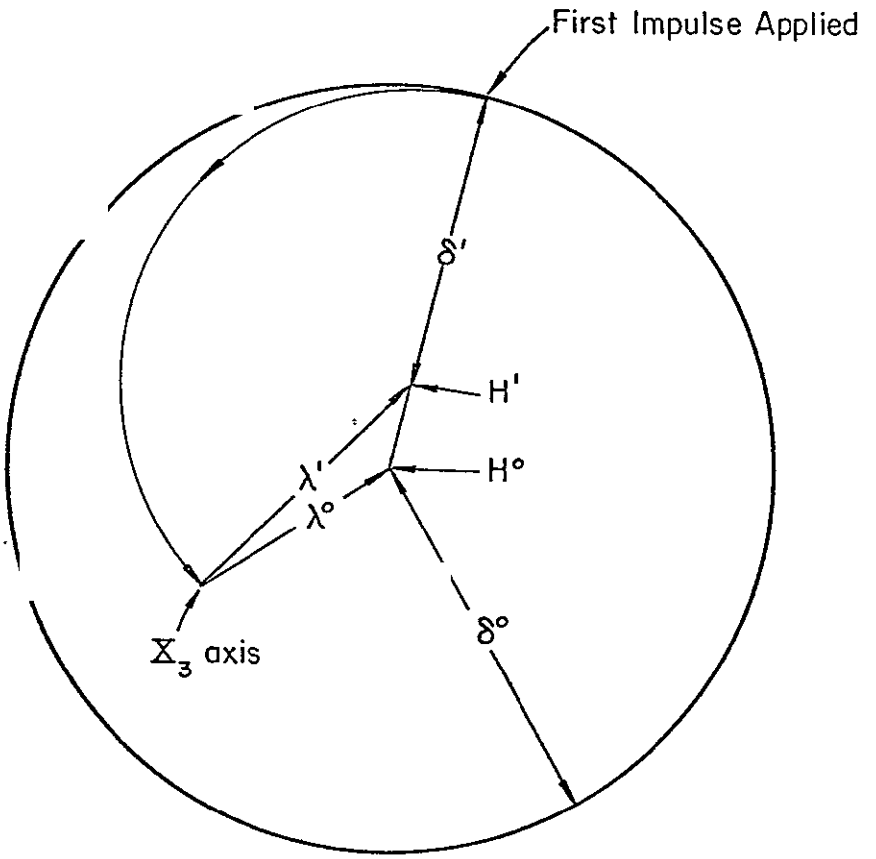

Figure 4
D. Childs

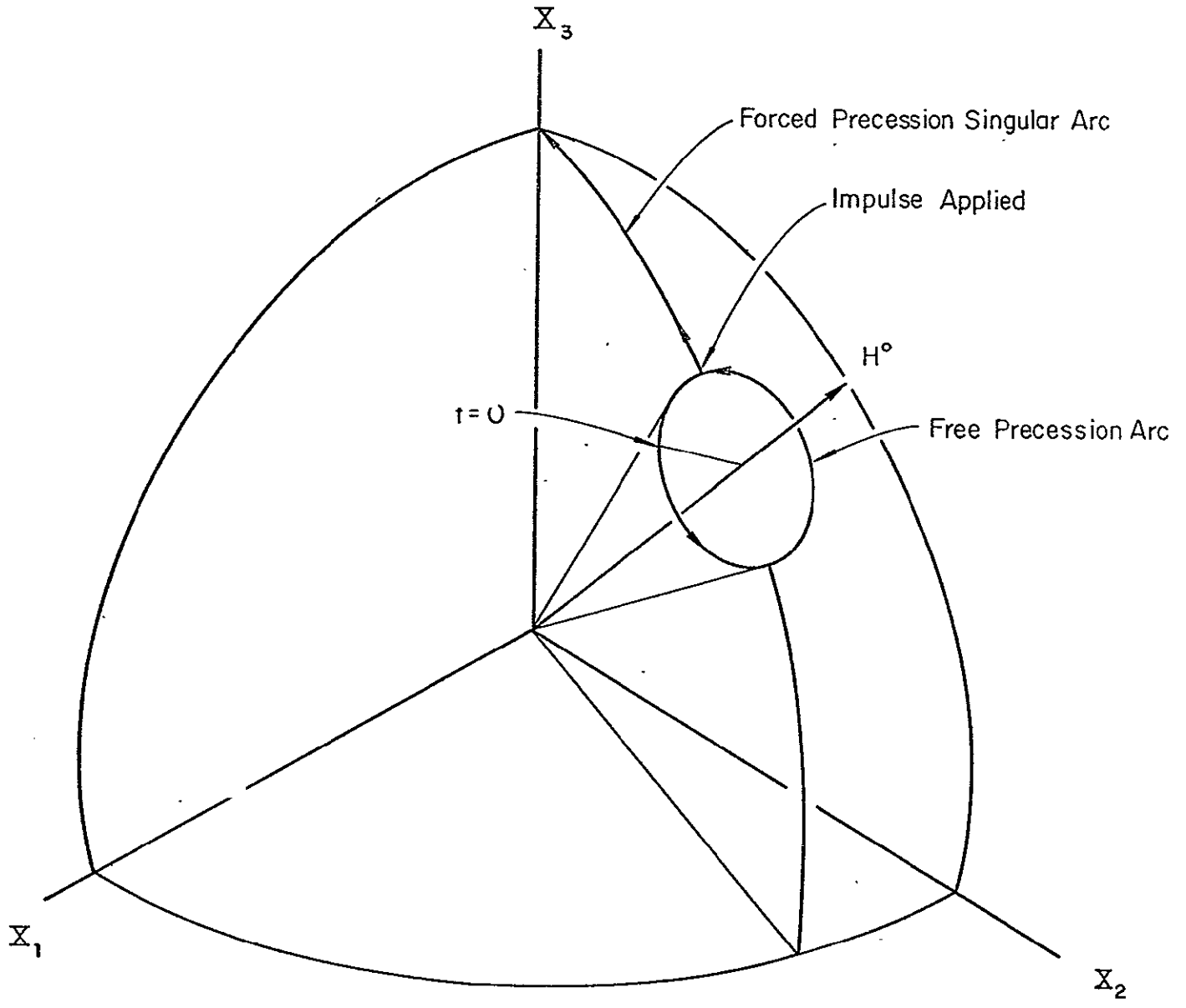

TORQUE FREE MOTION OF SPIN STABILIZED SPACECRAFT

D. C. Garvey

Abstract

This paper presents an approximate analytical solution for torque free motion of a slightly asymmetric spinning body. The solution developed is not restricted by either a constant spin speed or a small angle assumption. Accuracy comparisons between the approximate analytical solution and exact numerical integration solutions are provided for a particular inertia ratio and degree of asymmetry.

Introduction

Previous authors [1-5] have demonstrated the advantages of employing an impulsive attitude control logic for spin stabilized spacecraft. In each case a mathematical model of the torque free motion of a spinning body is presented in terms of a system of differential equations. For slightly asymmetric spacecraft these models employ the assumptions of constant spin speed and small Euler angles to obtain analytical solutions [2, 4]. When it becomes necessary to maintain attitude control through large angular displacements or the degree of asymmetry increases these assumptions are no longer applicable. Childs [5] has developed a mathematical model for an axisymmetric spacecraft which avoids the small angle restriction by employing direction cosines. This paper presents a mathematical model describing the torque free motion of a slightly asymmetric spacecraft in terms of direction cosines and avoids the assumptions of small angles and constant spin speed.

Analysis

Let R_i define the reference axes and let x_i denote the spacecraft fixed axes where the origin of both axes is located at the spacecraft center of mass. Thus Euler's equations for torque free motion are given by

$$\begin{aligned} \dot{\omega}_1 &= -((I_3 - I_2)/I_1)\omega_2\ \omega_3 \\ \dot{\omega}_2 &= ((I_3 - I_1)/I_2)\omega_1\ \omega_3 \\ \dot{\omega}_3 &= ((I_1 - I_2)/I_3)\omega_1\ \omega_2. \end{aligned} \tag{1}$$

Conservation of energy requires that

$$I_1\omega_1^2 + I_2\omega_2^2 + I_3\omega_3^2 = 2T \tag{2}$$

while conservation of angular momentum requires

$$(I_1\omega_1)^2 + (I_2\omega_2)^2 + (I_3\omega_3)^2 = H^2 \tag{3}$$

Employing (2) and (3) one obtains

$$\omega_1^2 = C_1^2 - C_2^2\omega_2^2 \tag{4}$$

$$\omega_3^2 = C_3^2 - C_4^2\omega_2^2 \tag{5}$$

where

$$C_1^2 = (H^2 - 2TI_3)/(I_1(I_1 - I_3))$$

$$C_2^2 = I_2(I_2 - I_3)/(I_1(I_1 - I_3))$$

$$C_3^2 = (2TI_1 - H^2)/(I_3(I_1 - I_3))$$

$$C_4^2 = I_2(I_1 - I_2)/(I_3(I_1 - I_3))$$

and $I_1 \leq I_2 < I_3$ or $I_1 \geq I_2 > I_3$

The general solution to (1) may be expressed in terms of elliptic integrals by utilizing (4) and (5) [6]. However, this form of a solution is awkward and does not provide a great deal of physical insight. Previous authors [2-4] have shown that for an axisymmetric spacecraft or a slightly asymmetric spacecraft with a constant spin speed assumption an analytical solution to (1) is readily obtained. Inspection of Euler's equations demonstrates that the assumption of constant spin speed becomes unacceptable as the degree of spacecraft asymmetry increases.

In this analysis a more general solution to (1) is developed in terms of a power series and is applicable to axisymmetric or slightly asymmetric spacecraft. Introduce the variables

$$\bar{I} = (I_1 + I_2)/2 \qquad \varepsilon = (I_1 - I_2)/\bar{I}$$

such that (1) can be written as

$$\begin{aligned} \dot{\omega}_1 &= -a\omega_2\omega_3 - \varepsilon P\omega_2\omega_3 \\ \dot{\omega}_2 &= a\omega_1\omega_3 - \varepsilon P\omega_1\omega_3 \\ \dot{\omega}_3 &= \varepsilon(\bar{I}/I_3)\omega_1\omega_2 \end{aligned} \tag{6}$$

where $a = (I_3 - \bar{I})/\bar{I}$ and $P = (\bar{I} - (I_3/2))/I_1$

and terms of order ε^2 are neglected. The solution to (6) can be demonstrated [7] to be

$$\begin{aligned} \omega_1(t) &= |\omega^0|\cos(a\Omega t+\rho^0)-\varepsilon|\omega^0|\{aK\sin(a\Omega t+\rho^0)\cdot N(t)+(P/a)\sin a\Omega t\sin\rho^0\} \\ \omega_2(t) &= |\omega^0|\sin(a\Omega t+\rho^0)+\varepsilon|\omega^0|\{aK\cos(a\Omega t+\rho^0)\cdot N(t)-(P/a)\sin a\Omega t\cos\rho^0\} \\ \omega_3(t) &= \Omega + \varepsilon K\{\cos 2\rho^0 - \cos(2(a\Omega t + \rho^0))\} \end{aligned} \tag{7}$$

where

$$N(t) = t\cdot\cos 2\rho^0 - (\sin(2(a\Omega t + \rho^0)) - \sin 2\rho^0)/(2a\Omega)$$

$$|\omega^0| = ((\omega_1{}^0) + (\omega_2{}^0)^2)^{\frac{1}{2}} \qquad \rho^0 = \tan^{-1}(\omega_2{}^0/\omega_1{}^0)$$

$$\Omega = \omega_3{}^0 \qquad \text{and} \qquad K = (\bar{I}|\omega^0|^2)/(4I_3\Omega a)$$

Previous authors have used Euler angles [2,3], direction cosines [5] and Euler's symmetrical parameters [8] as the kinematic variables defining body axes orientation relative to reference axes. Childs [5] has demonstrated the advantages of selecting direction cosines which are employed in this analysis.

To characterize the properties of the direction cosine matrix [A] consider an arbitrary vector v. This vector may be expressed in body axis coordinates as v_x and in reference axis coordinates as v_R. The

direction cosine matrix then satisfies

$$v_X = [A]v_R \quad , \quad v_R = [A]^T v_X \tag{8}$$
$$[A]^T[A] = [I]$$

where T denotes the transpose and [I] is the identity matrix. The relationship between the direction cosine matrix and the spacecraft angular velocity is given by [9]

$$\dot{[A]} = [W][A] \tag{9}$$

where

$$[W] = \begin{bmatrix} 0 & \omega_3 & -\omega_2 \\ -\omega_3 & 0 & \omega_1 \\ \omega_2 & -\omega_1 & 0 \end{bmatrix}$$

and is subject to the above constraint.

The direction cosines illustrated in Figure 1 are of particular interest in defining the attitude of a spin stabilized spacecraft. These terms define the spin axis orientation relative to a desired reference direction (R_3). From (9) one obtains

$$\begin{aligned} \dot{a}_{13} &= \omega_3 a_{23} - \omega_2 a_{33} \\ \dot{a}_{23} &= -\omega_3 a_{13} + \omega_1 a_{33} \\ \dot{a}_{33} &= \omega_2 a_{13} - \omega_1 a_{23} \end{aligned} \tag{10}$$

with $a_{13}^2 + a_{23}^3 + a_{33}^2 = 1.$

The orientation of body axes x_i relative to the reference axes R_i is defined in terms of an intermediate coordinate system X_i. For torque free motion it is convenient to choose this coordinate system such that

X_3 coincides with the angular momentum vector H. The angular rotations B^0 and λ^0 which orient the X_i coordinate system are defined in terms of the angular momentum vector at the initial time. The angular rotation B^0 is given by

$$B^0 = \tan^{-1}(H^0_{R2}/H^0_{R1}) + \pi \tag{11}$$

about R_3 and λ^0 is defined as

$$\lambda^0 = \cos^{-1}(H^0_{R3}/H) \tag{12}$$

about $-R_2$. Hence, an arbitrary vector v in the R_i coordinate system is expressed in the X_i coordinate system as

$$v_X = [\lambda^0][B^0]\, v_R \tag{13}$$

The orientation of body axes x_i relative to X_i is defined by the three Euler angle rotations ϕ about X_3, θ about X_2^1, and ψ about x_3 such that

$$v_X = [\psi][\theta][\phi]\, v_X \tag{14}$$

The angular velocity of the spacecraft is related to the three Euler angle rotations by

$$\begin{aligned} \dot{\phi} &= (\omega_2 \sin\psi - \omega_1 \cos\psi)/\sin\theta \\ \dot{\rho} &= \omega_1 \sin\psi + \omega_2 \cos\psi \\ \dot{\psi} &= \omega_3 + \cot\theta(\omega_1 \cos\psi - \omega_2 \sin\psi) \end{aligned} \tag{15}$$

A solution to (15) is readily obtained. The angular momentum vector in the X_i coordinate system is given by

$$\overline{H}_X = Hk \tag{16}$$

where k is a unit vector in the X_3 direction. This vector can be ex-

pressed in the x_i coordinate system as

$$H_X = [\psi][\theta][\phi]\, H_X \tag{17}$$

Expanding (17) into component form one obtains

$$\begin{aligned} I_1\omega_1 &= -H\cos\psi\sin\theta \\ I_2\omega_2 &= H\sin\psi\sin\theta \\ I_3\omega_3 &= H\cos\theta \end{aligned} \tag{18}$$

Thus angles ψ and θ are defined as

$$\psi = \tan^{-1}(I_2\omega_2/-I_1\omega_1) \tag{19}$$

$$\theta = \cos^{-1}(I_3\omega_3/H) \tag{20}$$

The remaining angle ϕ is obtained from (15). The above results, together with (3) and (5) yield

$$\dot{\phi} = H(2T - I_3\omega_3{}^2)/(H^2 - I_3{}^2\omega_3{}^2) \tag{21}$$

Neglecting terms of order ε^2 the solution to (21) is given by

$$\phi = \phi^0 + A_0 t + \varepsilon A_1(t\cdot\cos 2\rho^0 - (1/2a\Omega)(\sin(2(a\Omega t+\rho^0)) - \sin 2\rho^0)) \tag{22}$$

where

$$A_0 = H(2T - I_3\Omega^2)/(H^2 - I_3{}^2\Omega^2)$$

$$A_1 = H\bar{I}|\omega^0|^2(2TI_3 - H^2)/(2a(H^2 - I_3{}^2\Omega^2)^2)$$

and the initial condition ϕ^0 is unspecified.

The results obtained by introducing the additional kinematic variables are combined to yield analytical expressions for each of the direction cosine elements a_{ij}. From (13) and (14) one obtains

$$\bar{v}_X = [\psi][\theta][\phi][\lambda^0][\beta^0]\,\bar{v}_R \tag{23}$$

Performing the matrix multiplication yields [A]. In particular

$$\begin{aligned} a_{13} &= (\cos\psi\cos\theta\cos\phi - \sin\psi\sin\phi)\sin\lambda^0 - \sin\theta\cos\psi\cos\lambda^0 \\ a_{23} &= -(\sin\psi\cos\theta\cos\phi + \cos\psi\sin\phi)\sin\lambda^0 + \sin\theta\sin\psi\cos\lambda^0 \\ a_{33} &= \cos\theta\cos\lambda^0 + \sin\theta\sin\lambda^0\cos\phi \end{aligned} \tag{24}$$

In (24) ψ, θ and ϕ are given by (19), (20) and (22) with ϕ^0 defined in terms of a_{33} at the initial time.

Discussion

Equations (6) and (10) define a general mathematical model for torque free motion of an axisymmetric to slightly asymmetric spin stabilized spacecraft in terms of direction cosines. The analytical solutions to these equations are given by (7) and (24).

It is of interest to investigate the analytical solutions developed for a slightly asymmetric spacecraft. In general ($|\omega^0| \neq 0$) (7) indicates that the spin axis component of angular momentum is periodic. When this component of momentum is a maximum, conservation of angular momentum requires that the transverse component be a minimum. This result when combined with (20) defines a cone angle with a periodically varying amplitude. It is of particular interest to consider the final expression in (24) which may be written as

$$\cos\gamma_{33} = \cos\lambda^0\cos\theta + \sin\lambda^0\sin\theta\cos\phi \tag{25}$$

For the previously defined sequence of angular rotations ϕ, θ and ψ,

(25) is a statement of the Law of Cosines from spherical trigonometry. This result provides a simple geometrical description of spin axis motion relative to a desired reference direction and is depicted in Figure 2.

To form a measure of comparison between the analytical solution and the exact solution as determined by machine computation a numerical example is considered. In this example spacecraft initial conditions and moment of inertia ratio $(\bar{I}/I_3)$ remain constant while ε is varied. With this approach a measure of the effect of asymmetry upon agreement of the analytical solution with the exact or numerical solution is determined. The solutions are compared over a time interval approximating the time required for the spin axis to precess twice about the angular momentum vector. Table 1 lists the data employed in this example.

Figures 3 to 5 depict a comparison between the exact and analytical solutions for a_{33} with the data of Table 1. For an axisymmetric spacecraft the analytical solutions are the exact solutions as shown in Figure 3. The results for a slightly asymmetric spacecraft are illustrated in Figures 4 and 5. These figures demonstrate that for a constant moment of inertia ratio of

$$(\bar{I}/I_3) = 1.7$$

agreement between the two solutions is a function of both solution time and degree of asymmetry. In the example considered for which

$$0 < \varepsilon \leq 0.2$$

and the solution time approximates the time required for one precession of the spin axis about the angular momentum vector satisfactory agreement between the two solutions is achieved.

Summary

In this analysis a mathematical model of the torque free motion of an axisymmetric to slightly asymmetric spin stabilized spacecraft is developed. The differential equations describing spacecraft dynamics are given by (6) and spacecraft kinematics are defined in terms of direction cosines by (10). Analytical solutions to these differential equations without the assumptions of small angles or constant spin speed are given by (7) and (24).

Analysis of the analytical solutions has shown that for a slightly asymmetric spacecraft both the spin axis component of angular momentum and the amplitude of the cone angle are periodic. It has also been demonstrated that the motion of the spin axis about the angular momentum vector may be expressed in terms of the Law of Cosines for sides of a spherical triangle.

The analytical solutions obtained are the exact solutions for an axisymmetric spacecraft. For a slightly asymmetric spacecraft the study of a numerical example with moment of inertia properties

$$(\overline{I}/I_3) = 1.7 \quad \text{and} \quad 0 < \varepsilon \leq 0.2.$$

indicates that the approximate analytical solution compares favorably with the exact solution over one precession cycle.

Table 1 Example Data

Initial Conditions		
$a_{11} = 0.877583$	$a_{12} = 0.22984$	$a_{13} = -0.420735$
$a_{21} = 0.000000$	$a_{22} = 0.877583$	$a_{23} = 0.479426$
$a_{31} = 0.479426$	$a_{32} = -0.420753$	$a_{33} = 0.770151$
$\omega_1 = 0.150000$	ω_2 0.150000	$\omega_3 = 0.628319$

Moment of Inertia Parameters

I_1	I_2	I_3	$\bar{I}$	ε
3400.	3400.	2000.	3400.	0.0
3740.	3060.	2000.	3400.	0.2
3910.	2890.	2000.	3400.	0.3

References

1. Grubin, C., "Generalized Two-Impulse Scheme for Reorienting a Spin Stabilized Vehicle," Progress in Astronautics and Rocketry, Academic Press Inc., New York, 1962, Vol. 8, pp. 649-668.

2. Dobrotin, B. and Nicklas, J., "Spin Stabilized Spacecraft," JPL Space Programs Summary No. 37034, Vol. IV, pp. 66-77.

3. Porcelli, G. and Connolly, A., "Optimal Attitude Control of a Spinning Space-Body a Graphical Approach," IEEE Trans. Automatic Control, Vol. AC-12, June 1967, pp. 41-49.

4. Wheeler, P. C., "Two-Pulse Attitude Control of an Asymmetric Spinning Satellite," Progress in Astronautics and Aeronautics, Academic Press Inc., New York, 1964, Vol. 13, pp. 261-287.

5. Childs, D., "Direction-Cosine Attitude-Control Logic for Spin-Stabilized Axisymmetric Spacecraft," Accepted for publication in AIAA Journal of Spacecraft and Rockets, 14 April 1970.

6. Whittaker, E. T., "Analytical Dynamics of Particles and Rigid Bodies," Cambridge University Press, New York, 1964, pp. 144-152.

7. Moulton, F. R., "Differential Equations," Dover, New York, 1958, pp. 39-56.

8. Mitchell, E. E. and Rogers, A. E., "Quaternion Parameters in the Simulation of a Spinning Rigid Body," Simulation, McGraw-Hill, New York, 1968, pp. 33-39.

9. Sabroff, A., et al., "Investigation of the Acquisition Problem in Satellite Attitude Control," Tech. Report AFFDL-TR-65-115, Dec. 1965, Air Force Flight Dynamics Laboratory, Wright Patterson Air Force Base, Ohio.

LIST OF FIGURES

Fig. 1. D. Garvey

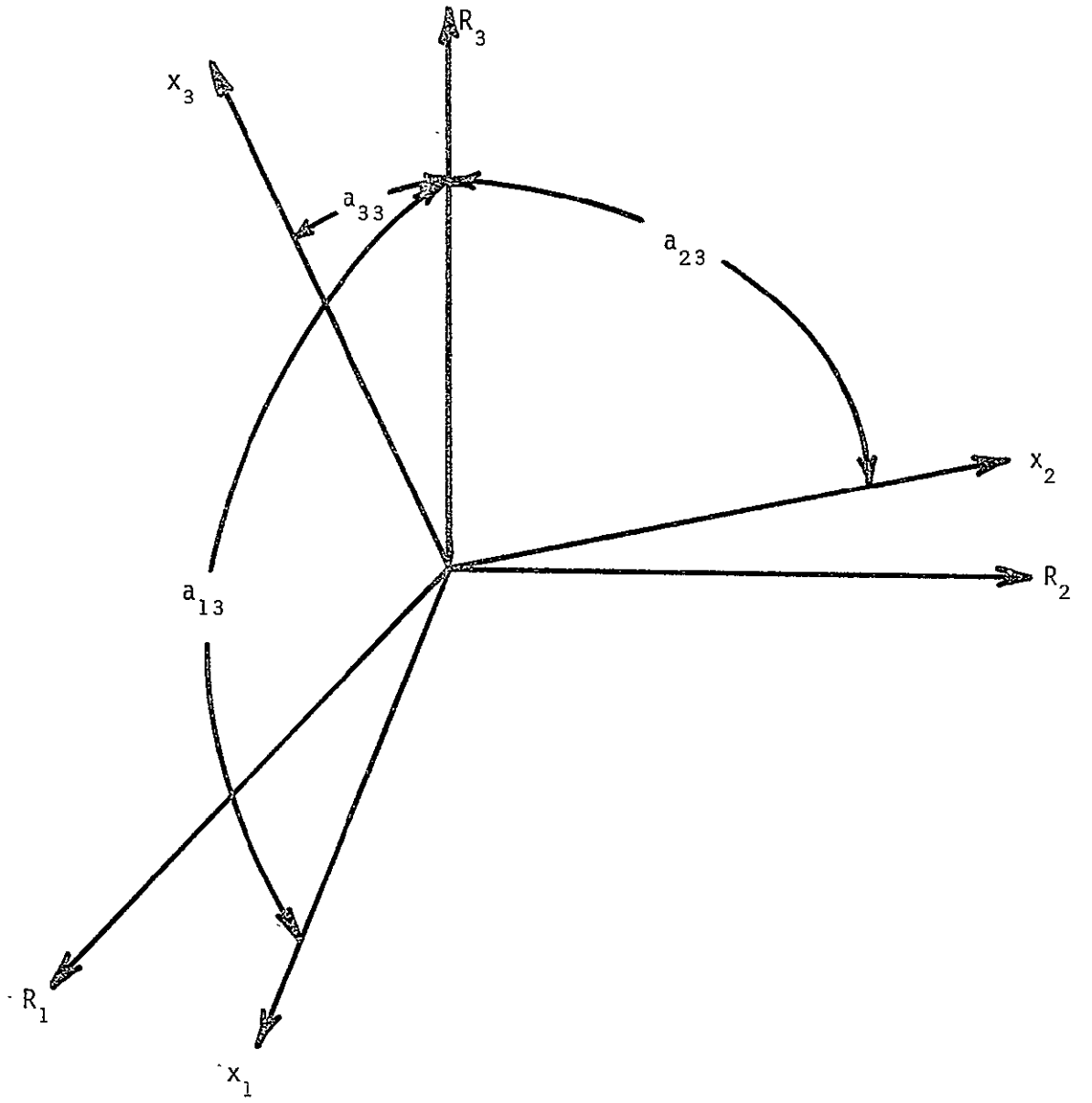

Fig. 2. D. Garvey

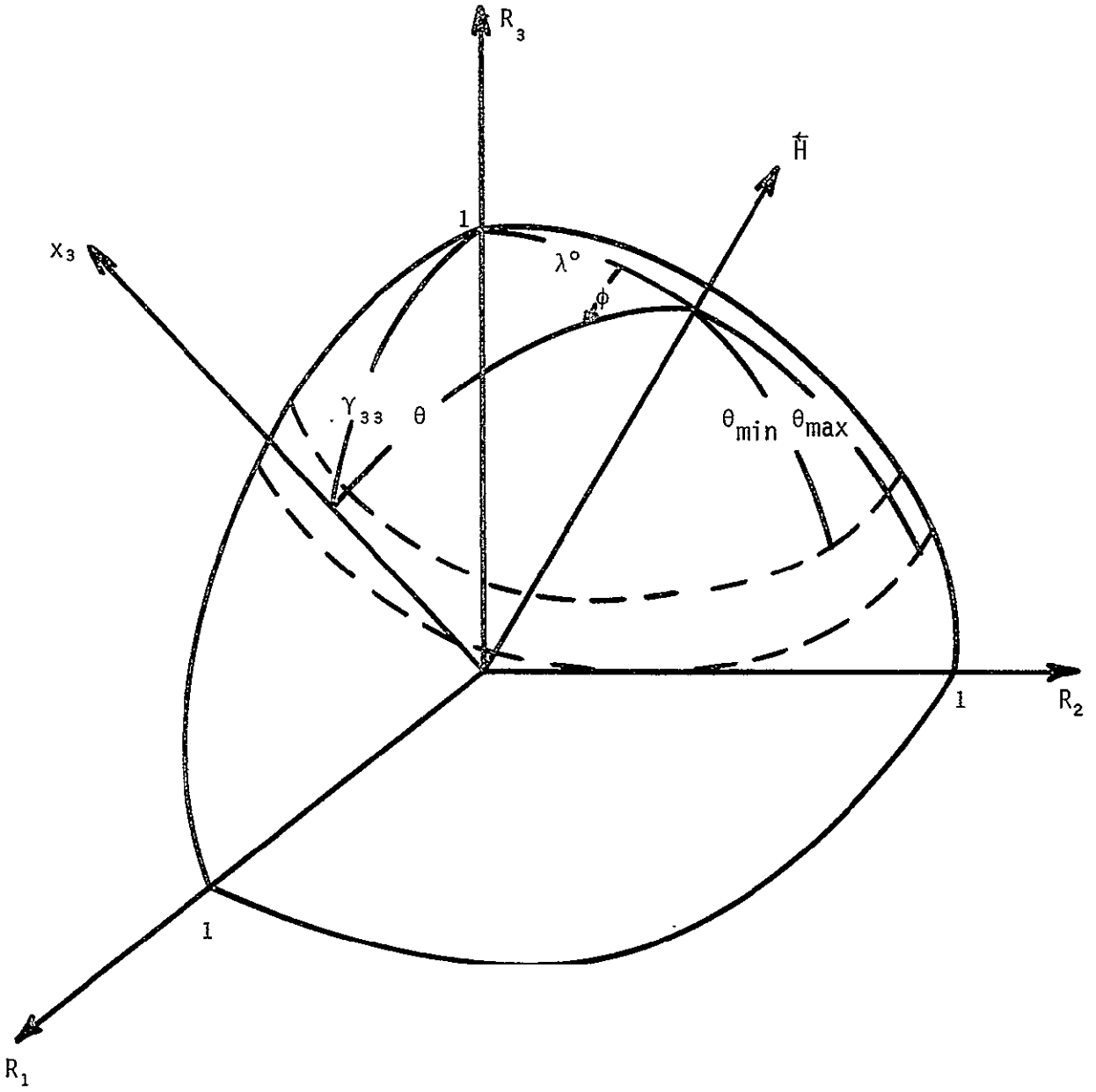

Fig. 3. D. Garvey

——— Analytical and Numerical Solution

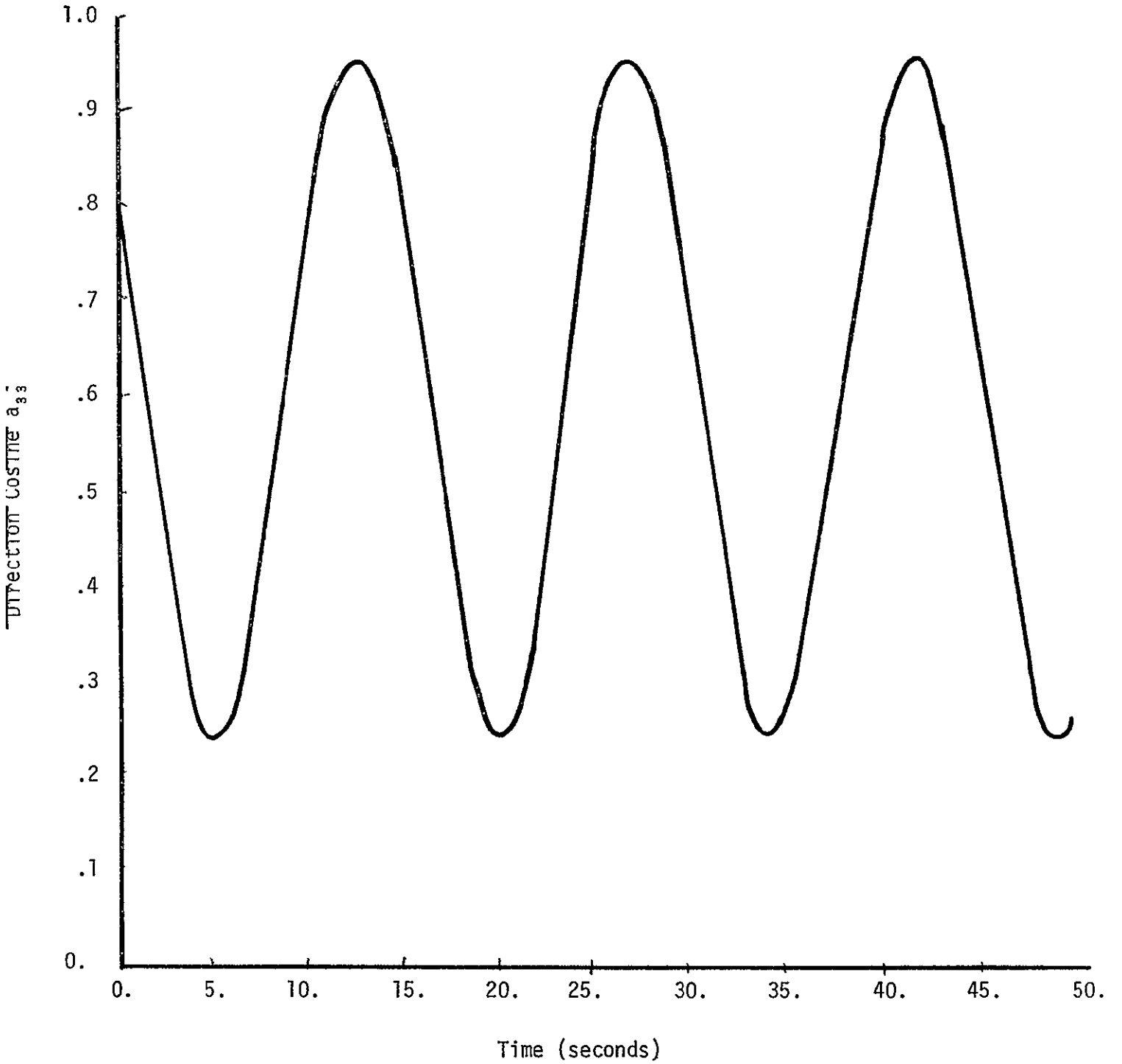

Fig. 4. D. Garvey

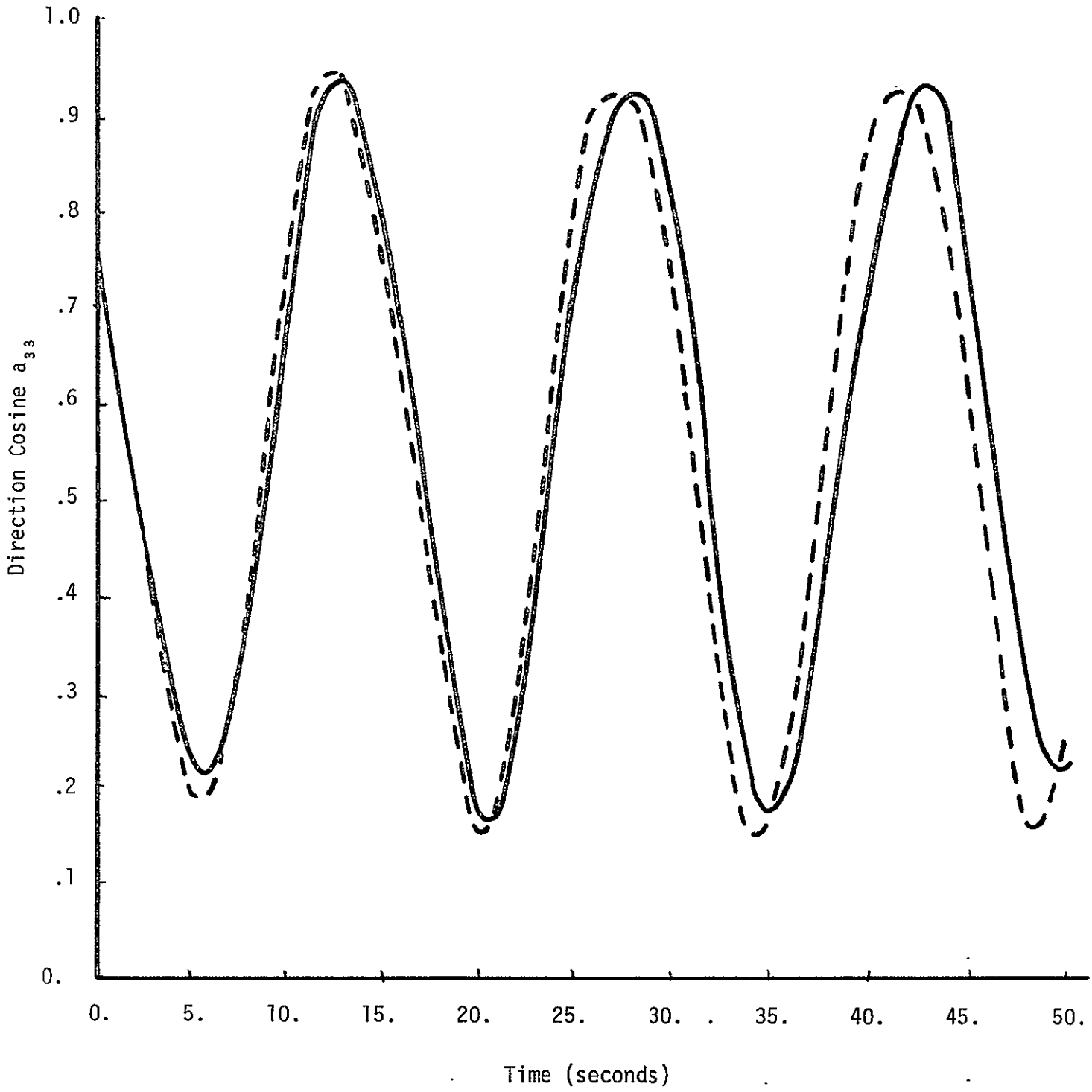

Fig. 5. D. Garvey

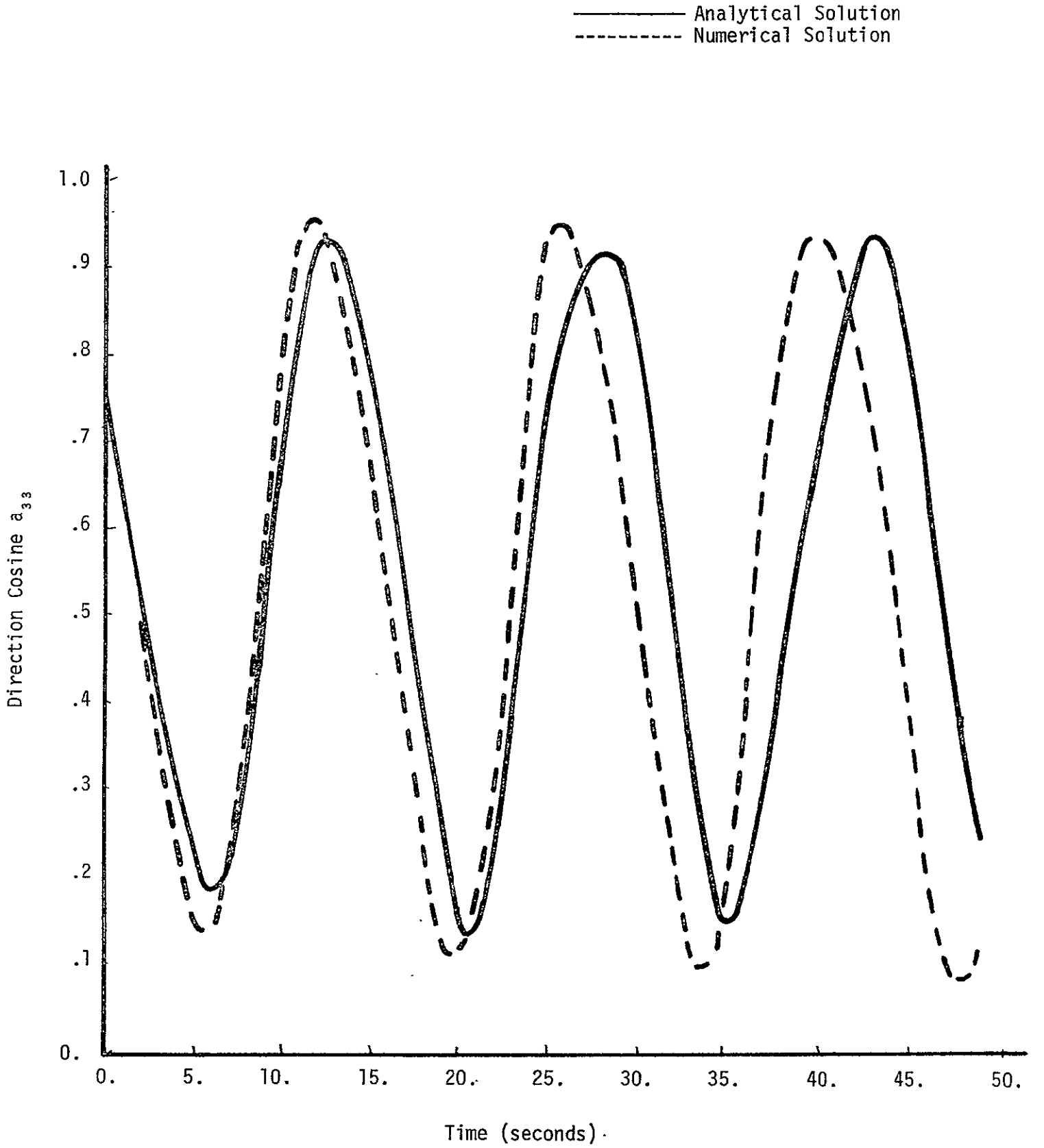

SPACE-BASED ORBIT DETERMINATION*

N. Duong**
C. Byron Winn+

ABSTRACT

Techniques are investigated for orbit determination using range-only data. Two specific problems are examined; the first is the determination of arbitrary orbits using range information obtained from a space base in synchronous orbit while the second problem is the determination of the orbit of a near synchronous satellite. Specific examples are presented and comparisons are made between orbit determination by use of ground stations and by satellites.

---

*This work was supported in part under NASA Research Grant NGR 06-002-085. This financial support is gratefully acknowledged.

**Graduate Student, Mechanical Engineering, Colorado State University.

+Associate Professor, Mechanical Engineering, Colorado State University.

Nomenclature

Symbols	Definitions	Units
a	semi-major axis of the orbit of the target satellite	earth-radii
e	eccentricity of the orbit of the target satellite	non-dimensional
i	inclination of the target satellite orbit plane	radians
Ω	longitude of the ascending node of target sat. orbit	radians
ω	argument of perigee of target satellite orbit	radians
T	time of perigee passage of target satellite	seconds
r_s	distance from target satellite to geocenter	earth-radii
V_s	velocity of target satellite	radii/sec
E	eccentric anomaly of target satellite	radians
ρ	slant-range	earth-radii
μ	gravitational constant of the Earth	$(\text{radii})^3/\text{sec}^2$
δ	declination of the tracking satellite	radians
α	right ascension of the tracking satellite	radians
d	distance from tracking satellite to geocenter	earth-radii
δ_s	declination of the geostationary target satellite	radians
α_s	right ascension of the geostationary target satellite	radians
d_s	distance from geostationary target satellite to geocenter	earth-radii
t_o	time starting the range measurements	seconds
ω_E	angular velocity of the rotation of the Earth	radians/sec

1. Introduction

Techniques involving range only data for orbit determination have been investigated by several researchers in the past. The method of R. M. L. Baker, Jr., based on the synthesis of the classical f and g series of celestial mechanics with certain unified formulae developed by S. Herrick, has been applied to range only orbit determination using ground-based tracking stations [Baker]. The technique does not give adequate information for orbit determination when the tracking stations are near the poles or equator. In addition, the ground based tracking stations provide limited coverage. Consequently some investigations into the use of space-based tracking stations have been conducted. The feasibility of using range only data to determine circular orbits has been demonstrated [Ball]. The possibility of using range and range rate information and combining tracking data obtained from satellites with ground based data to improve orbit determination accuracy has also been investigated [Johnson, Mullin, and Steiner].

The purpose of this research has been to develop a general method for determining the orbit of a target satellite from range only data obtained from a single space-based tracking station.

2. Description of the Method

For the purpose of this initial study, it has been assumed that the earth is spherical and that no perturbations appear as the result of air drag, solar radiation, lunar attraction, or any other cause. It is further assumed that approximate values of position and velocity, $\vec{r}_s$ and $\vec{v}_s$,

at a certain time t are known. The situation is described by the following sketch.

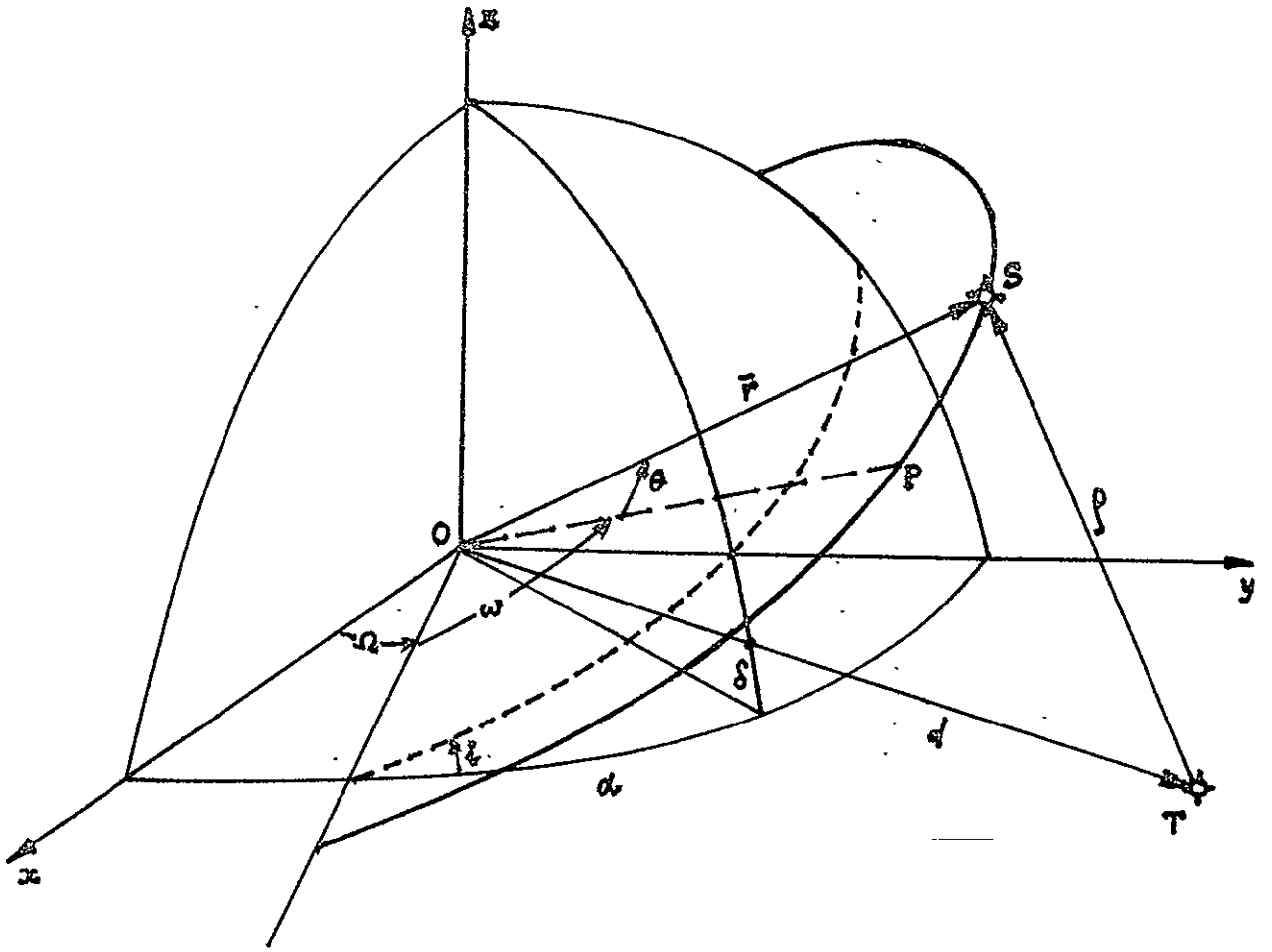

From the basic vector relationship

$$\vec{\rho} = \vec{r} - \vec{d}$$

or

$$\vec{\rho}\cdot\vec{\rho} = \rho^2 = r^2 + d^2 - 2\vec{r}\,\vec{d} \qquad (1)$$

one can get an expression for ρ in terms of the orbital elements a, e, i, Ω, ω, E of the target satellite S and the elements of position

α, δ, d of the tracking satellite T in the form

$$\rho(a, e, i, \Omega, \omega, E, \alpha, \delta, d) \tag{2}$$

Let ρ_o be the observed value of range, and ρ_c the computed value of range from expression (2). The range residuals are

$$\Delta\rho = \rho_o - \rho_c \tag{3}$$

Calculating ρ_c requires initial estimates of a, e, i, Ω, ω, E, which can be computed from approximate values of $\vec{r}_s$ and $\vec{v}_s$.

Using Kepler's equation

$$E - e \sin E = \sqrt{\frac{\mu}{a^3}}\,(t - T) \tag{4}$$

one can write $\Delta\rho$ in terms of the corrections Δa, Δe, Δi, $\Delta\Omega$, $\Delta\omega$, ΔT as

$$\Delta\rho = \left\{\frac{\partial\rho}{\partial a} + \frac{\partial\rho}{\partial E}\frac{\partial E}{\partial a}\right\}\Delta a + \left\{\frac{\partial\rho}{\partial e} + \frac{\partial\rho}{\partial E}\frac{\partial E}{\partial e}\right\}\Delta e + \left\{\frac{\partial\rho}{\partial i}\right\}\Delta i$$

$$+ \left\{\frac{\partial\rho}{\partial\Omega}\right\}\Delta\Omega + \left\{\frac{\partial\rho}{\partial\omega}\right\}\Delta\omega + \left\{\frac{\partial\rho}{\partial E}\frac{\partial E}{\partial T}\right\}\Delta T \tag{5}$$

The coefficients of Δa, Δe, Δi, $\Delta\Omega$, $\Delta\omega$, ΔT can be found by differentiating equation (2) with respect to a, e, i, Ω, ω, E and taking account of relation (4).

The equation (5) represents a set of equations (one for each observation time) which can be solved for Δa, Δe, Δi, $\Delta\Omega$, $\Delta\omega$, and ΔT by the method of least squares.

The next approximations to the orbital elements of the target satellite is:

$$\begin{aligned} a' &= a + \Delta a \\ e' &= e + \Delta e \\ i' &= i + \Delta i \end{aligned} \tag{6}$$

$$\Omega' = \Omega + \Delta\Omega$$

$$\omega' = \omega + \Delta\omega$$

$$T' = T + \Delta T$$

One can obtain the new value of E by solving Kepler's equation. The a', e', i', Ω', ω', E' are then substituted back into equation (2) and ρ_c is computed again.

New residuals are formed from equation (3), and new corrections to a, e, i, Ω, ω, E are computed from (5) and (4). After which we get the next approximation to a, e, i, Ω, ω, T from equation (5). This process is repeated until the residuals $\Delta\rho$ are sufficiently small.

3. Range Equation and its Partial Derivatives

With respect to the geocentric inertial frame Oxyz, the coordinates of the tracking satellite T are

$$x_\tau = d \cos\delta \cos\alpha$$

$$y_\tau = d \cos\delta \sin\alpha$$

$$z_\tau = d \sin\delta$$

and the coordinates of the target satellite S are

$$x_s = a\{(\cos E - e)(\cos\Omega \cos\omega - \sin\Omega \sin\omega \cos i) - \sqrt{1-e^2} \sin E(\cos\Omega \sin\omega + \sin\Omega \cos\omega \cos i)\}$$

$$y_s = a\{(\cos E - e)(\sin\Omega \cos\omega + \cos\Omega \sin\omega \cos i) - \sqrt{1-e^2} \sin E(\sin\Omega \sin\omega - \cos\Omega \cos\omega \cos i)\}$$

$$z_s = a\{(\cos E - e) \sin\omega \sin i + \sqrt{1-e^2} \sin E \cos\omega \sin i\}$$

Equation (1) then becomes

$$\rho^2 = a^2(1-e\cos E)^2 + d^2 + 2ad\cos\delta\{[\cos i \sin(\Omega-\alpha) - \tan\delta \sin i][\sin\omega(\cos E-e) + \sqrt{1-e^2}\cos\omega \sin E] - \cos(\Omega-\alpha)[\cos\omega(\cos E-e) - \sqrt{1-e^2}\sin\omega \sin E]\} \quad (7)$$

If the tracking satellite T is in the equatorial plane, $\delta = 0$, then

$$\rho^2 = a^2(1-e\cos E)^2 + d^2 + 2ad\{\cos i \sin(\Omega-\alpha)[\sin\omega(\cos E-e) + \sqrt{1-e^2}\cos\omega \sin E] - \cos(\Omega-\alpha)[\cos\omega(\cos E-e) - \sqrt{1-e^2}\sin\omega \sin E] \quad (8)$$

The partial derivatives of equation (7) with respect to a, e, i, Ω, ω, E are, respectively,

$$\frac{\partial\rho}{\partial a} = \frac{a^2(1-e\cos E)^2 - d^2}{2a\rho} + \frac{\rho}{2a}$$

$$\frac{\partial\rho}{\partial e} = -\frac{a^2}{\rho}(1-e\cos E)\cos E - \frac{ad}{\rho}\cos\delta\{[\cos i \sin(\Omega-\alpha) - \tan\delta \sin i][\sin\omega + \frac{e}{\sqrt{1-e^2}}\cos\omega \sin E] - \cos(\Omega-\alpha)[\cos\omega - \frac{e}{\sqrt{1-e^2}}\sin\omega \sin E]\}$$

$$\frac{\partial\rho}{\partial i} = -\frac{ad}{\rho}\cos\delta[\sin i \sin(\Omega-\alpha) + \tan\delta \cos i][\sin\omega(\cos E-e) + \sqrt{1-e^2}\cos\omega \sin E]$$

$$\frac{\partial\rho}{\partial\Omega} = \frac{ad}{\rho}\cos\delta\{\cos i \cos(\Omega-\alpha)[\sin\omega(\cos E-e) + \sqrt{1-e^2}\cos\omega \sin E] + \sin(\Omega-\alpha)[\cos\omega(\cos E-e) - \sqrt{1-e^2}\sin\omega \sin E]\}$$

$$\frac{\partial\rho}{\partial\omega} = \frac{ad}{\rho}\cos\delta\{[\cos i \sin(\Omega-\alpha) - \tan\delta \sin i][\cos\omega(\cos E-e) - \sqrt{1-e^2}\sin\omega \sin E] + \cos(\Omega-\alpha)[\sin\omega(\cos E-e) + \sqrt{1-e^2}\cos\omega \sin E]\}$$

$$\frac{\partial\rho}{\partial E} = \frac{a^2}{\rho}(1-e\cos E)e\sin E + \frac{ad}{\rho}\cos\delta\{[\cos i \sin(\Omega-\alpha) - \tan\delta \sin i][-\sin\omega \sin E + \sqrt{1-e^2}\cos\omega \cos E] + \cos(\Omega-\alpha)[\cos\omega \sin E + \sqrt{1-e^2}\sin\omega \cos E]\}$$

and from Kepler's equation

$$\frac{\partial E}{\partial a} = \frac{-1.5\mu^{\frac{1}{2}}(t-T)}{a^{5/2}(1-e\cos E)}$$

$$\frac{\partial E}{\partial e} = \frac{\sin E}{1-e\cos E}$$

$$\frac{\partial E}{\partial T} = \frac{-\mu^{\frac{1}{2}}}{a^{3/2}(1-e\cos E)}$$

4. Tracking a Geostationary Satellite

In order to apply the above method in the case of a geostationary target satellite, the tracking satellite should not be geostationary. Let a_T, e_T, i_T, Ω_T, ω_T, T_T be the orbital elements of the tracking satellite and α_s, δ_s, d_s be the elements of position of the target satellite with respect to the geocentric equatorial inertial frame; then equation (7) becomes

$$\begin{aligned}\rho^2 = {} & a_T^2 (1-e_T\cos E_T)^2 + d_s^2 + 2a_T d_s \cos\delta_s\{[\cos i_T \sin(\Omega_T-\alpha_s) \\ & - \tan\delta_s \sin i_T][\sin\omega_T(\cos E_T - e_T) + \sqrt{1-e_T^2}\cos\omega_T \sin E_T] \\ & - \cos(\Omega_T-\alpha_s)[\cos\omega_T(\cos E_T - e_T) - \sqrt{1-e_T^2}\sin\omega_T \sin E_T]\}\end{aligned} \tag{9}$$

where E_T is obtained by solving Kepler's equation.

The right ascension of the target satellite can be written as

$$\alpha_s = \alpha_{s_0} + \omega_E(t-t_0) \tag{10}$$

If the orbital elements of the tracking satellite are known, then equation (9) has the form

$$\rho = \rho(\alpha_{s_0}, \delta_s, d_s)$$

One can express the range residuals $\Delta\rho$ in terms of the corrections $\Delta\alpha_{s_o}$, $\Delta\delta_s$, Δd_s as

$$\Delta\rho = \left\{\frac{\partial\rho}{\partial\alpha_{s_o}}\right\}\Delta\alpha_{s_o} + \left\{\frac{\partial\rho}{\partial\delta_s}\right\}\Delta\delta_s + \left\{\frac{\partial\rho}{\partial d_s}\right\}\Delta d_s \tag{11}$$

where

$$\frac{\partial\rho}{\partial\alpha_{s_o}} = -\frac{a_T d_s}{\rho}\cos\delta_s\{\cos i_T\cos(\Omega_T-\alpha_s)\,[\sin\omega_T(\cos E_T-e_T)$$

$$+\sqrt{1-e_T^2}\cos\omega_T\sin E_T] + \sin(\Omega_T-\alpha_s)[\cos\omega_T(\cos E_T-e_T)$$

$$-\sqrt{1-e_T^2}\sin\omega_T\sin E_T]\}$$

$$\frac{\partial\rho}{\partial\delta_s} = -\frac{a_T d_s}{\rho}\{[\sin\delta_s\cos i_T\sin(\Omega_T-\alpha_s) + \cos\delta_s\sin i_T]$$

$$[\sin\omega_T(\cos E_T-e_T) + \sqrt{1-e_T^2}\cos\omega_T\sin E_T]$$

$$-\sin\delta_s\cos(\Omega_T-\alpha_s)\,[\cos\omega_T(\cos E_T-e_T) - \sqrt{1-e_T^2}\sin\omega_T\sin E_T]\}$$

$$\frac{\partial\rho}{\partial d_s} = \frac{\rho}{2d_s} + \frac{d_s^2 - a_T^2(1-e_T\cos E_T)^2}{2d_s\rho}$$

The next approximations to the elements of position of the target satellite are

$$\alpha_s' = \alpha_{s_o} + \Delta\alpha_{s_o} + \omega_E(t-t_o)$$

$$\delta_s' = \delta_s + \Delta\delta_s$$

$$d_s' = d_s + \Delta d_s \tag{12}$$

The process is then continued as in section 3.

5. Preliminary Results

The above formulation has been simulated for a simple least squares approach. First, the target satellite selected for study was an elliptical earth satellite having the following known orbit parameters

a =	1.6	earth radii
e =	0.05	
i =	1.138991	radian
Ω =	1.796065	radian
ω =	1.004865	radian

and the tracking satellite was taken as a geostationary satellite. Then the more general case of an elliptical non-equatorial earth synchronous tracking satellite was considered to compare the results obtained with a ground-based tracking station, and to track a geostationary target satellite. In all cases the observed ranges were simulated by a program written in double precision for FORTRAN IV on a CDC 6400 digital computer.

The entire orbit determination program was also written in double precision because of the number of trigonometric functions involved in the expressions and the similarity of the observed values of ρ, and to diminish the detrimental effect of truncation in calculation and to avoid difficulty in performing inversion of the normal matrix.

The program started from approximate values of components of position and velocity vectors of the target satellite at time t_o = T + 1800 seconds

True Position and Velocity		Approximate Position and Velocity		
r_x =	-0.3115940360324	r_x =	-0.33	(radii)
r_y =	-1.0161619714329	r_y =	-0.96	(radii)
r_z =	1.1516722843306	r_z =	1.00	(radii)
V_x =	0.0004110148706	V_x =	0.00038	(radii/sec)
V_y =	-0.0007627143063	V_y =	-0.00078	(radii/sec)
V_z =	-0.0004996964384	V_z =	-0.00052	(radii/sec)

Using well-known formulas one can obtain the first estimates for orbital elements of the target satellite as

a =	1.3559298580661	(radii)
e =	.0878878577706	
i =	1.1232204187772	(radian)
Ω =	1.7322918670788	(radian)
ω =	-0.0091516259974	(radian)
T =	-896.7222616242500	(sec.)

All range residuals were reduced to a value smaller than 10^{-13}. Using ten observations with a 100-sec interval between two observations, after six iterations the best estimates for the orbital elements of the target satellite were

a =	1.5999999996368	(radii)
e =	0.0499999999891	
i =	1.1389909994616	(radian)
Ω =	1.7960649999600	(radian)
ω =	1.0048649967139	(radian)
T =	-0.0000051365072	(sec.)

The effects of the number of observations and the time interval used were also considered in this study, and gave the following results:

1. The value of the normal matrix increases as the number of observations increases (i.e., when the number of observations changes from 10 to 20, with the same time interval, the value of the normal matrix changes from 10^{-35} to 10^{-24}); that facilitates the inversion process and allows larger (or smaller) guesses for the first estimates of the orbital elements.
2. With the same number of observations and iterations, the accuracy increases slightly as the time interval increases (Table I).
3. Small time intervals (less than about 10 sec.) must be avoided in order that the ranges vary significantly enough so that the inversion of the normal matrix is possible.

The method also works well for different values of inclination angle of the target satellite orbit plane, including $i = 90°$.

For $i = 0$, the tracking satellite should be in a slightly inclined orbit so that $\frac{\partial \rho}{\partial i} \neq 0$, making the inversion of the normal matrix possible.

	10 observations & after 3 iterations		
	40-sec interval	60-sec interval	100-sec interval
a	1.5999993646172	1.5999998812537	1.5999999851120
e	0.0499999675940	0.0499999664185	0.0500000005377
i	1.1389894947893	1.1389906906153	1.1389909143707
Ω	1.7960647775925	1.7960649476248	1.7960649987362
ω	1.0048618674775	1.0048645161761	1.0048650009421
T	-0.0056788572160	-0.0009357441760	-0.0000297907105

Table 1. Effects of Time Interval Variations

Because space-based tracking stations offer better geometry between stations and target satellites, by choosing suitable positions for tracking satellites one can get larger variations in slant-ranges in the same time intervals than in the case of an Earth-based tracking station. Consequently, in orbit determination problems using single station with range-only data, space based tracking stations will give better results in a shorter computer time.

The results below represent the tracking of an elliptical earth-satellite by using both ground and space-based stations (making 10 observations from each) to track during the same time intervals (100-sec).

Orbital elements of target satellite	
a = 1.6	(radii)
e = 0.1	
i = 1.138991	(radian)
Ω = 1.796065	(radian)
ω = 1.004865	(radian)
T = 0.	(sec.)

Estimates for orbital elements of target satellite	
a = 1.5961457660781	(radii)
e = 0.0979824812812	
i = 1.1394144718751	(radian)
Ω = 1.7967958707145	(radian)
ω = 0.9959110790266	(radian)
T = 9.2644292404117	(sec.)

Orbital elements of tracking satellite	
a = 6.592185612541	(radii)
e = 0.05	
i = 0.02	(radian)
Ω = 1.50	(radian)
ω = 0.70	(radian
T = 1000.	(sec.)

Coordinates of earth-based tracking station	
d = 1.0	(radii)
δ = .5934	(radian)
α_o = 2.295889	(radian)
(at t = 0)	

Tracking satellite (after 3 iterations)	
a = 1.6000000111919	(radii)
e = 0.1000000009737	
i = 1.1389910470895	(radian)
Ω = 1.7960650022364	(radian)
ω = 1.0048649819020	(radian)
T =-0.0000059857304	(sec.)

Earth-based tracking station (after 4 iterations)	
1.6000000277239	(radii)
0.1000000028427	
1.1389913824938	(radian)
1.7960653060371	(radian)
1.0048646107041	(radian)
-0.0002198539483	(sec.)

Using the same elliptical non-equatorial earth synchronous tracking satellite, with 6 observations starting from perigee at 100-sec. intervals the problem of tracking a geostationary satellite which has been moved to a neighboring position from a nominal point by perturbation effects was examined. With the method described in Section 4, and assuming that the perturbation motion of the target satellite was very slow so that one can consider the target satellite to be fixed with respect to the earth during any measurement period, the results are

Position of geostationary target satellite			1st approximation for elements of position (using position of nominal point)	
α_{s_o}	2.5124666666667	(radian)	2.4958	(radian)
δ_s	0.0166666666666	(radian)	0.0	(radian)
d_s	6.6704676659106	(radii)	6.592185612541	(radii)

Best estimates (after 8 iterations)		
α_{s_o}	2.5124666669423	(radian)
δ_s	0.0166666674769	(radian)
d_s	6.6705781317991	(radii)

To get better results and faster convergence for the process, one should increase the number of observations if the curvature of the portion of the tracking satellite orbit used during the measurement period decreases.

Further analysis of the method will be made to determine a suitable weighting matrix for laser range data, and to examine the effects of the geometry of the orbits, especially in the case of tracking satellites on parabolic and hyperbolic orbits. In addition, an examination of the effects of using two or more tracking satellites is being conducted.